The Pennsylvania State University

The Graduate School

College of Earth and Mineral Sciences

EVALUATING AVULSION CONTROLS ON FLUVIAL SAND BODY ARCHITECTURE AND CONNECTIVITY

A Thesis in

Geosciences

by

Tramond Baisden

Submitted in Partial Fulfillment
of the Requirements
for the Degree of

Master of Science

December 2015

The thesis of Tramond Baisden was reviewed and approved* by the following:

Elizabeth Hajek
Assistant Professor of Geosciences
Thesis Advisor

Rudy Slingerland
Professor of Geosciences

Demian Saffer
Professor of Geosciences

Michael Arthur
Interim Associate Head of the Graduate Program

*Signatures are on file in the Graduate School

ABSTRACT

Various scales of heterogeneity affect fluvial reservoir performance and are typically difficult to predict. Channel-belt-scale heterogeneity results from fluvial processes such as bar migration and reworking, and avulsion processes which build multi-story sand bodies (MSBs). Depending on basin conditions and avulsion patterns, channel belts may stack vertically or laterally, with each potentially affecting reservoir area and connectivity. The well-exposed Wasatch Formation (Paleocene/Eocene, Piceance Basin, Colorado, USA) exhibits three distinct styles of fluvial sand bodies and serves as the study area for this work. Using LiDAR and panoramic photo panels, field observations of the internal and external geometry of sand bodies were made and used to construct generalized channel elements for two net-to-gross (high and low) scenarios.

Simplified two-dimensional models generate reservoirs ranging from one to five stories. A suite of vertical aggradation rates and model widths develop domains that facilitate both lateral and vertical stacking of channel elements. Maximum connected areas and number of compartments are recorded for each model run. Results suggest high net-to-gross scenarios typically result in higher reservoir areas and lower compartmentalization. As aggradation and model width increase, reservoir area decreases while compartmentalization increases. High quality reservoirs are dominated by vertical stacking for low and high-net scenarios. There exist at least two scenarios where low-net, vertically stacked channels result in better connected, larger reservoirs than high-net, laterally stacked channels.

TABLE OF CONTENTS

LIST OF FIGURES

LIST OF TABLES

ACKNOWLEDGEMENTS

I am extremely grateful to Dr. Elizabeth Hajek, my thesis advisor, for her continuous support, guidance, and motivation throughout both my undergraduate career and graduate research. I am also grateful to Dr. Rudy Slingerland and Dr. Demian Saffer for their valuable discussion and advice while serving as members of my committee. Probing and analytical discussion with them helped me to focus my research goals and hypotheses. Ellen Chamberlin, Sheila Trampush, and Ryan Creitz were instrumental in data collection and discussions in the field.

For my family and friends who have supported me through all of my endeavors, I am thankful. Restless nights and long days were made easier with their kind words and encouragement. Lastly, I appreciate the camaraderie and friendship of fellow graduate students in the Geosciences Department and College of Engineering. I am especially thankful to MEGA, NSBE, NABG, and the Office of Engineering Diversity for providing resources, mentorship, and a space to relax during this process. Thank you!

1. Introduction

The connectivity of fluvial reservoirs is inherently difficult to predict, due to the presence of lithologic heterogeneities (Larue and Hovadik, 2006; Pranter et al., 2007) and complex internal architecture (Willis and Tang, 2010). Heterogeneities of various scales arise from a variety of fluvial processes, including bar migration and reworking, channel thread abandonment and reoccupation, and discharge variations. At the smallest scale, variations in grain size can affect connectivity within individual channel-bodies, while channel-belt-scale heterogeneities can significantly compartmentalize reservoirs and reduce flow efficiency (Pranter et al, 2007). Both geologic and engineering data can be used to infer connectivity in the subsurface (Larue and Hovadik, 2006), but are not commonly available in the exploration or development phases. Furthermore, without close well spacing, these sub-seismic resolution features are all but impossible to identify and increase risks when fluvial reservoirs are produced (Pranter et al., 2011).

At basin scale, large-scale channel avulsion patterns influence sand-body distribution, the overall net-to-gross of fluvial deposits, as well as heterogeneity and size of high-net intervals (Allen, 1978; Mackey and Bridge, 1995; Heller and Paola, 1996; Larue and Hovadik, 2006; Hajek et al., 2010). Modeling and field studies have explored how bar formation and channel migration can impact connectivity and compartmentalization in channel-belt deposits at various scales (Donselaar and Overeem, 2008; Willis and Tang, 2010; Labourdette, 2011; Pranter et al, 2011). However, the role of channel avulsion patterns and processes on controlling connectivity and

compartmentalization of multi-story, channel-belt-scale sand bodies remains poorly understood.

In order to better understand how avulsion reoccupations can impact reservoir connectivity and compartmentalization, we characterized a range of sand-body architecture in well exposed outcrops of the Wasatch Formation (Paleocene-Eocene, Piceance Basin, Colorado, USA). Using field observations, we generated simplified geometric models and investigated the effects of channel-belt-scale avulsion on fluvial reservoir connectivity. Specifically, we aimed to determine the effects of vertical versus lateral stacking on static connectivity, which is defined as the largest connected area resulting from model generated sand-bodies. Here, we show vertical stacking results in greater connectivity in both high-net and low-net cases. However, there exist some cases where low-net, vertically stacked sand bodies are of higher reservoir quality than high-net, laterally stacked sand bodies.

2. Fluvial process controls on reservoir connectivity

Fluvial processes – such as, channel incision, widening, and migration, bar formation and growth, and channel avulsion – control the development and architecture of facies in fluvial sand bodies, particularly the arrangement of reservoir and non-reservoir facies. Consequently, understanding the effects of channel and bar formation, evolution, and migration have been the focus of many fluvial reservoir quality and connectivity studies.

Generally, sand-rich channel-belt deposits will be better connected and less compartmentalized than muddier fluvial reservoirs (e.g. Allen, 1978; Larue and Friedmann, 2005; Larue and Hovadik, 2006; Pranter et al., 2011); however, even within relatively sandy channel-belts, the character and architecture of channel fills and bar deposits can have significant impact on reservoir performance. For example, low channel aggradation and finer-grained abandonment fill result in channel belts with relatively low overall recovery factors (Willis and Tang, 2010) and bar-scale shale drapes on accretion surfaces can significantly reduce breakthrough time and sweep efficiency (Pranter et al., 2007). These types of differences in bar and channel-fill sedimentology and architecture are influenced by several factors, including levee cohesion (Eaton et al., 2009), abandonment period length (Stouthamer, 2001) and variations in flow velocity (Thomas et al. 1987; Lynds and Hajek, 2006). At a larger scale, the stacking and arrangement of individual channel-belt deposits can substantially influence reservoir connectivity and compartmentalization. Multi-story sand bodies (Fig. 2.1.), referred to as MSBs

henceforth, are defined as amalgamated channel deposits with through-going erosional surfaces, representing multiple episodes of channel-belt deposition (Friend et al., 1979; Gibling, 2006; Chamberlin and Hajek, 2015).

The architecture and arrangement of MSBs is largely influenced by subsidence and aggradation, where relatively slow subsidence or aggradation results in more interconnected channel-belt deposits (Bridge and Leeder, 1979; Blakey and Gubitosa, 1983; Bristow and Best, 1993; Paola and Heller, 1996; Labourdette, 2011), and avulsion patterns, where clustered paleo-avulsion patterns yield interconnected MSBs that contain more channel-belt deposits than random avulsion patterns (Chamberlin and Hajek, 2015). The degree of amalgamation and arrangement of stories – or channel elements – in MSBs can change connectivity. For example, increased connectivity has been attributed to vertically stacked, ribbon sand bodies deposited in high accommodation settings, which can connect laterally stacked sand bodies formed in low accommodation settings (Labourdette, 2011).

Despite progress in understanding how fluvial processes can be used to predict reservoir connectivity, outstanding questions remain. In particular, it is unclear how avulsion patterns and MSB architecture control reservoir connectivity. In light of recent results, which suggest that fluvial systems may be predisposed to certain avulsion styles and patterns (e.g. Flood and Hampson, 2014; Chamberlin and Hajek, 2015)---, understanding the degree to which avulsion-derived MSB architecture influences inherent reservoir connectivity is important for improving subsurface prediction.

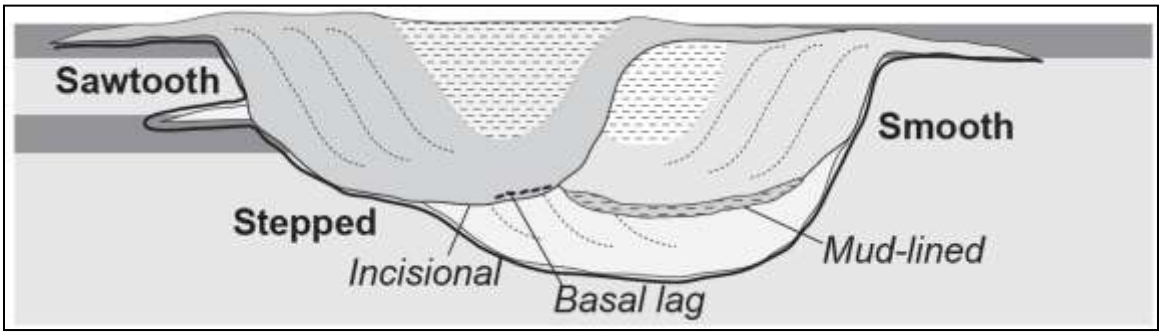

Fig. 2.1. Schematic diagram of a multi-story sand-body (MSB) showing characteristics of published descriptions of origin interpretations. Floodplain shown in light and dark grey. Stippled pattern represents abandonment fill (mud plugs). Various shades of gray with clinoforms represent channel fill. The external geometry of channel sand-bodies has been shown to be strong evidence of MSB origin in some cases. Left, stepped margin characteristic of MSBs formed through abandonment/reoccupation. Right, smooth margin characteristic of MSBs formed through intra-channel-belt processes, such as bar migration and meander cutoff. From Chamberlin and Hajek, 2015.

In order to understand the influence avulsion patterns have on MSB connectivity and compartmentalization, we evaluate channel-body architecture in well-exposed field examples and use geometric models to explore MSB architecture and compartmentalization under different generic stacking conditions. We focus specifically on channel-belt-element stacking consistent with the definition of Chamberlin and Hajek (2015), where individual stories comprise the deposits of channel-belt activity between avulsion. Internally, channel-belt elements may exhibit a large degree of variability, including a variety of bar-deposit styles and arrangements (e.g. Pranter et al., 2007; Labourdette et al., 2011; Labrecque et al., 2011) and different populations and preservation of intra-channel mudstone accumulations (e.g. Donselaar and Overeem, 2008; Reijenstein et al., 2011) that significantly affect reservoir connectivity and compartmentalization. Additionally, the composition and heterogeneity of overbank deposits, particularly proximal-overbank and avulsion deposits, can vary widely among ancient fluvial deposits (e.g., Hajek and Edmonds, 2014) and impact the connectedness of channel-belt elements (e.g., Jones and Hajek, 2007). Here, we aimed to isolate the specific effects of MSB stacking; we focused primarily on the architecture of MSBs as a whole rather than the architecture of individual channel-belt elements.

3. Architecture of avulsion-generated sand bodies: examples from the Wasatch Formation

In order to gain a better sense of avulsion-generated MSB architecture, we evaluated sand-body architecture in the well-exposed Wasatch Formation (Paleocene/Eocene, Piceance Basin, USA). This unit provides an example of diverse fluvial sand-body styles across its three members, while having similar scales, sediment source, and tectonic setting (Foreman et al., 2012). We identified the best-exposed sand bodies and mapped their internal and external geometry in order to characterize the range of avulsion-related channel-belt architecture present across the formation.

3.1. Study Area

The Paleocene-Eocene Wasatch Formation fills the central part of the Piceance Basin (western Colorado, USA; Fig 3.1.1), and comprises fluvial sands, overbank muds, levee and splay deposits, and coals (Lorenz and Nadon, 2002; Johnson and Flores, 2003; Foreman et al., 2012). The Wasatch Formation ranges from about 600m to 1200m thick (Lorenz and Nadon, 2002), and broadly thins from west to east (Johnson and Flores, 2003). Donnell (1969) subdivided the Lower Tertiary strata of the region into three members, the Paleocene Atwell Gulch, and Eocene Molina and Shire members of the Wasatch Formation (Fig. 3.1.2).

Basin subsidence reconstructions (Johnson, 1992) indicate that the Piceance Basin experienced broadly similar subsidence rates through the Paleocene and Eocene, as well as relatively similar sedimentation rates. Recent work shows that although various

episodes of Laramide uplift created new highlands in the region (thus potential source areas), the sediment source for each member of the Wasatch Formation remained largely constant (Foreman et al., 2012).

Despite similarities in subsidence and sedimentation rates, distinct channel styles characterize each member of the Wasatch Formation. Single story sand bodies dominate the Atwell Gulch, while multi-story sheet sands are common to the Molina. Shire sand bodies are multi-story, yet not as wide as those seen in the Molina. Foreman et al. (2012) argue the shift in channel styles was a response to the abrupt climate change of the Paleocene-Eocene Thermal Maximum. This variation in channel style, coupled with a lack of structural complexity and sparse vegetation, make the Wasatch Formation an ideal location for this study.

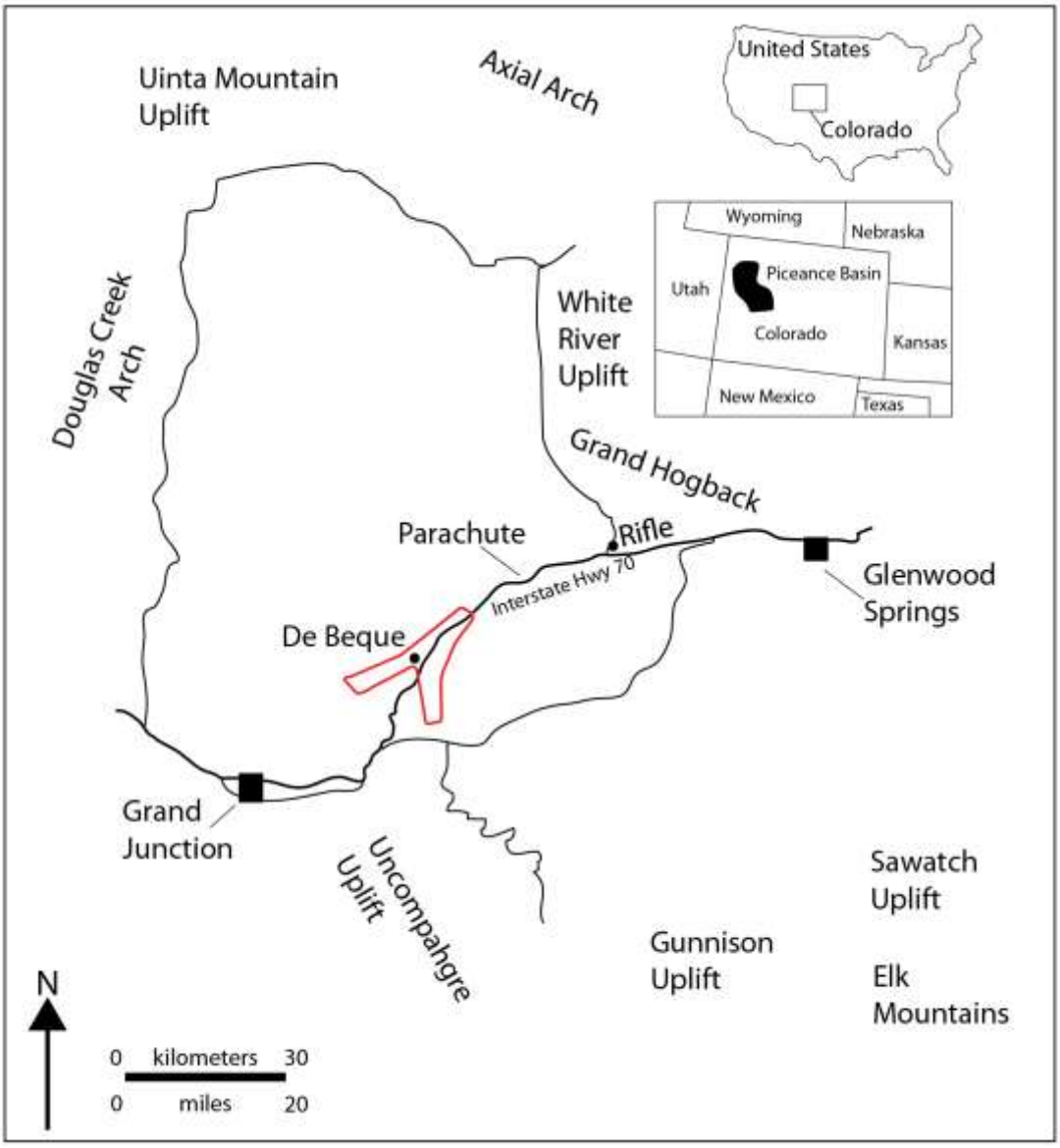

Fig. 3.1.1. Location map of the Piceance Basin, Colorado, USA. Study area outlined in red. The basin is bound to the west by the Douglas Creek Arch, to the south by the Uncompahgre and Sawatch Uplifts, to the east by the White River Uplift, and to the north by the Uinta Mountain Uplift. This study is limited to the area near De Beque and Parachute, along the I-70 Corridor. Modified from Pranter et al., 2007.

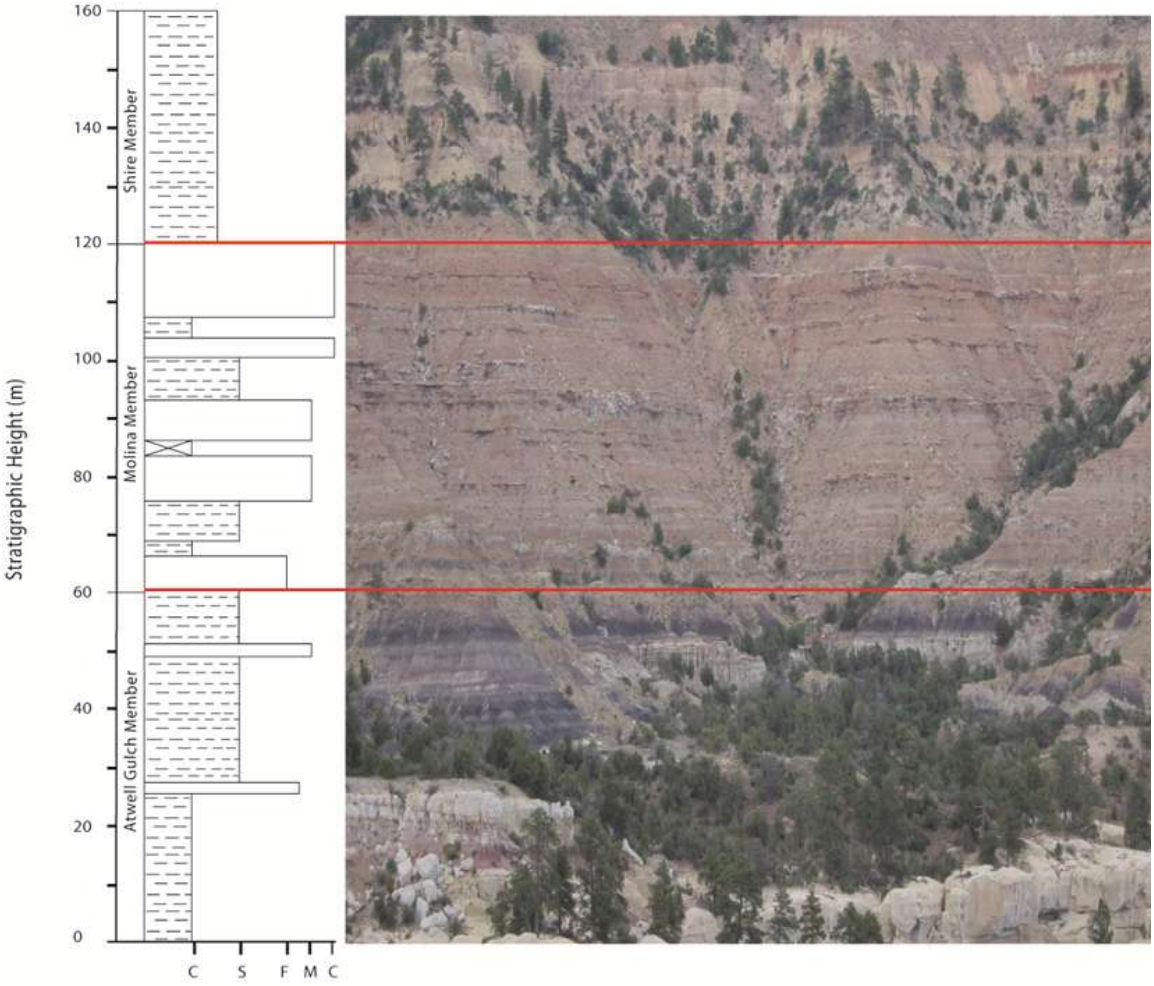

Fig. 3.1.2. Representative stratigraphic column of the Wasatch Formation (left). The mud-dominated Atwell Gulch Member is overlain by the sand-rich Molina Member. Sand content decreases in the uppermost Shire Member. Modified from Foreman et al., 2012. Photograph of complete Wasatch Formation exposure (right) near of De Beque, Colorado. Member boundaries on photo are approximate. Photo courtesy of Leah Toms.

3.1.1 Atwell Gulch Member

The base of the Wasatch Formation is marked by the mud-dominated Atwell Gulch Member, which unconformably overlies the Ohio Creek Conglomerate (Johnson and Flores, 2003). It comprises thin, laterally restricted, predominantly single story sand bodies, encased in variegated red, purple, and orange floodplain paleosols. Paleosols become progressively grayer up-section, with coal deposits cropping out near the Atwell Gulch-Molina boundary, indicating a shift towards a wetter climate (Foreman et al., 2012). With average flow depths of about 1m and average flow widths of about 4m, relatively shallow and narrow rivers deposited these sand bodies in lower-energy environments (relative to the Molina and Shire Members), as evidenced by the dominance of trough crossbedding (Foreman et al., 2012). Atwell Gulch sand bodies typically have preserved levees, while splays are rare in floodplain deposits.

3.1.2 Molina Member

Sand content increases markedly in the Molina Member. Channel sand bodies are relatively thick, laterally continuous, sheet-like, and typically multistory. Paleo-rivers, on average, were about 1.5m deep and 10m wide, and show a greater range in scale than the underlying Atwell Gulch or overlying Shire members (Foreman et al., 2012). Molina sand bodies typically lack distinct levee deposits; however, crevasse-splay deposits are ubiquitous. Paleosols are generally gray-green with purple mottling, and overall weakly developed relative to other Wasatch Formation members.

Lorenz and Nadon (2002) interpreted a distinct shift in channel style, from meandering in the Atwell Gulch, to a more braided depositional style in the Molina.

Several hypotheses related to climate and tectonics have been proposed to explain this occurrence. Foreman et al. (2012) argues an increase in precipitation, related to the onset of the Paleocene-Eocene Thermal Maximum (PETM), resulted in an increased sediment load and influx of sand. This is supported by the dominance of upper-plane bed laminations in Molina channels and an abundance of crevasse splay deposits in Molina floodplains.

3.1.3 Shire Member

The Shire Member is the youngest section of the Wasatch Formation and is dated to the Eocene. Following the main portion of the PETM carbon-isotope excursion, sand-content diminishes and the Wasatch returns to mud-dominated basin fill. Sand bodies, both single and multistory, are thicker than those of the Atwell Gulch, but not nearly as laterally extensive as those in the Molina. Paleoflow depths and widths are, on average, about 1m and 5m, respectively (Foreman et al., 2012). Paleosols are generally well developed and range from red, orange, purple, and green with strong horizonation and mottling. Channel sand bodies are often incised into underlying floodplain material and other times underlain by splays (Hajek and Edmonds, 2014). The Shire Member grades into the overlying lacustrine Green River Formation.

3.2. Field Study

The goal of this portion of the study was to characterize the range of channel-belt architecture present in the Wasatch Formation. Channel-belt elements are stacked both vertically and laterally, and also show evidence of both lateral migration and channel-belt-scale avulsion. We used terrestrial lidar scans and high resolution photo panels, supplemented by direct field measurements, to map the best- exposed representative sand bodies in each member.

3.2.1 Terrestrial lidar and Photography

In order to characterize the geometries present, well-exposed outcrops were identified and targeted for interpretation. Four high-quality sand bodies from each member and additional, large swaths of outcrop were selected for terrestrial lidar scanning (TLS) equipment. The TLS equipment used, the Riegl VZ-1000, captures scans with up to ~10 cm resolution, with finer resolution possible at shorter scan distances. Targeted sand bodies were scanned at ~10cm resolution, while larger swaths were scanned at lower resolution in order decrease scanning times. All scans were coupled with high-resolution photomosaics, taken using a Nikon D5000 digital camera and Gigapan Epic PRO. Using the combination of Gigapan photos and high-resolution LiDAR scans, sand-body geometry and internal architecture were interpreted. GPS coordinates and links to Gigapans of interpreted outcrops can be found in Appendix A.

3.2.2 Sand-body measurements and Interpretation Criteria

Following Chamberlin and Hajek (2015), external geometries of the sand bodies were evaluated in order to identify channel-belt sand bodies that resulted from avulsion (Fig. 3.2.1). The classification scheme of Allen (1983) was modified and used to identify and interpret internal architecture and external geometry of the sand bodies (Fig. 3.2.2; Table 3.2.1.) Key surfaces, such as those of basal erosion, through-going erosive boundaries, lateral accretion surfaces, bar-set surfaces, and dune sets, when possible, were identified.

Overall sand body and individual story widths and thicknesses were measured. Lateral migration distance was calculated by taking the bar-set width and dividing by the average bar width. Aspect ratio of the sand bodies and average story dimensions were then calculated. The ratio of number of stories to average story width and thickness was also determined. All measurements were made using TLS scans or were taken directly with a laser range finger in the field. These observations and measurements allow us to determine the degree to which avulsions resulted in lateral or vertical stacking of channel belts in each member.

Stories are interpreted as separate channel belts following criteria from Chamberlin and Hajek (2015), where stepped boundaries and preserved floodplain deposits indicate reoccupation of a channel belt. Story boundaries are represented by prevalent, laterally persistent surfaces, typically marked by incision and abandonment fill which bound large-scale packages of channel sands. Depending on perspective, they may be convex or planar.

Bar-sets are defined as packages of one channel-belt that represent multiple areas/events of accretion, i.e. two bars in one channel that are both accreting downstream represent two separate bar-sets. Bar-sets are defined by discontinuous basal surfaces, higher order internal surfaces marking accretion, and may have preserved fine-grain deposits which may represent interbar muds. Evidence to the contrary is required in order for a potential bar-set to be interpreted as a story.

Lateral accretion/Bar surfaces are defined by mostly continuous surfaces lined with channel fines which bound small scale packages of channel sands. Perpendicular or slightly oblique to paleoflow, they may be convex to sigmoidal, or relatively planar when viewed along paleoflow.

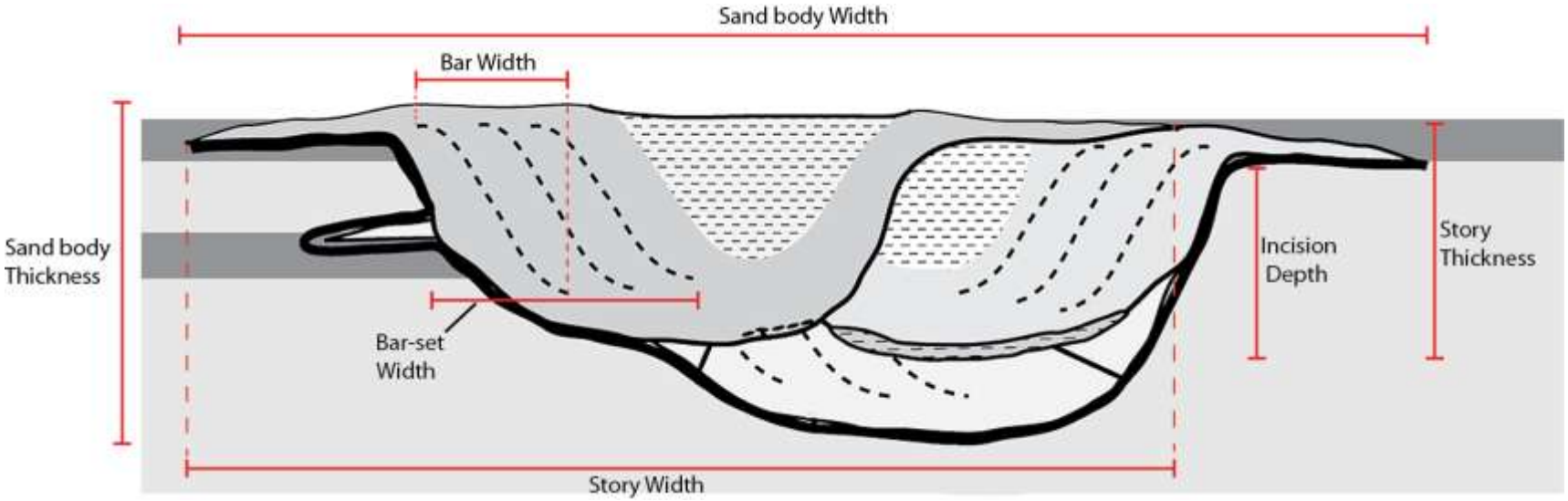

Fig. 3.2.1. Schematic diagram of a MSB with field measurements. Bar width was measured from the crest to the base of the bar. Total bar-set width was measured from the crest of the first bar to the base of the last bar. Incision depth was measured from the base of levees to the lowest point of the basal scour surface. Story width was measured from exposed end to end. Story thickness was measured from the top of the story to the basal scour surface. Modified from Chamberlin and Hajek (2015).

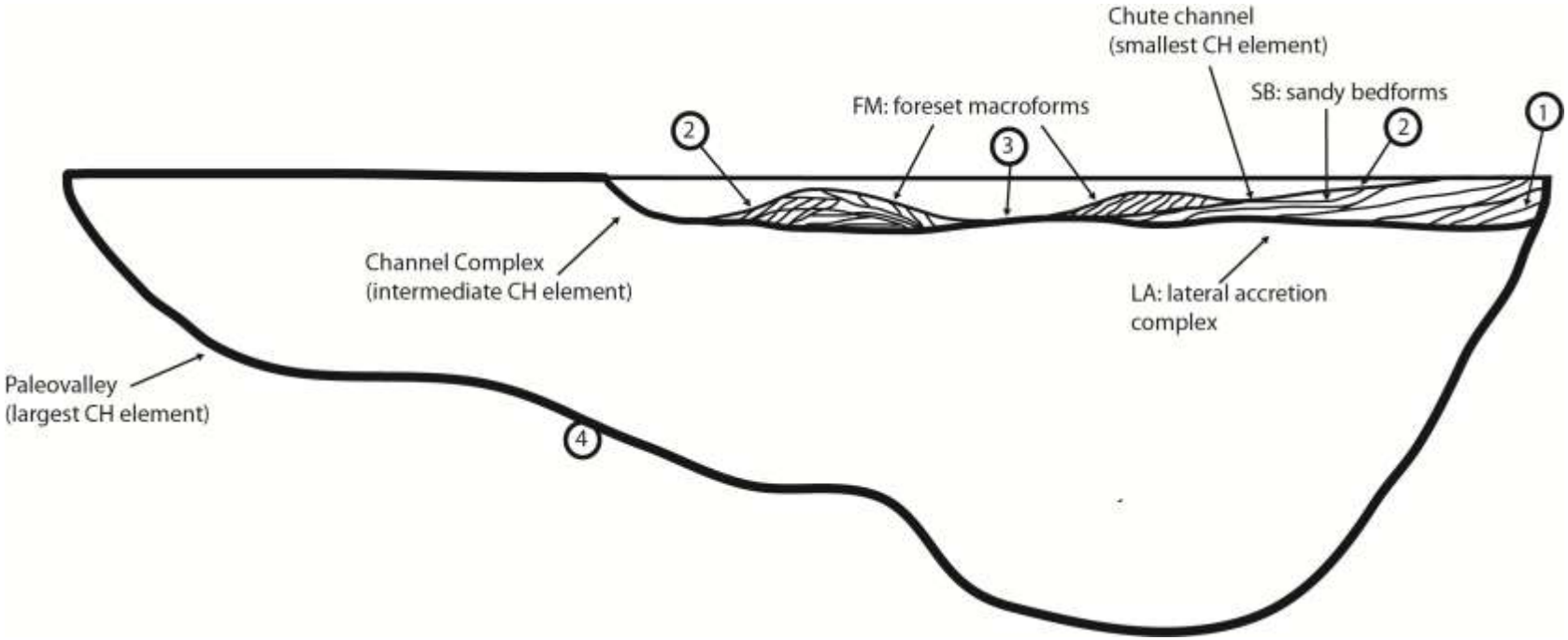

Fig. 3.2.2. Classification scheme of Allen (1983). First order surfaces delineate bedsets, such as crossbed sets. Second order surfaces bound cosets, i.e. macroforms such as laterally or downstream accreting bars. Third order surfaces are prevalent surfaces of erosion, marking channel complexes or groups of architectural elements. Fourth order surfaces represent groups of channels. Modified from Miall (1985).

Table 3.2.1. Classification Scheme and Comparison to Allen (1983)

Order of Surfaces	This Study	Allen (1983)
1	Bedsets	Bedsets
2	Lateral accretion surfaces	Cosets
3	Bar-sets	Groups of architectural elements or complexes
4	Basal Scour/Channel Complex	Paleovalleys

3.3 Results and Interpretations

Four of the best-exposed channel-belt sand bodies from each member were evaluated in detail (Figs. 3.3.1-3.3.12). Measurements and full descriptions for each sand-body can be found in Appendix B and C, respectively.

The three members of the Wasatch Formation exhibit a wide range of architecture, evidenced by the internal and external geometry of sand bodies, inferred facies and their arrangement, and channel-belt-scale stacking patterns. In the Atwell Gulch Member, sand bodies are typically single story and show strong evidence of lateral migration (e.g., Fig 3.3.1). Well-defined bar clinoforms were measured to estimate migration distances, which ranged from 1.4 to about 2.1 average bar widths. Proximal overbank and splay deposits were rare, only observed at Atwell Gulch-3. Based on these observations, intra-channel-belt processes are interpreted as the predominant controls on channel-belt architecture.

Sand bodies become much more laterally extensive, thick, and multi-storied in the Molina Member. The number of stories ranges from 2-5, with most stories comprising multiple bar-sets. Channel fines line the majority of interpreted higher order surfaces and mark abandonment or reduced-flow conditions. Interpreted lozenge-shaped, downstream accreting bars in Molina-2 and the overall lack of lateral accretion deposits suggest lower sinuosity, consistent with braided-river archetypes and previous interpretations of Molina fluvial style (Lorenz and Nadon, 2002; Foreman et al., 2012). Proximal overbank and splay deposits commonly surround Molina channel-belt deposits.

The Shire member is characterized by steep basal scour surfaces and deep incision with relatively fine-grained fill. Channel-belt elements more closely resemble Atwell

Gulch channel-belt elements, but are dominantly arranged in MSBs comprising 2-4 stories. Stories typically contain one or two bar-sets.

Overall, vertical stacking dominates in the Molina and the Shire Member, with a slight component of vertical stacking (Fig. 3.3.13). Atwell Gulch channel-belt complexes are single story, though lateral stacking dominates in the one interpreted MSB (Fig. 3.3.3). Molina and Shire Members both show evidence for common avulsion reoccupation.

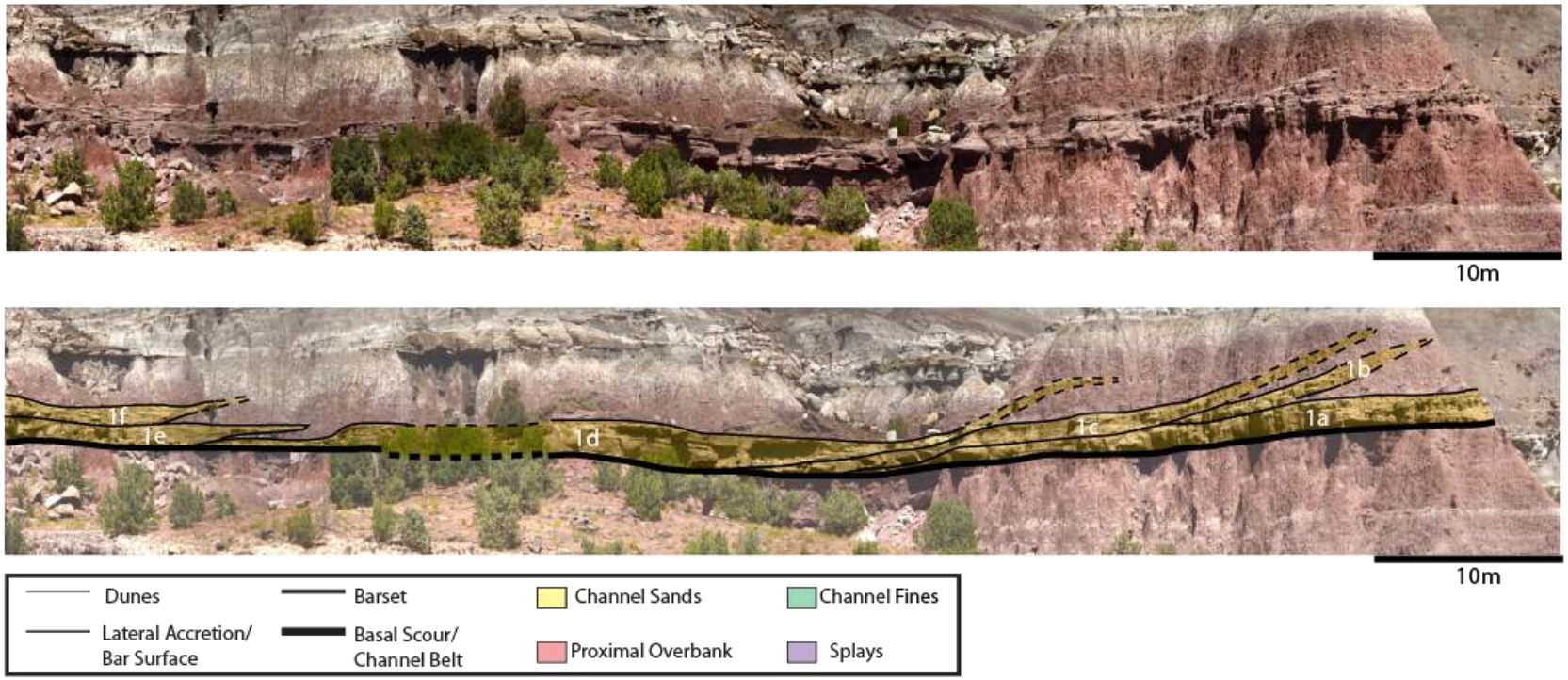

Fig. 3.3.1. Sand body Atwell Gulch-1. Single-story sand-body with evidence of lateral migration. Dashed lines represent lower confidence in interpretations.

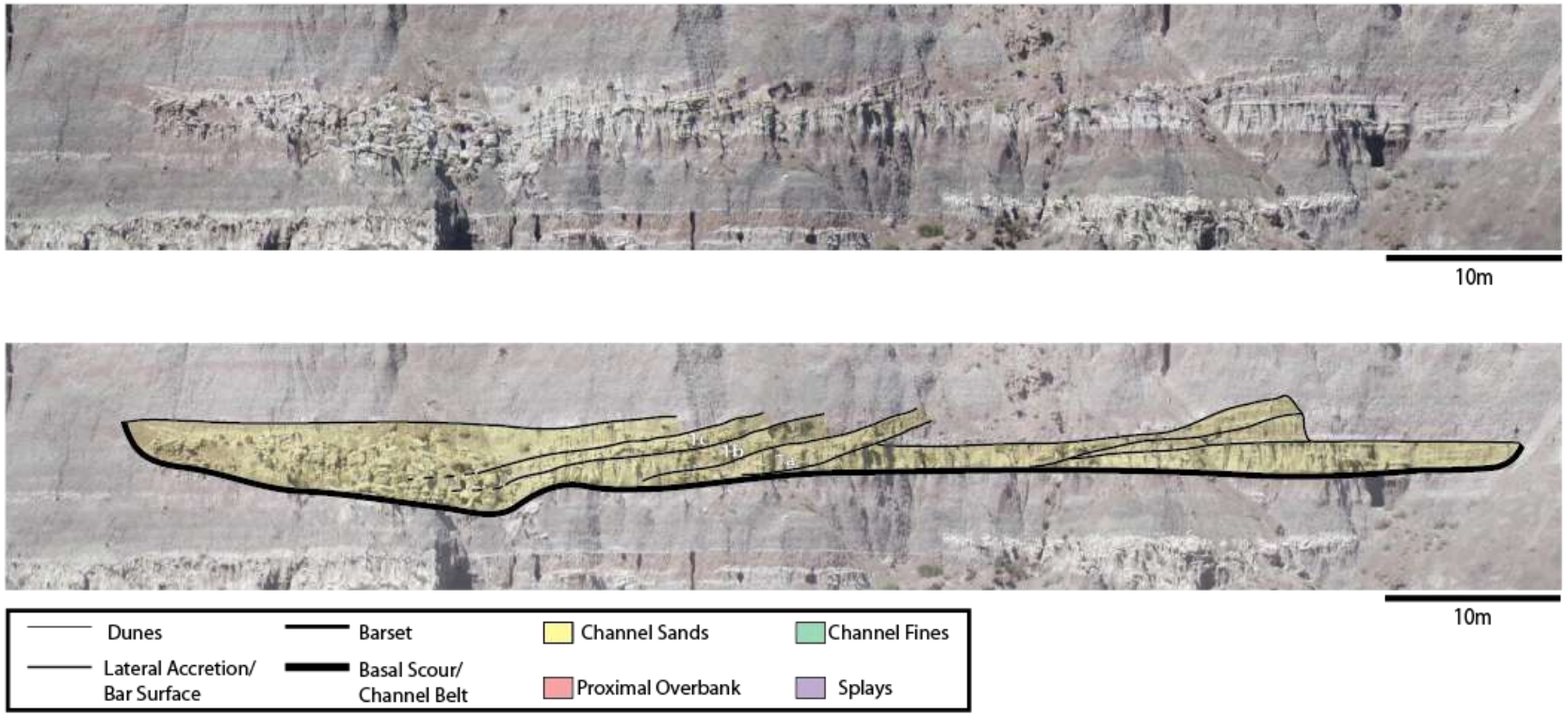

Fig. 3.3.2. Sand body Atwell Gulch-2. Single-story sand-body with evidence of lateral migration. Dashed lines represent lower confidence in interpretations.

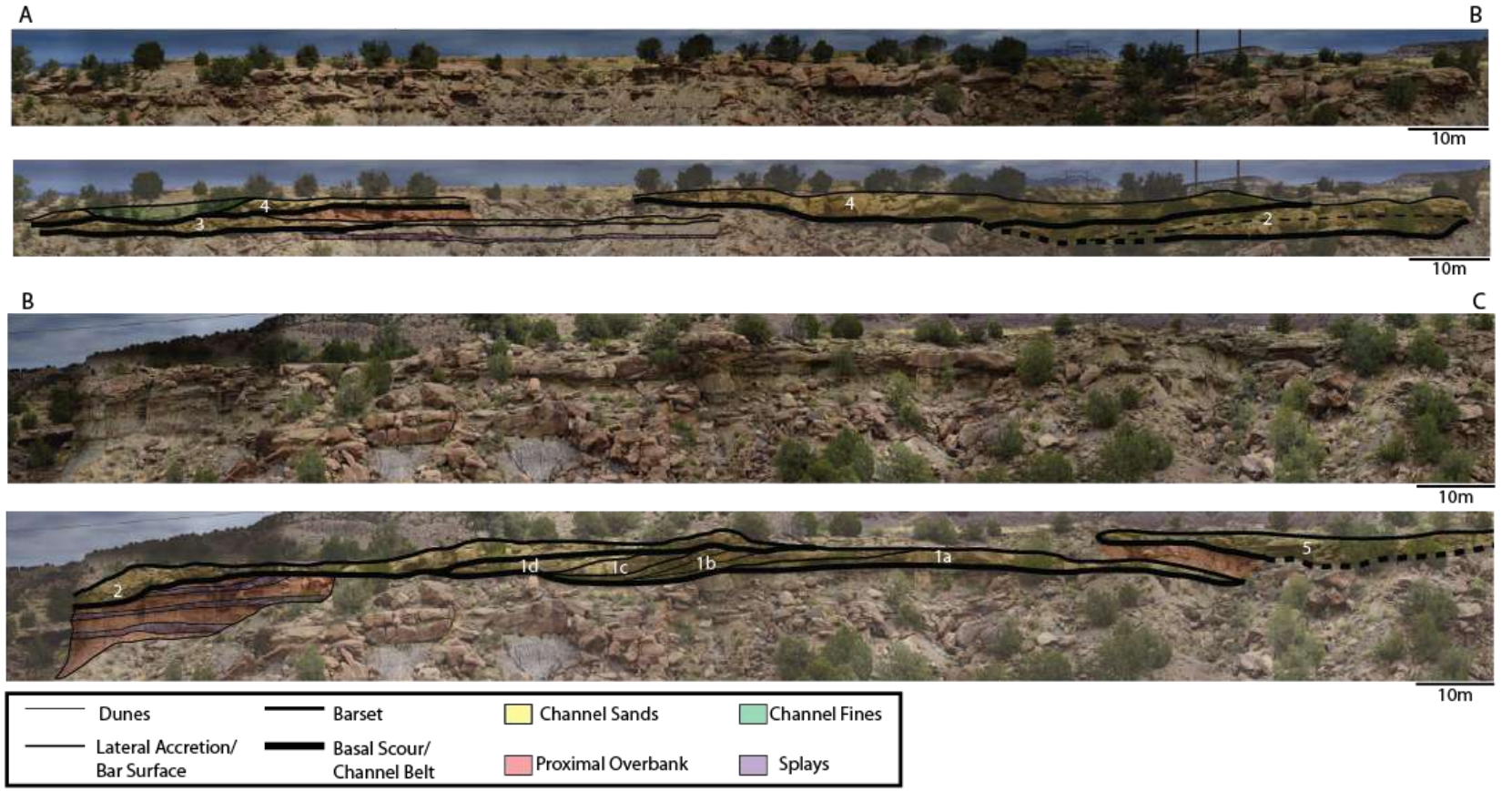

Fig. 3.3.3. Sand body Atwell Gulch-3. Multi-story (5) sand-body with evidence of lateral migration and abandonment/reoccupation. Dashed lines represent lower confidence in interpretations.

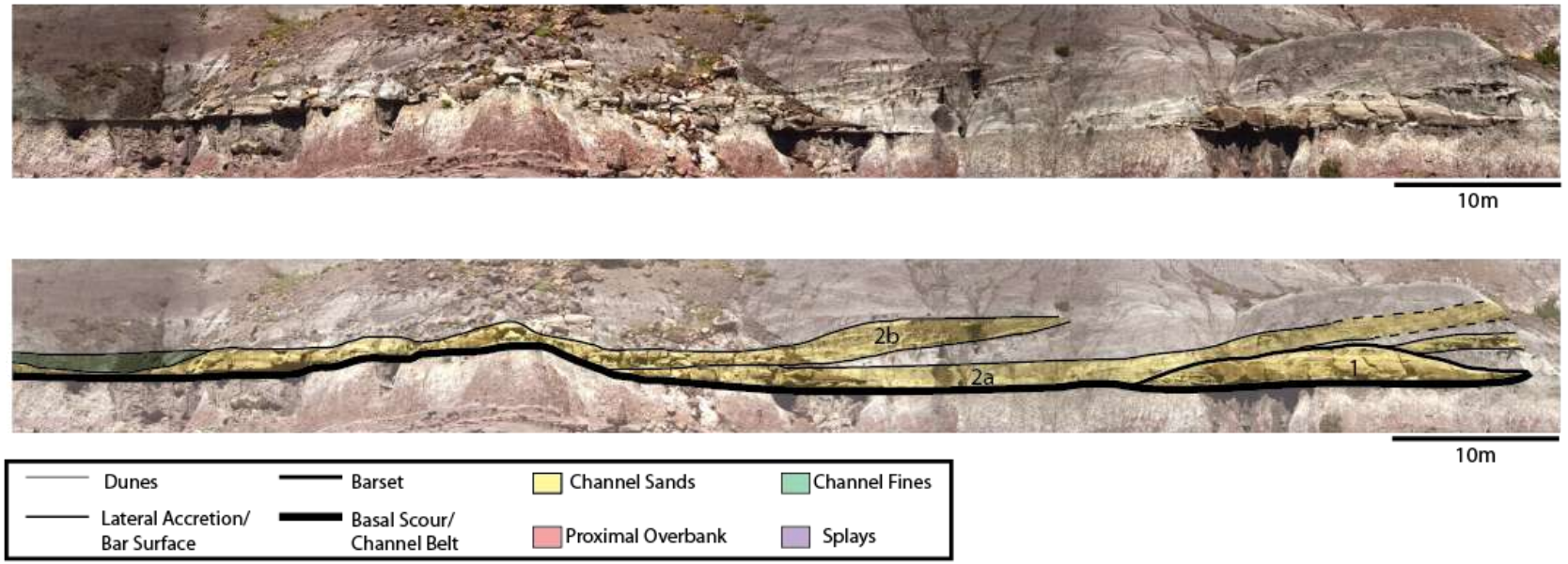

Fig. 3.3.4. Sand body Atwell Gulch-4. Single-story sand-body with evidence of lateral migration. Lower bar-set is truncated by an upper bar-set, potentially a meander cutoff. Dashed lines represent lower confidence in interpretations.

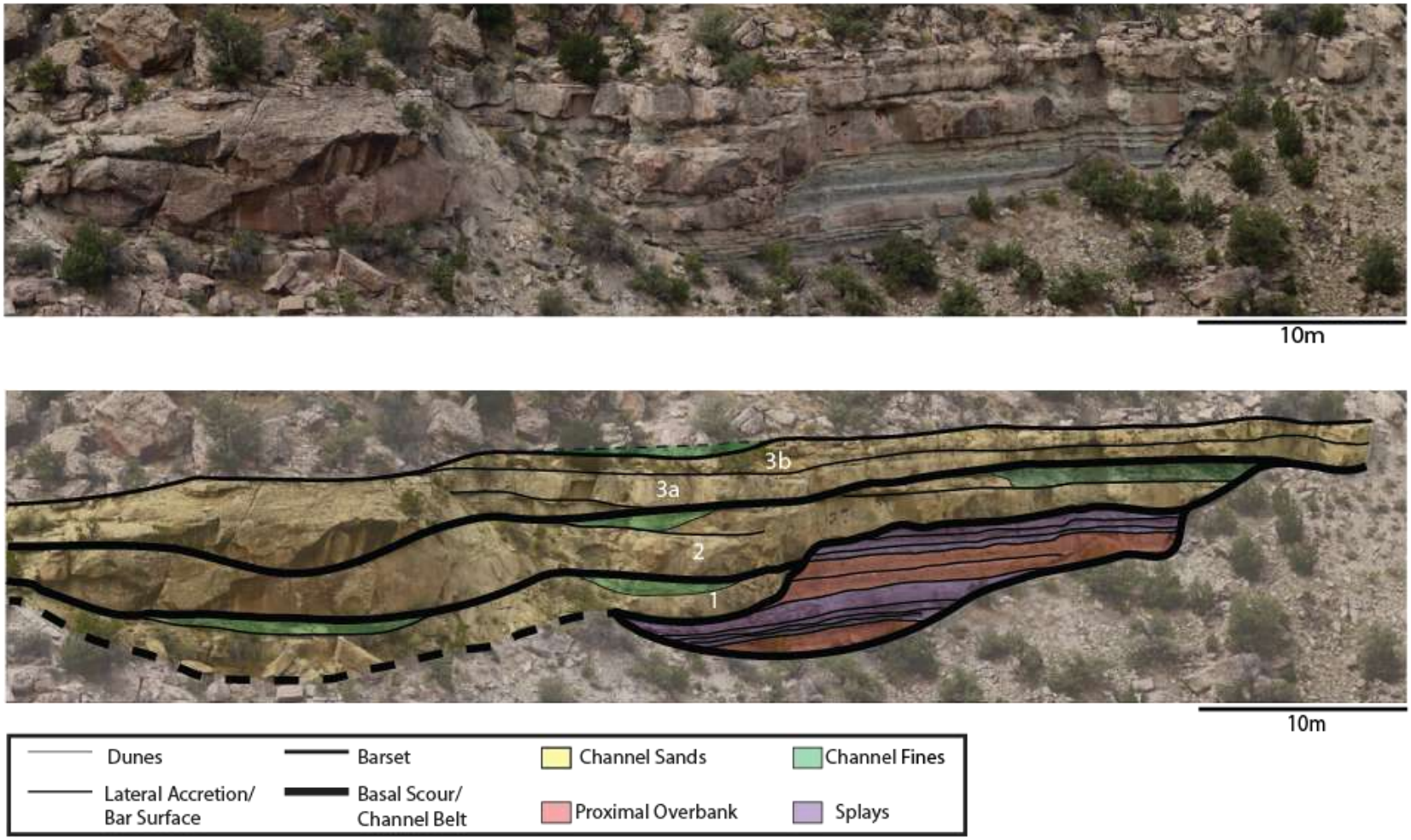

Fig. 3.3.5. Sand body Molina-1. Three-story sand-body dominated by vertical stacking and marked by deep incision. Fine-grained channel fill is preserved throughout. Dashed lines represent lower confidence in interpretations.

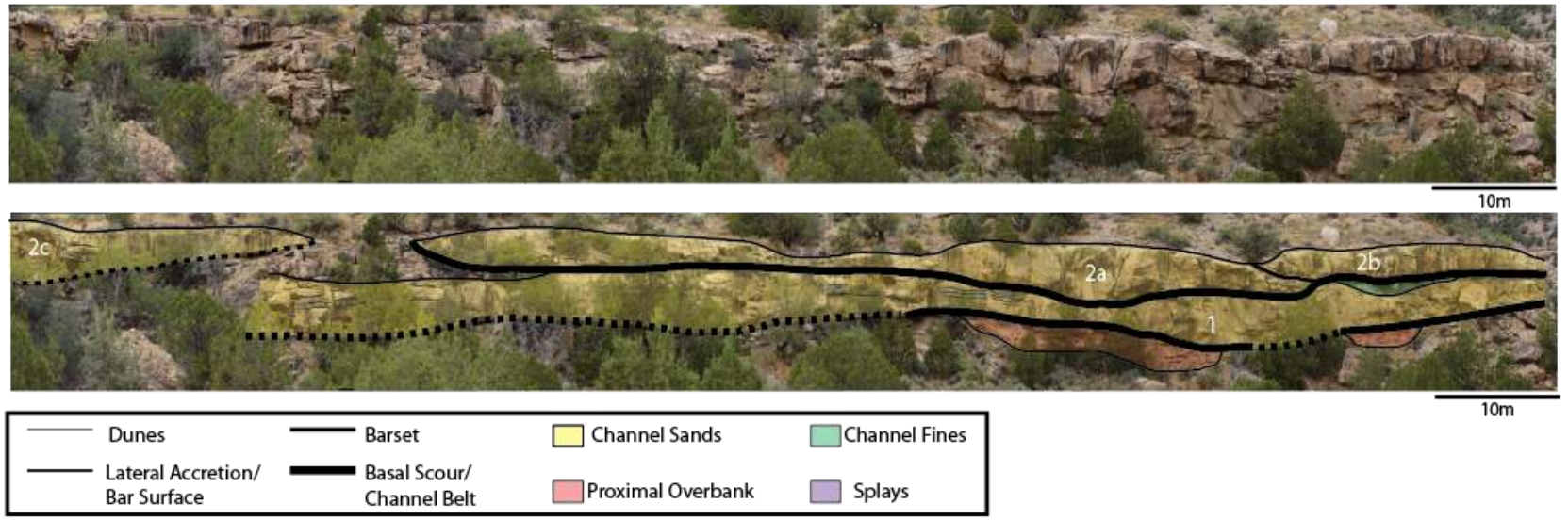

Fig. 3.3.6. Sand body Molina-2. Two-story sand-body with evidence of abandonment/reoccupation. Lower story represents a single channel belt, while the upper story represents downstream accreting bars or a braided stream. Dashed lines represent lower confidence in interpretations.

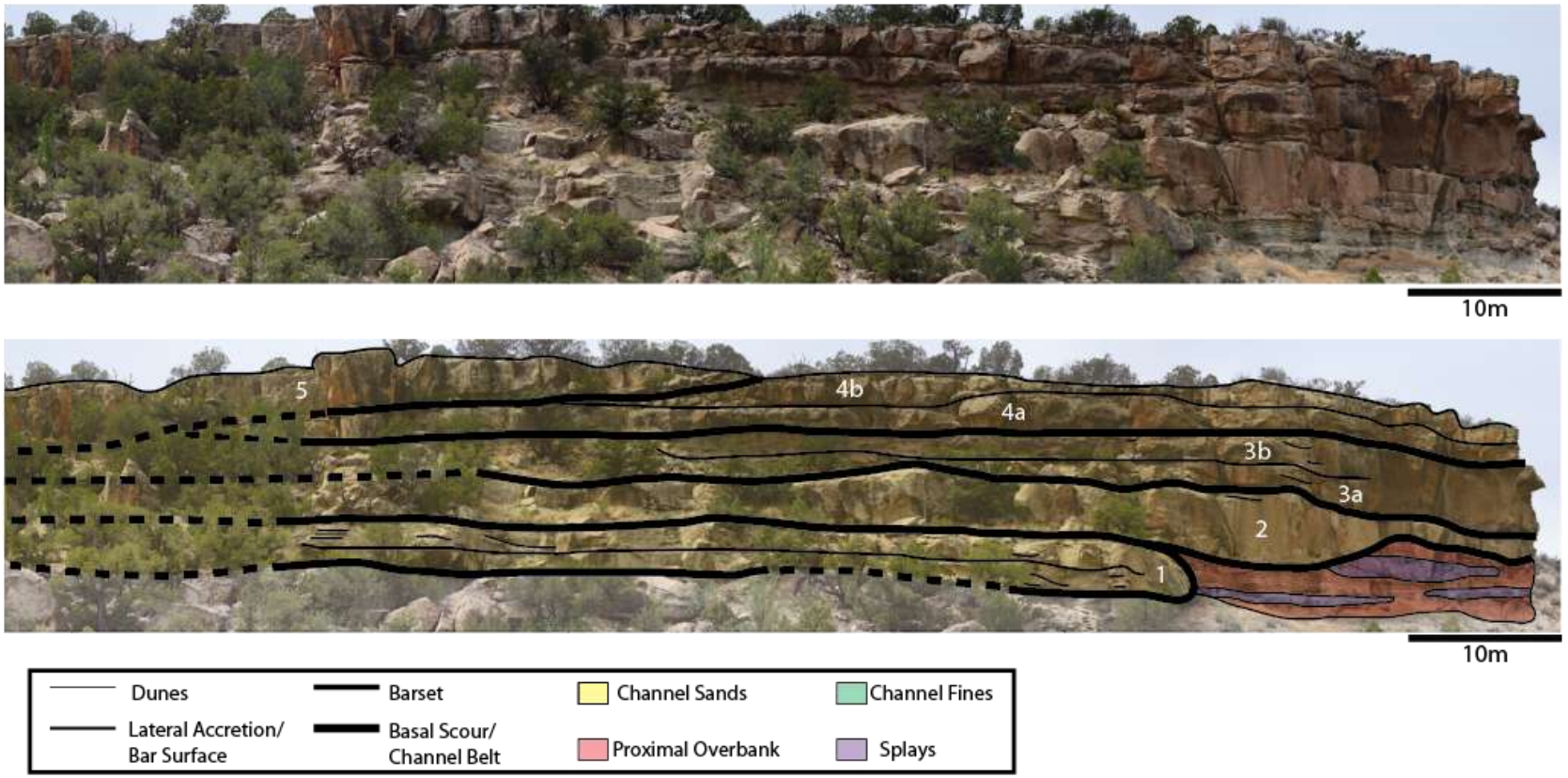

Fig. 3.3.7. Sand body Molina-3. Five-story sand-body with evidence of abandonment/reoccupation and lateral migration. Each story represents a separate channel belt, and sometimes comprises multiple bars. Dashed lines represent lower confidence in interpretations.

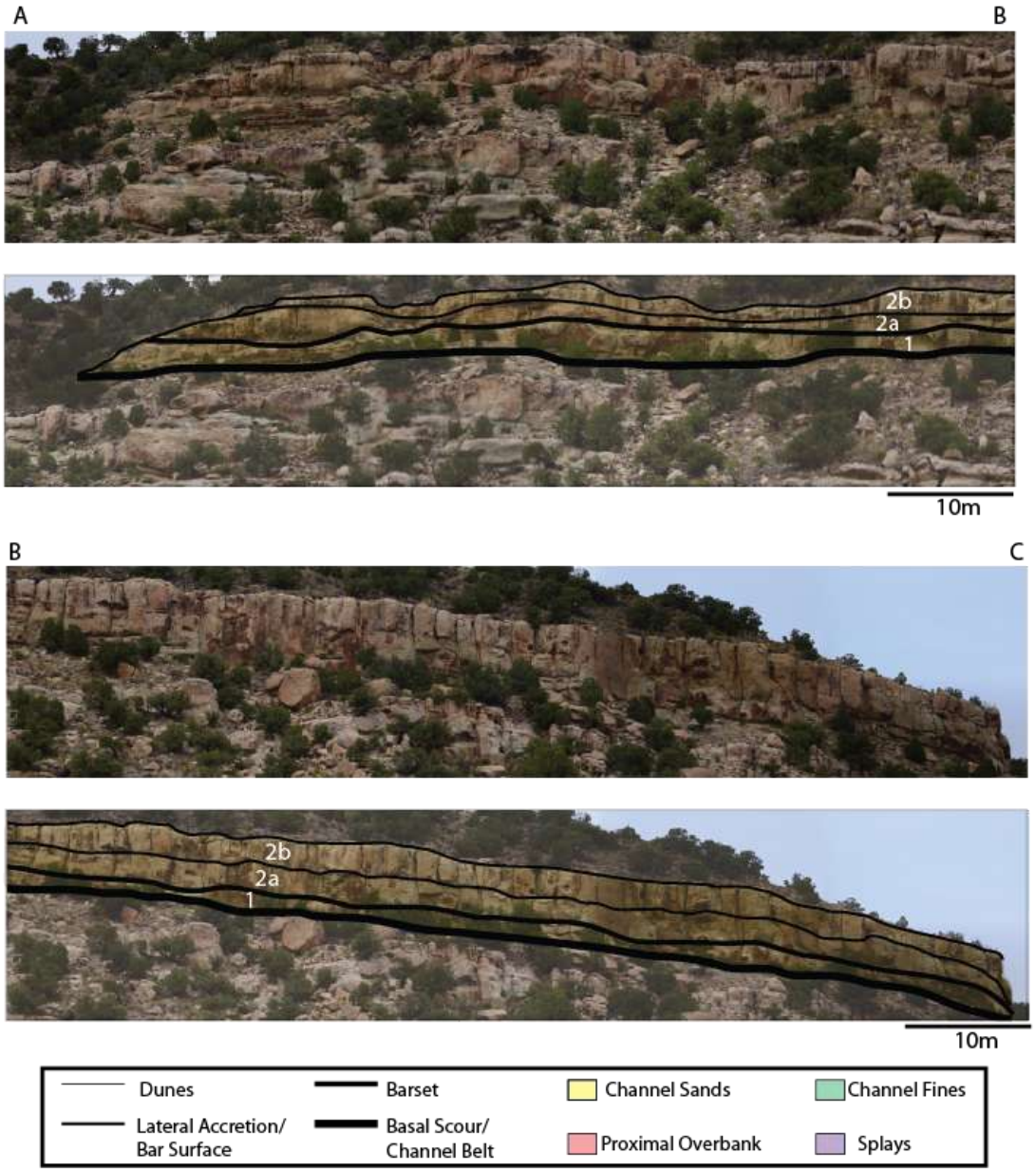

Fig. 3.3.8. Sand body Molina-2. Two-story sand-body with evidence of intra-channel-belt processes. Each story represents one channel-belt, with the upper bar-set comprising two bars (2a-2b). Internal surfaces are somewhat difficult to trace continuously, but are well-exposed at the margins of the MSB.

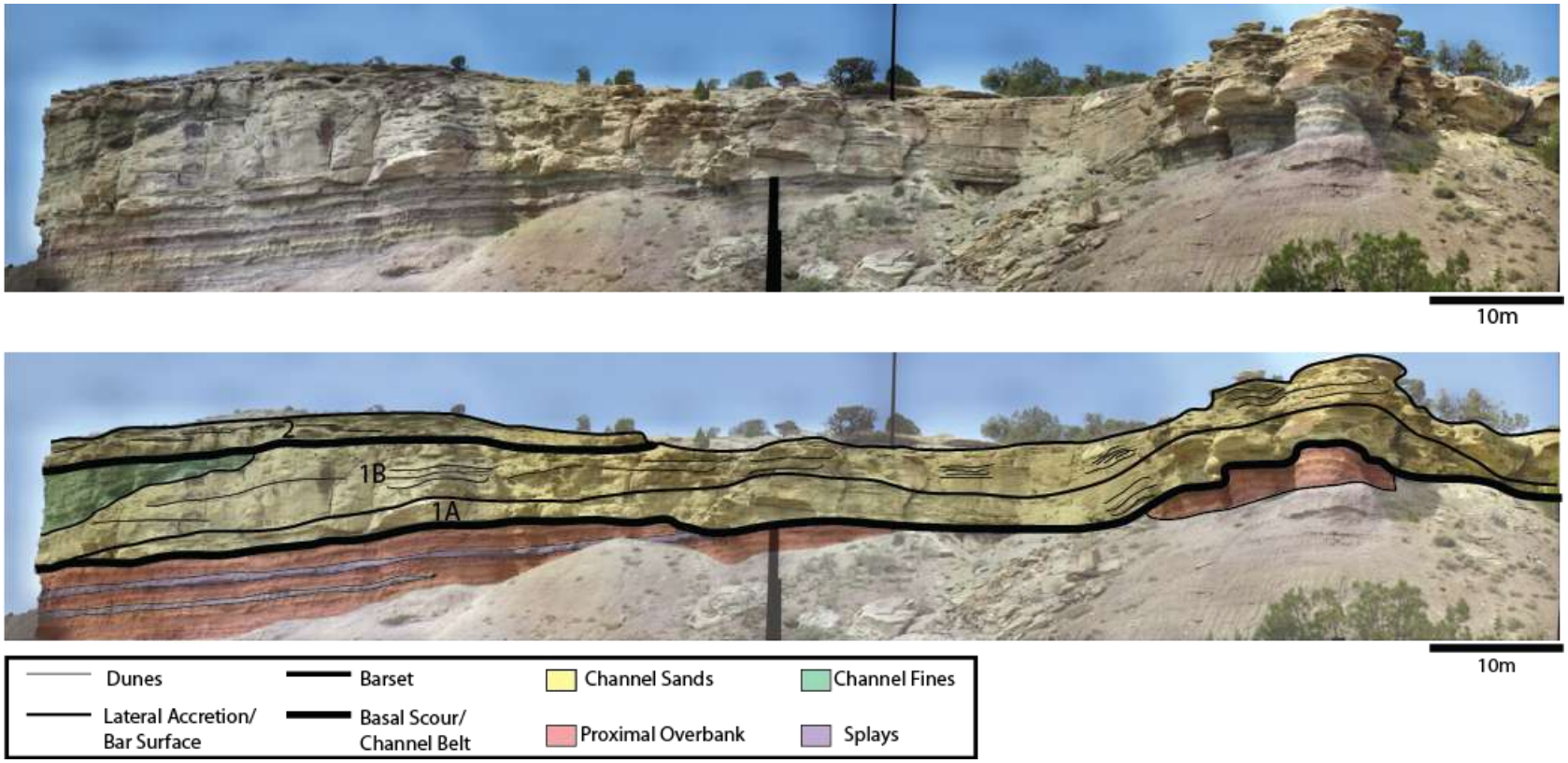

Fig. 3.3.9. Sand body Shire-1. Two-story sand-body, with evidence of lateral migration and abandonment/reoccupation. A steep-sided mud-plug marks abandonment, while a 4th order, basal scour surface related to story 2 truncates story 1b.

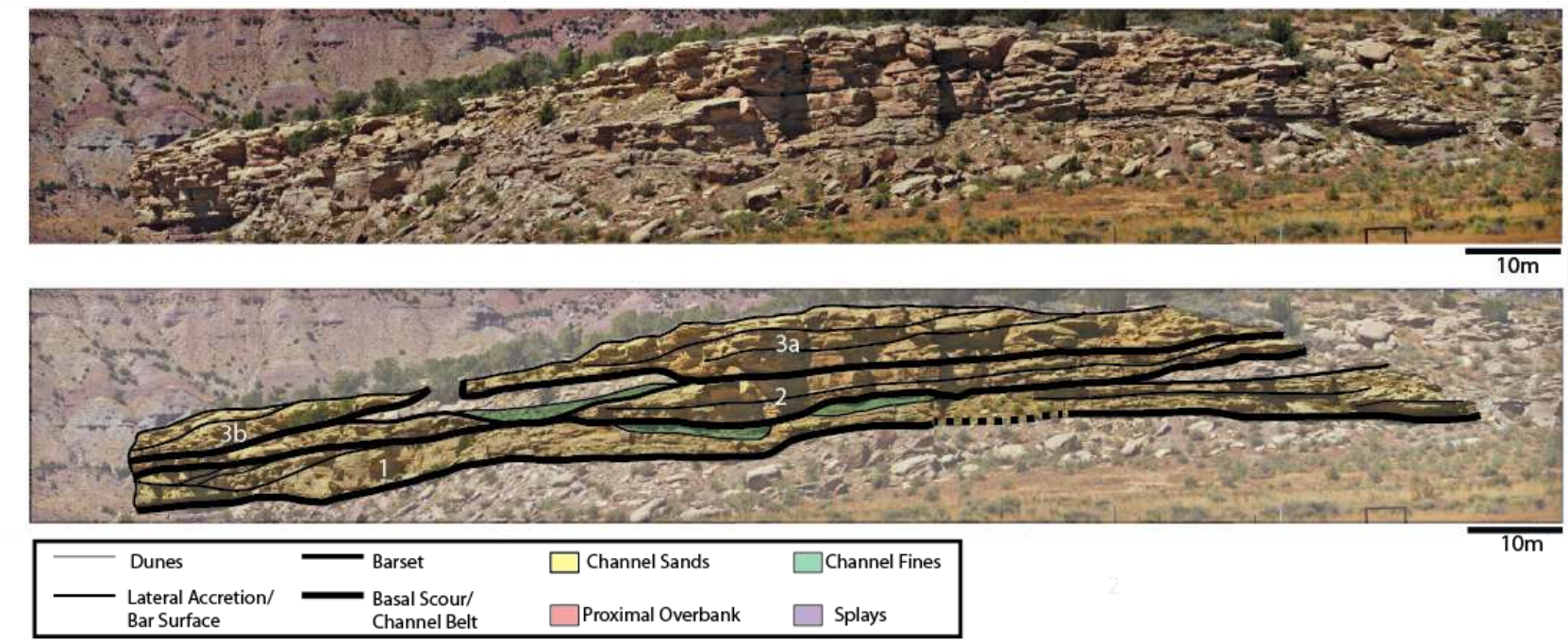

Fig. 3.3.10. Sand body Shire-2. Three-story sand-body with complex internal structure. Stories 1 and 2 represent two channel belts comprising bar deposits. Mud-plug at top of story 2 represents abandonment fill. 3a and 3b are nested bar-sets of the same channel belt. Preserved channel fines and stepped margins indicate abandonment/reoccupation. Dashed lines represent lower confidence in interpretations.

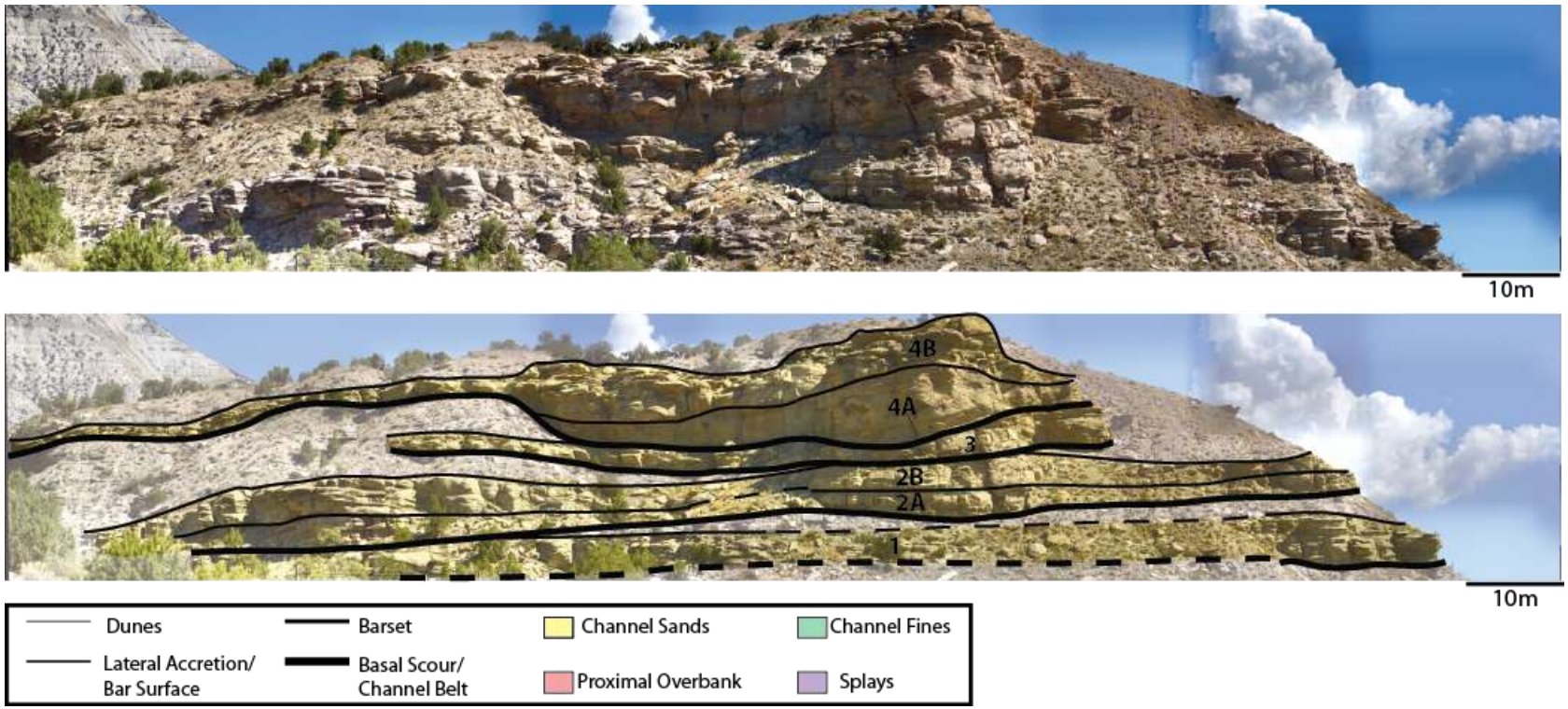

Fig. 3.3.11. Sand body Shire-3. Four-story sand-body, constructed through channel-belt abandonment/reoccupation and intra-channel-belt processes. Stories represent individual channel belts. Stepped margins and preserved floodplain between stories are readily visible. Dashed lines represent lower confidence in interpretations.

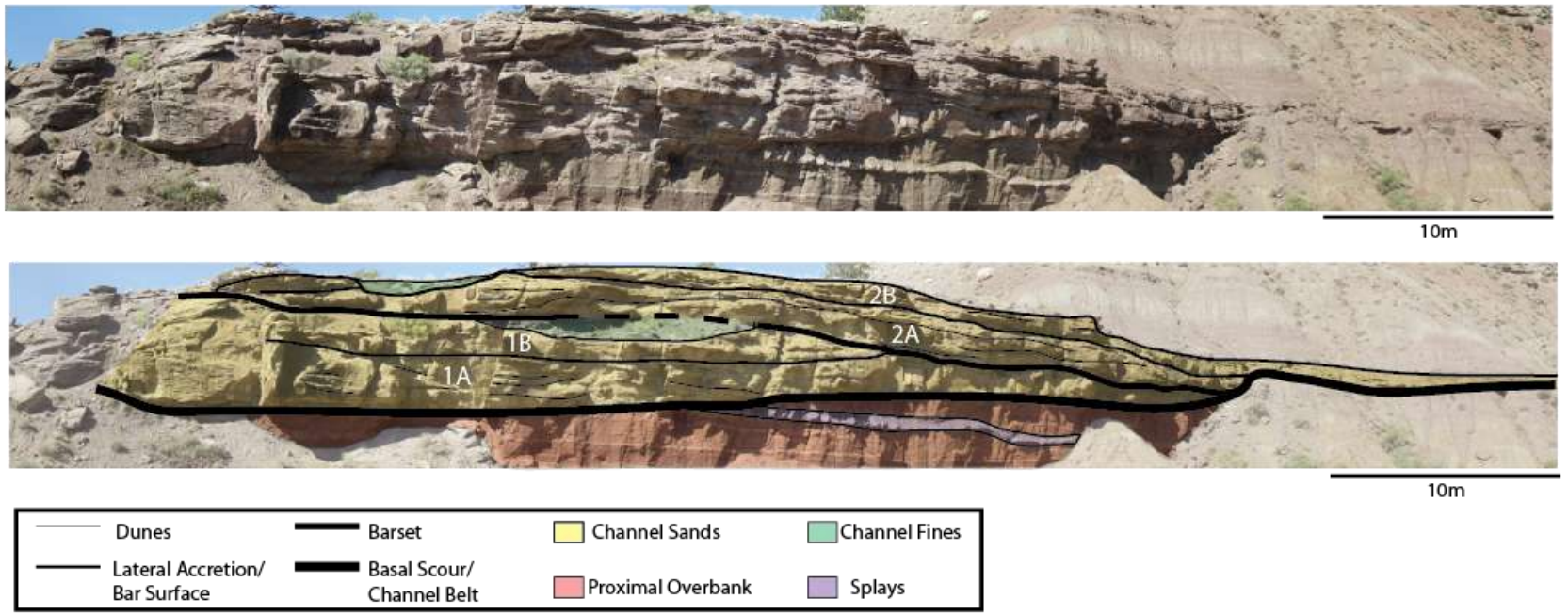

Fig. 3.3.12. Sand body Shire-4. Two-story sand-body formed through intra-channel-belt processes. Smooth bounding surface is visible at right margin. Stories are nested bars of a single channel-belt. Interbar muds preserved between 1b and 2a. Dashed lines represent lower confidence in interpretations.

Fig. 3.3.13. Relative stacking patterns of MSBs. Values are equal to the ratio of number of stories to average story width and thickness for vertical and lateral stacking, respectively. One Atwell Gulch sand body is multistory, and is dominated by lateral stacking. Molina and Shire MSBs are typically stacked vertically, with a slight component of lateral stacking.

4. Reservoir Modelling

While this study relied on outcrop examples to inform the models, we did not purely model interpreted outcrops (e.g. Pranter et al., 2007; Labourdette, 2011). Based on observations made in the field, simplified geometric reservoir models were developed to investigate the effects of vertical and lateral stacking of avulsion-generated channel belts on reservoir connectivity and compartmentalization. The purpose of the model is to develop predictions of reservoir connectivity based upon aggradation conditions, floodplain width, and stacking patterns for a given avulsion frequency.

4.1 Model Description

4.1.1 Model Design

The MATLAB code (Appendix D) used in this study was designed to randomly place five channel-belt elements in a model domain, creating multi-story sand bodies. Vertical aggradation (Eq. 1), which represents the steady build-up of the floodplain between channel avulsions, is the product of the channel element height and a vertical aggradation factor. This variable controls the height above the base of the previous channel-belt element at which the next centroid is placed. The domain height (Eq. 2) is defined by five times the vertical aggradation plus one-half element height. The model width (Eq. 3) represents the area over which an avulsion can occur, i.e. the range of values in the model domain over which element centroids can be placed laterally, and is a specified multiplier of the channel-belt element width. The domain width (Eq. 4) is defined by the model width plus the one-half the channel width, which is added to each

side of the domain to provide a buffer zone. This ensures each channel element is placed completely in the domain. The range of values chosen for both factors is listed in Table 4.1.1 and a schematic diagram of all values described above is shown in Fig**.** 4.1.1.

The lateral position of each channel-belt-element centroid is randomly selected from within the model width and the orientation of each element (left- or right-facing) is randomly determined. The channel elements are then placed in the domain in stratigraphic order, forming MSBs. Nine total simulations were run, spanning a range of vertical aggradation and model widths. The total number of compartments and the maximum compartment area were recorded for each run (n=100). Number of compartments ranged from four in a fully amalgamated sand body, to 20 in runs that produced five isolated sand bodies. Maximum connected area, or the largest compartment, is also recorded and normalized to the maximum compartment size in an individual element. Values closer to 6 indicate low amalgamation, while values closer to 1 indicate higher amalgamation.

Eq. 1)

$$Vertical\ Aggradation\ = Element\ Height * Vert.Agg.Factor$$

Eq. 2)

$$Domain\ Height = 5 * VA + \frac{Element\ Height}{2}$$

Eq. 3)

$$Model\ Width = Lateral\ Position\ Multiplier * Element\ Width$$

Eq. 4)

$$Domain\ Width = (Element\ W.\ * Lateral\ Position\ Mult. + Element\ Width$$

Table 4.1.1. Vertical aggradation factors and lateral position multipliers

Scenario	Vertical Aggradation Factor	Lateral Position Multiplier	Domain Area (Pixels)
1	0.25 (Low)	1.5 (Low)	1080000
2	0.25 (Low)	2.5 (Medium)	1512000
3	0.25 (Low)	3.5 (High)	1944000
4	0.50 (Medium)	1.5 (Low)	1620000
5	0.50 (Medium)	2.5 (Medium)	2268000
6	0.50 (Medium)	3.5 (High)	2916000
7	0.75 (High)	1.5 (Low)	2295000
8	0.75 (High)	2.5 (Medium)	3213000
9	0.75 (High)	3.5 (High)	4131000

Table 4.1.1. Each vertical aggradation factor and lateral position multiplier combination was tested, for a total of 9 model runs. Model runs will be referred to by the following: Low Aggradation, Low Width = LALW; Low Aggradation, Medium Width = LAMW; Low Aggradation, High Width = LAHW. Following the same convention, the remaining cases are MALW, MAMW, MAHW, HALW, HAMW, and HAHW.

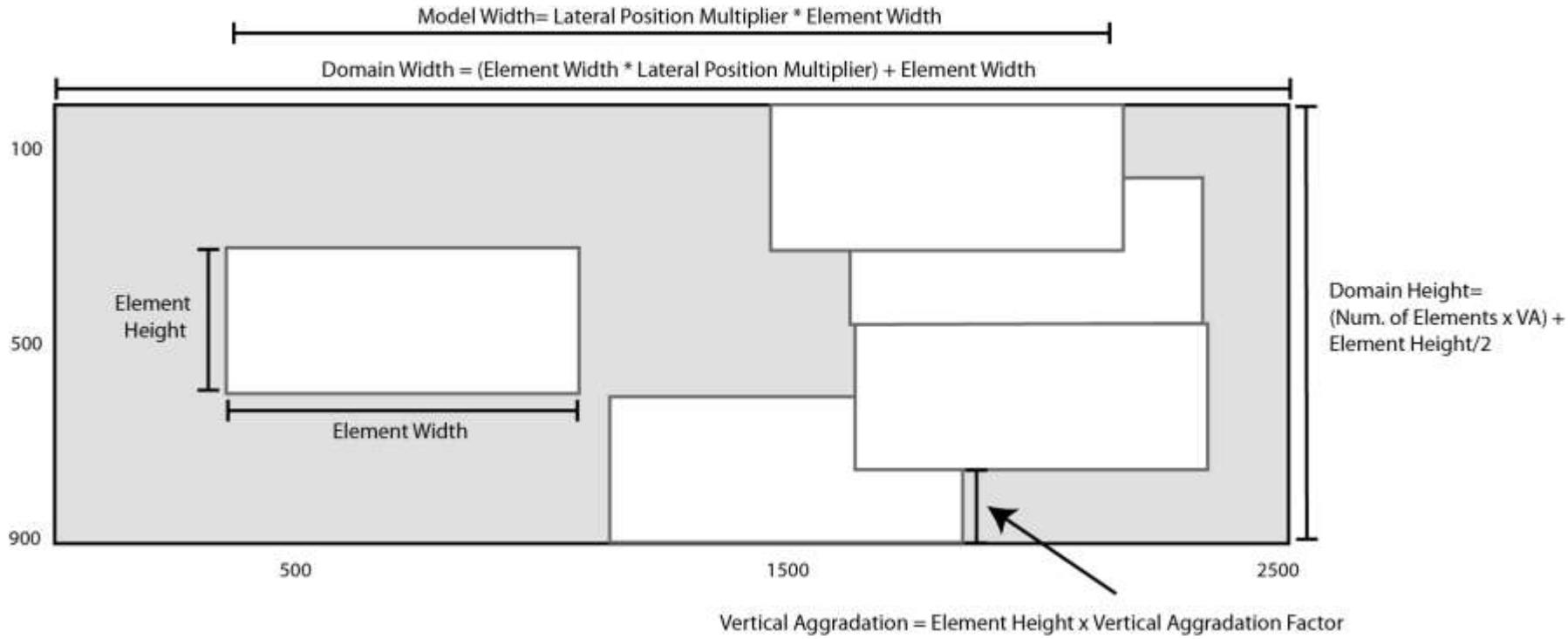

Fig. 4.1.1. Schematic diagram of reservoir model. In this example (MAMW), vertical aggradation is set to 0.5 times the element height. The lateral migration factor is 2.5 times the element width. The model width represents the area in which an avulsion can occur, i.e. the range of x-values in the model domain from which centroid lateral position may be selected. Buffers (equal to ½ the element width) on each side of the domain ensure all the full extent of all elements will fit in the domain.

4.1.2 Channel-belt Elements

Two cartoonized channel elements were developed (Fig. 4.1.2) and are loosely constrained by observations from outcrop in the Wasatch Formation. The elements represent generic high net-to-gross and low net-to-gross channel-belt scenarios. Net-to-gross is controlled by the thickness of bar-top muds and abandonment fill at the top of each element. The low-net case (Fig. 4.1.2a) is approximately 44% net-to-gross, while the high-net case (Fig. 4.1.2b) is 70% net-to-gross. This generally captures the range of net-to-gross exhibited by the muddy Atwell Gulch Member and Shire Members, and the sandy Molina Member. Each element contains four compartments, three of which are small, fully separated compartments and one larger compartment, containing the majority of the sand in the element. Based on the width of the bar-set and average bar width, these geobodies represent channels that have migrated 1.8 bar-widths, consistent with observations in the Atwell Gulch member.

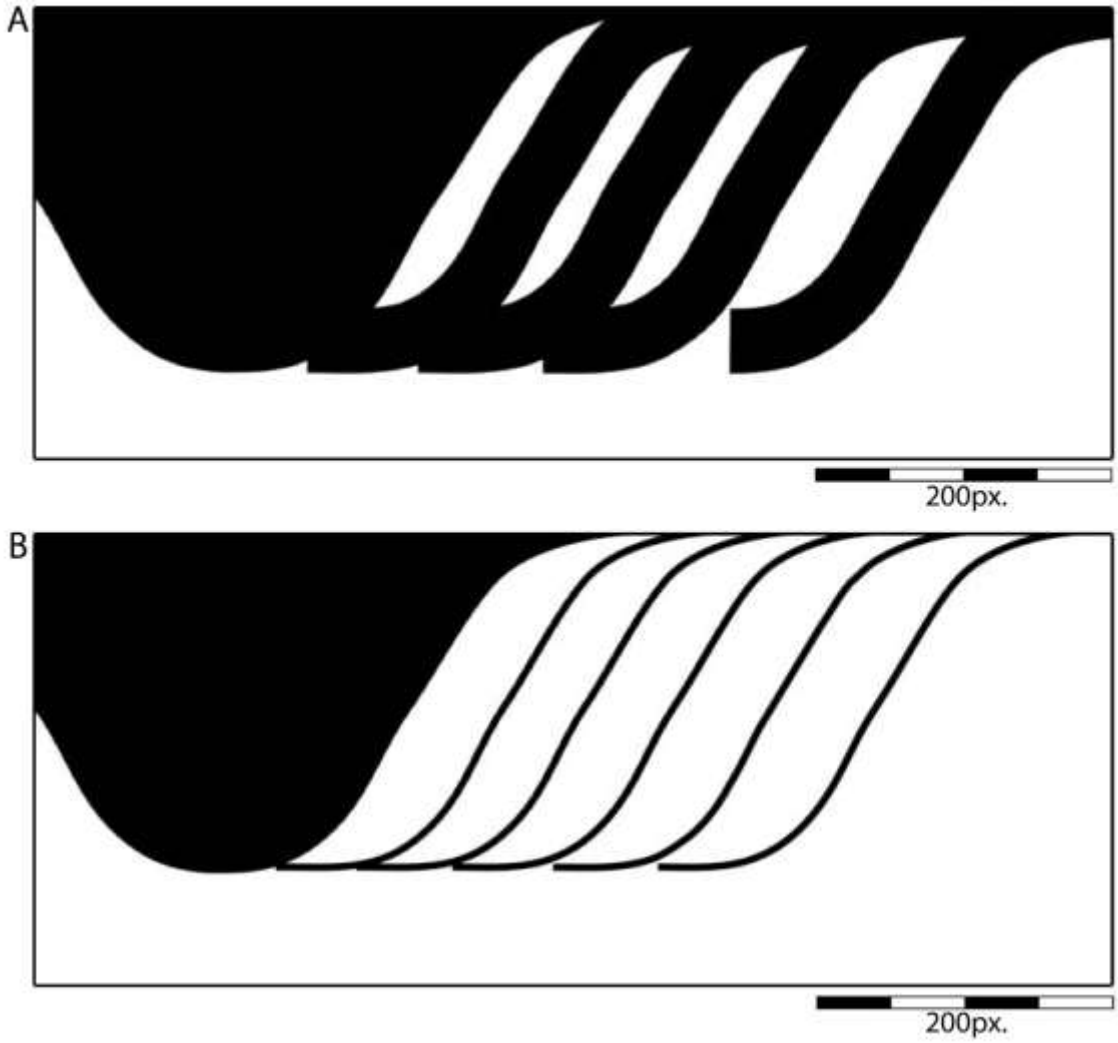

Fig. 4.1.2. Channel-belt elements for reservoir models. White represents reservoir quality channel sands; black represents channel fines, i.e. mud plugs and shale drapes on clinoform tops. A) Low net-to-gross channel element with thick bar top muds and abandonment fill. Net-to-gross is ~44%. Three small compartments and one large compartment result from the position of bar top muds. B) High net-to-gross (~70%) channel element. Bar top muds also result in three small compartments and one large compartment. Abandonment fill at top is nonexistent. Both models are 720 x 300 pixels.

4.1.3 Lateral versus Vertical Stacking

In order to more directly test the effects of lateral versus vertical stacking in multi-story sand bodies, a second round of modelling was carried out. Here, we sought to determine if vertical stacking in high and/or low-net cases produced the largest NMCA and lowest compartmentalization. In each run, vertical aggradation rates and lateral migration distances were varied to create equal-area model domains (Table 3.2). Each run featured two model domains, one of which had a higher probability of vertical stacking and the other, lateral (Fig. 4.1.3). Both high-net and low-net scenarios were tested, with maximum connected area and number of compartments recorded. Maximum connected area was normalized by multiplying the largest compartment size by five and dividing by the total number of pixels in the model domain. Amalgamation, in terms of normalized connected area, increased from 0 to values greater than 1, while sand-body isolation decreases. It is not possible, however, to determine if amalgamation or isolation contribute more to this index.

Table 4.1.2. Vertical vs. lateral stacking models

Model Run	Vertical Aggradation Factor	Lateral Migration Factor	Model Domain Area (pixels)
1 Vertical	0.25	1.25	
1 Lateral	0.05	2.75	972,000
2 Vertical	0.5	2.0	
2 Lateral	0.15	4.625	1,944,000
3 Vertical	0.75	1.25	
3 Lateral	0.2	4.3125	2,065,500

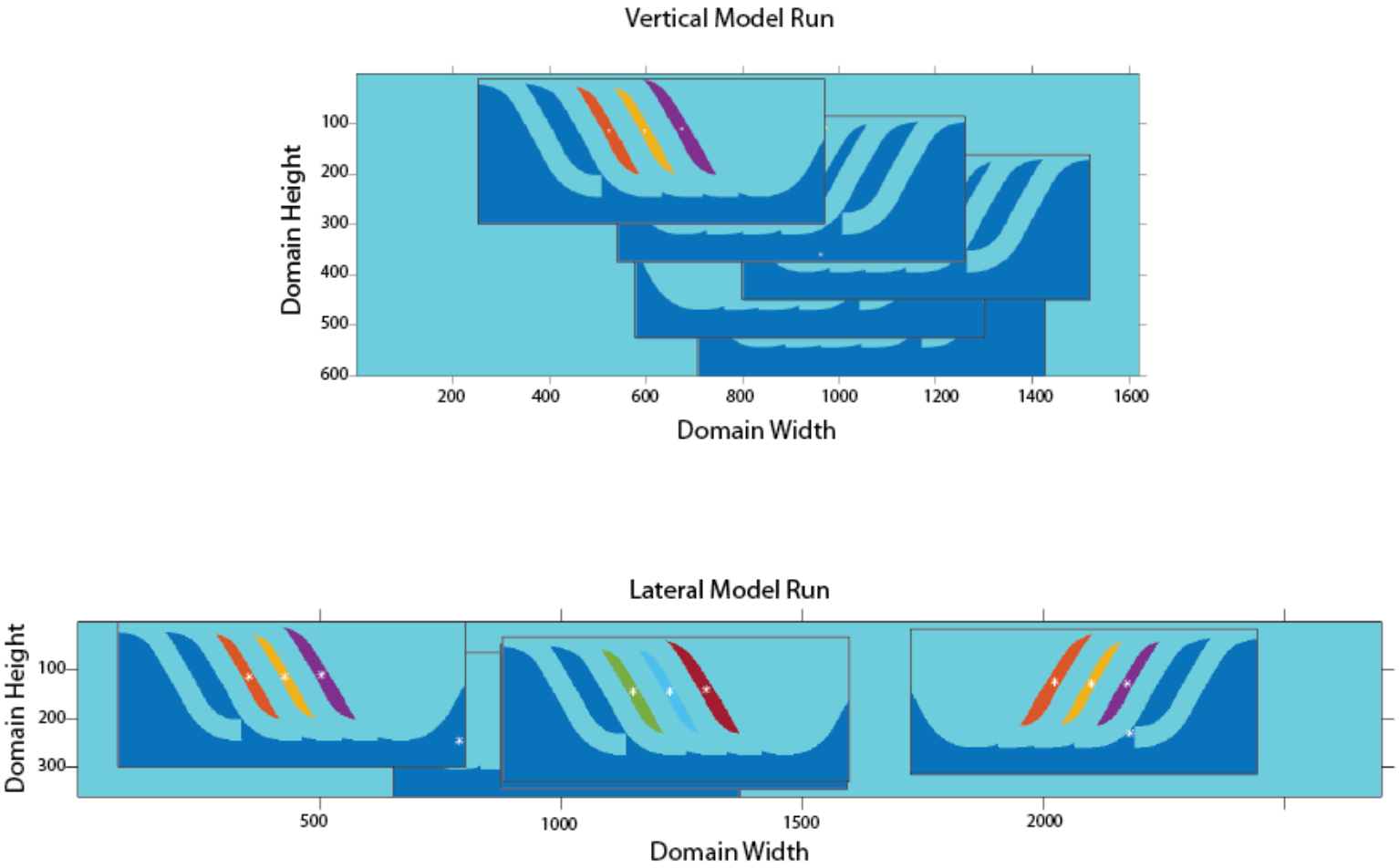

Fig. 4.1.3. Example output from vertical (top) and lateral (bottom) models. Vertical aggradation for the vertical case is 0.5 and model domain width is 2 times the element width. Vertical aggradation for the lateral case is 0.15 and model domain width is 4.625 times the element width. Connected compartments are the same color. White stars are compartment centroids. Light-blue represents background deposition and channel muds.

4.2 Results

4.2.1 High-Net Model Runs

Output from each model run was compared to determine which scenarios produced the least compartmentalized reservoirs with the largest connected areas. Mean normalized maximum connected area (NMCA) was greatest with medium aggradation for low and medium model widths (Fig 4.2.1.a-b – 4.2.3a-b; Fig. 4.2.4b – 4.2.6b). At high model width, mean NMCA decreases uniformly as aggradation increases (Fig 4.2.9b). The HALW case produced the largest spread in NMCA, ranging from 1 to 5.6 (Fig 4.2.7b). Far more MSBs with NMCA greater than 5 were produced by the high-net runs, relative to low-net cases. There was a uniform increase in number of compartments with increases in both model width and vertical aggradation (Fig. 4.2.7 – 4.2.9d). MAHW, HAMW, and HAHW cases produce fully isolated sand bodies (20 isolated compartments) (Fig. 4.2.8d – 4.2.9d). ANOVA testing revealed that the number of compartments and NMCA was statistically similar for the scenarios shown in Tables 4.2.1 and 4.2.2.

4.2.2 Low-Net Model Runs

Low-net cases show trends similar to those in the high-net case, with overall smaller NMCA and more compartmentalization. NMCA generally decreased as aggradation and model width increased (Fig 4.2.1d-f – 4.2.3d-f; Fig. 4.2.7a – 4.2.9a). The only exception occurred at low model widths; the MALW case resulted in the largest mean normalized connected area, while the HALW case produced the largest spread

(without outliers) in NMCA (Fig. 4.2.7a). Low aggradation cases did not produce any MSBs with NMCA greater than 5 (Fig. 4.2.7a – 4.2.9a), while MALW and HALW repeatedly produced compartments of this size (Fig. 4.2.7a).

Relative to all model widths, the number of compartments increased drastically between the low and medium aggradation cases, while the increase was more subtle between medium and high aggradation (Fig 4.2.4d-f – 4.2.6d-f; Fig. 4.2.7c – 4.2.9c). MAMW, MAHW, HAMW, and HAHW cases all produced runs that did not yield MSBs (i.e. 20 isolated compartments) (Fig. 4.2.8c, 4.2.9c). The data also show that low-net cases were less likely to produce fully amalgamated MSBs with only 4 compartments. ANOVA testing revealed that the number of compartments and NMCA was statistically similar for the scenarios shown in Tables 4.2.3 and 4.3.4.

4.2.3 High-Net versus Low-Net Model Runs

ANOVA testing revealed that several high-net and low-net cases were statistically similar in NMCA and number of compartments. Tables 4.2.5 and 4.2.6 contain results from the statistical analysis. The majority of statistically similar runs represent at least one instance of medium or high aggradation or model width. 67% of cases with statistically similar number of compartments are medium or high aggradation and width. There was slightly more overlap with low aggradation and low width cases in NMCA, but 47% of the similar cases are medium and high aggradation and width only. Based on the shape of the model domains, special attention was paid to cases which represent potential vertically dominant stacking (e.g. HALW) and laterally dominant stacking (e.g. LAHW). Figures 4.2.10 and 4.2.11 show cumulative distributions of NMCA and number

of compartments for some of these cases; boxplots of the same data are shown in Figures 4.2.12 and 4.2.13.

Though statistically similar, HALW (low-net) runs produce larger NMCAs than the LAHW (high-net) case. In LAHW cases, low and high-net runs produce nearly identical results. Interestingly, the high-net, HALW case actually produced a greater number of *smaller* connected areas than the low-net LAMW case.

4.2.4 Vertical versus Lateral Model Runs

These model runs were designed to force vertical or lateral stacking of sand bodies in domains of equal area. Domain area increased significantly between run 1 and run 2, but only slightly between run 2 and run 3. Broadly similar ranges and distributions of NMCA and number of compartments resulted from model runs 2 and 3. This holds true for both the vertical and lateral cases, across both net-to-gross scenarios. Model run 1, however, produced results that are noticeably different from runs 2 and 3.

Figures 4.2.14 – 4.2.15 and 4.2.18 show that as domain area increased, both vertical and lateral cases show decreases in mean NMCA. Mean number of compartments increased with domain area (Fig. 4.2.16-4.2.17, 4.2.19). For each model run scenario, vertical cases had higher mean NMCA and lower mean number of compartments than lateral cases. The same was true for high-net versus low-net cases in mean NMCA (e.g. high net, vertical NMCA > low-net, vertical NMCA). Compartmentalization, however, varied by less than 2% for each lateral run. The low net, vertical case in model run 2 (Fig. 4.2.17b, 4.2.19e) had the largest spread in number of compartments, the result of the domain area being greatest here. Modeled sand bodies

ranged from completely isolated (20 compartments) to fully amalgamated (1 large compartment, plus three smaller compartments) (Fig. 4.2.20). This was also the only scenario (Low-V2) which produced completely isolated sand bodies.

ANOVA tests were also carried out for these model results. Tables 4.2.7 – 4.2.12 highlight similar model runs. Internal to low-net runs, several showed similar compartmentalization, while only lateral runs 2 and 3 showed similar NMCA. None of the high-net cases were similar in NMCA, and only V2 and V3 showed similar compartmentalization. Across net-to-gross scenarios (Tables 4.2.11 and 4.2.12), 6 of the 36 runs had similar number of compartments (Fig. 4.2.21), while only 2 have similar NMCA (Fig. 4.2.22). These cases have the potential to create reservoirs of equal quality, despite differences in net-to-gross.

Figure 4.2.23 compares the low-net, vertical case for model run 1 to the high-net, lateral cases for runs 2 and 3. NMCA for Low-V1 (Fig. 4.2.23a, b) was always higher than that of the lateral cases, which were also more compartmentalized (Fig. 4.2.23c, d). These represent the only cases where vertical stacking of low-net elements resulted in a better-connected reservoir.

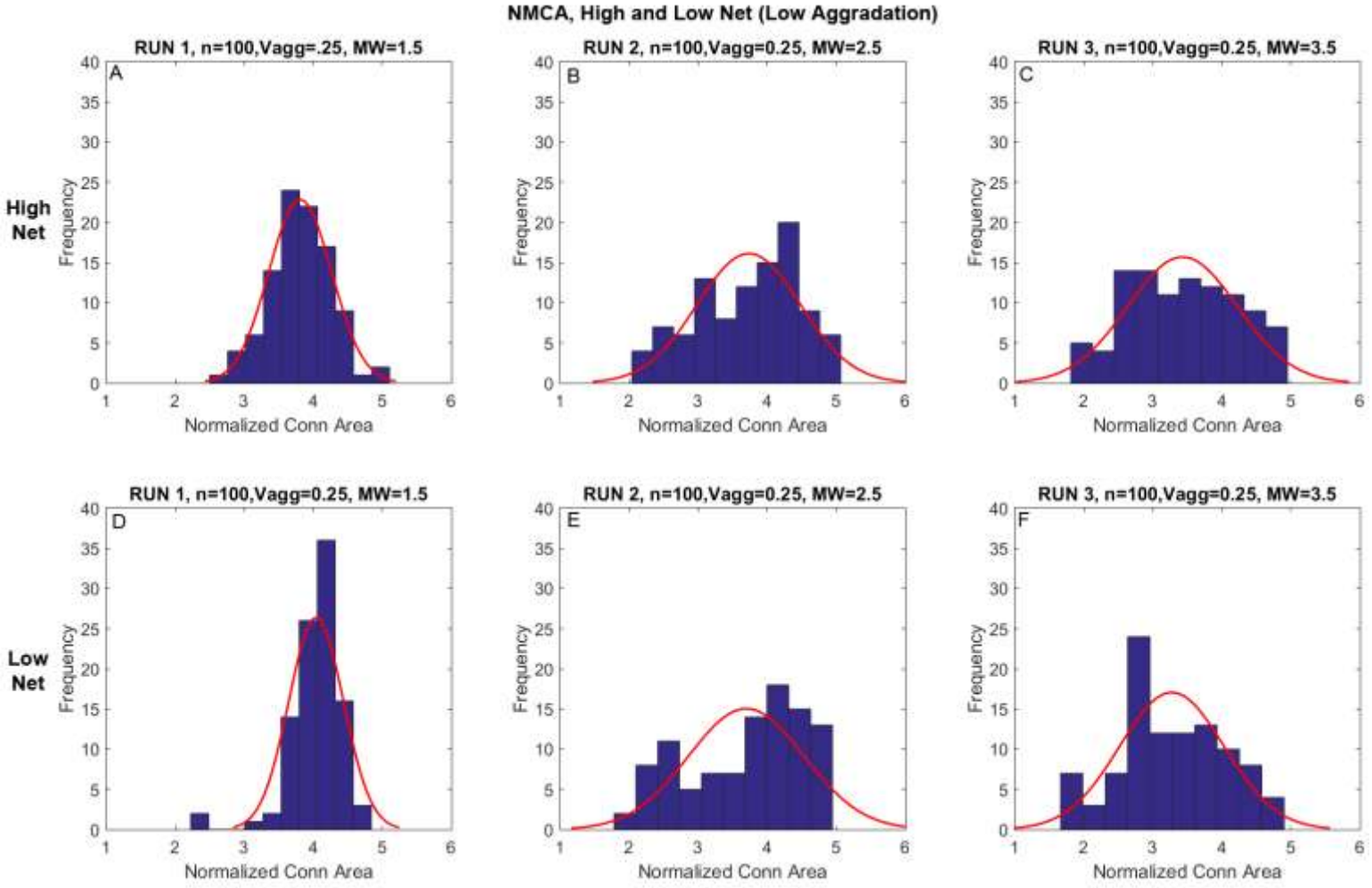

Fig. 4.2.1. Histograms showing NMCA for low aggradation cases. Both high-net (top) and low-net (bottom) runs are shown. Aggradation is constant while model width varies from 1.5-3.5 times the element width. Red line is a normal distribution which approximates the histogram.

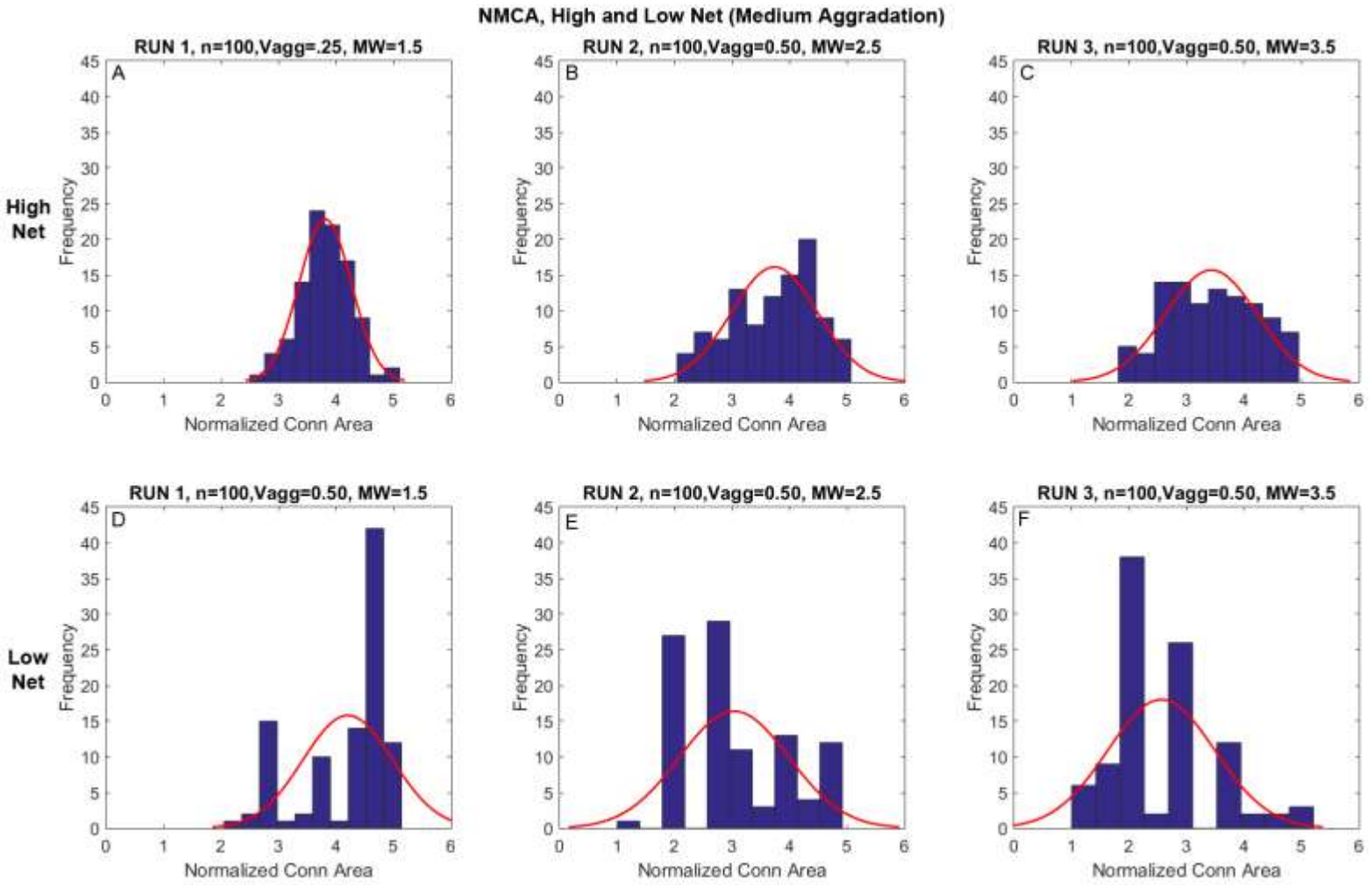

Fig. 4.2.2. Histograms showing NMCA for medium aggradation cases. Both high-net (top) and low-net (bottom) runs are shown. Aggradation is constant while model width varies from 1.5-3.5 times the element width.

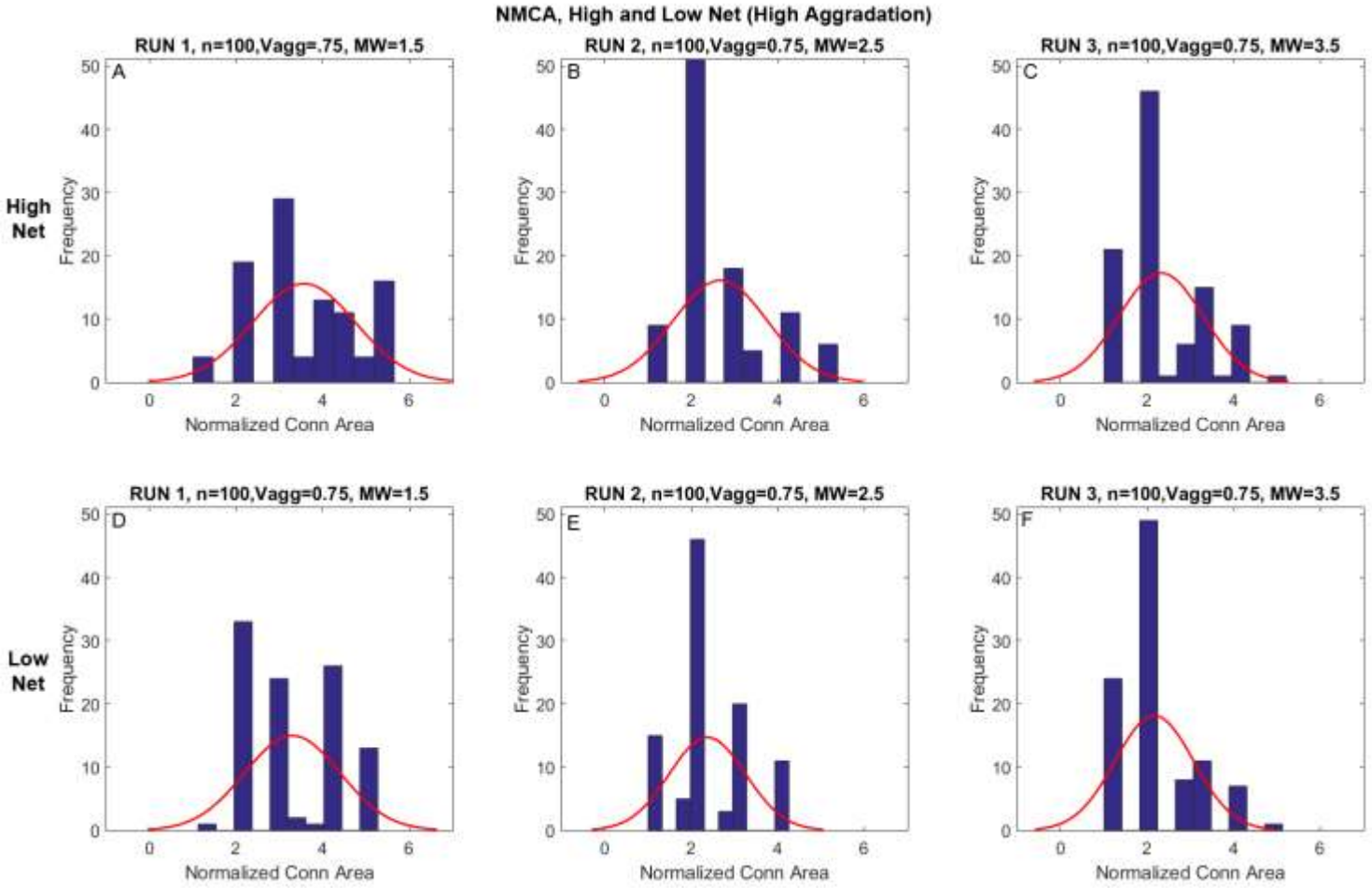

Fig. 4.2.3. Histograms showing NMCA for high aggradation cases. Both high-net (top) and low-net (bottom) runs are shown. Aggradation is constant while model width varies from 1.5-3.5 times the element width.

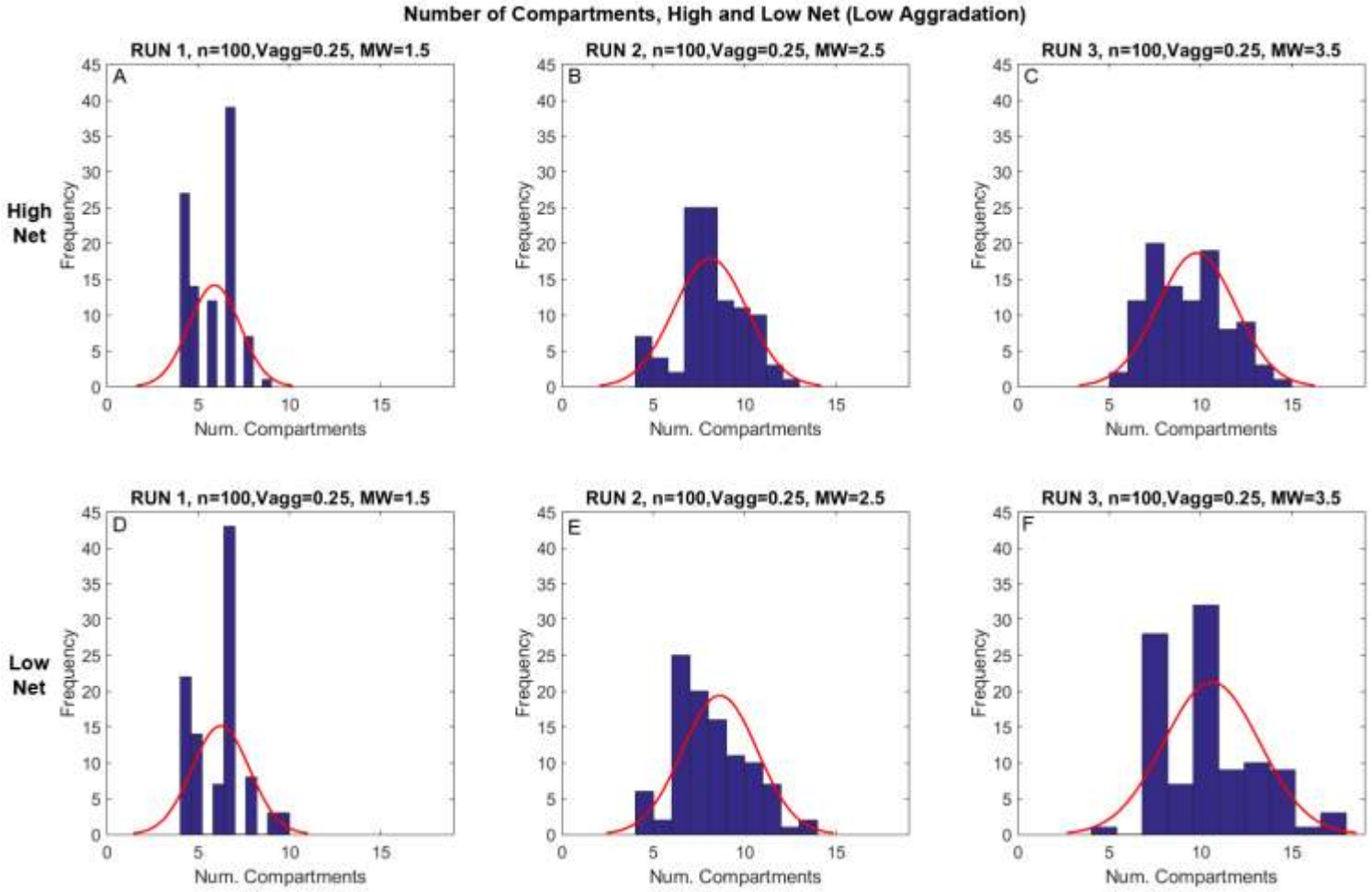

Fig. 4.2.4. Histograms showing number of compartments for low aggradation cases. Both high-net (top) and low-net (bottom) runs are shown. Aggradation is constant while model width varies from 1.5-3.5 times the element width.

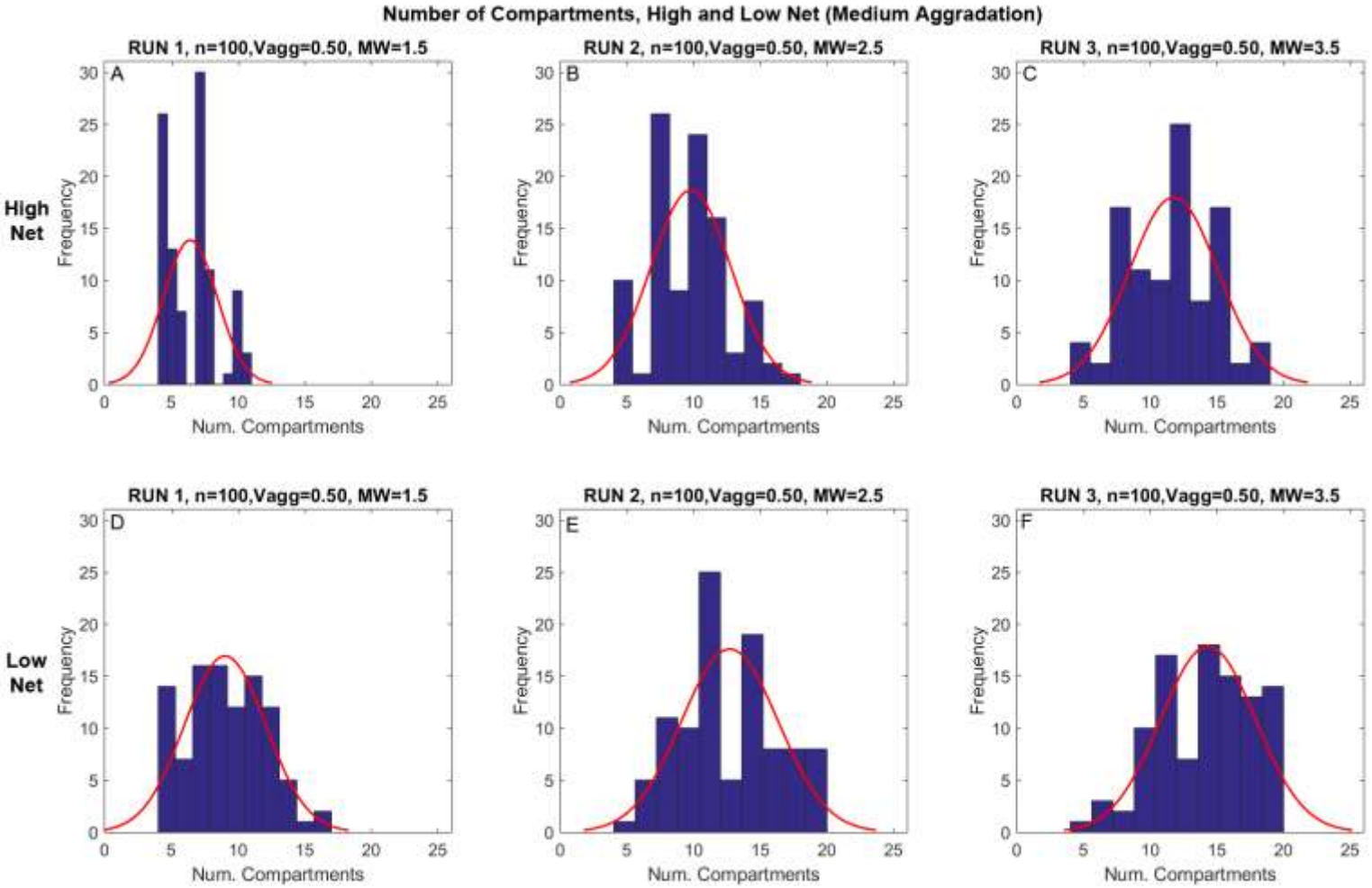

Fig. 4.2.5. Histograms showing number of compartments for medium aggradation cases. Both high-net (top) and low-net (bottom) runs are shown. Aggradation is constant while model width varies from 1.5-3.5 times the element width.

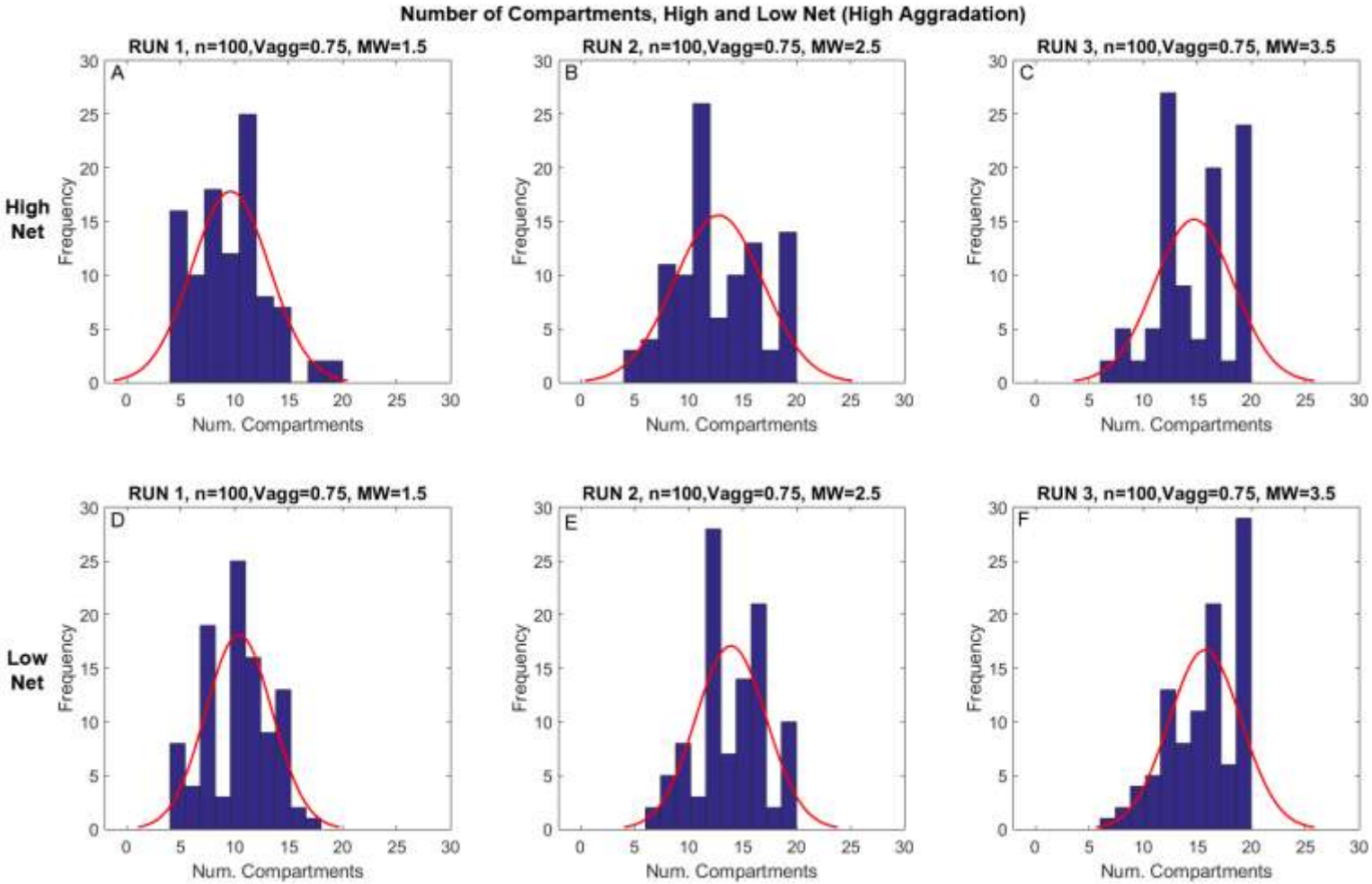

Fig. 4.2.6. Histograms showing number of compartments for high aggradation cases. Both high-net (top) and low-net (bottom) runs are shown. Aggradation is constant while model width varies from 1.5-3.5 times the element width.

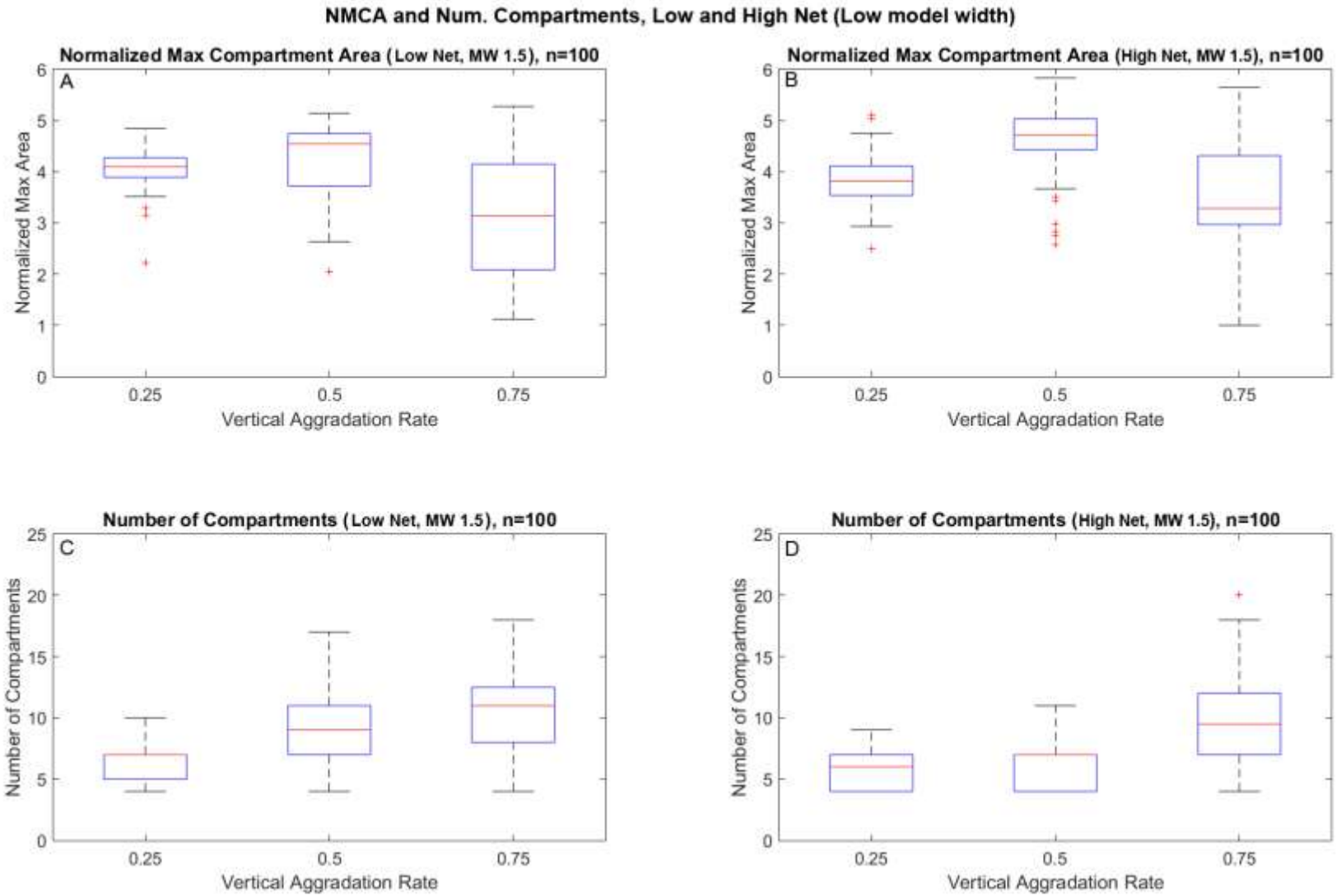

Fig. 4.2.7. Boxplots showing NMCA (top) and number of compartments (bottom) for low-net (left) and high-net (right) low model width runs. Model width is constant while vertical aggradation varies from 0.25 to 0.75 times the element height. Red line is median value. Blue box represents 25th-75th percentile. Red stars are outliers (beyond 1.5 times the inter-quartile range)

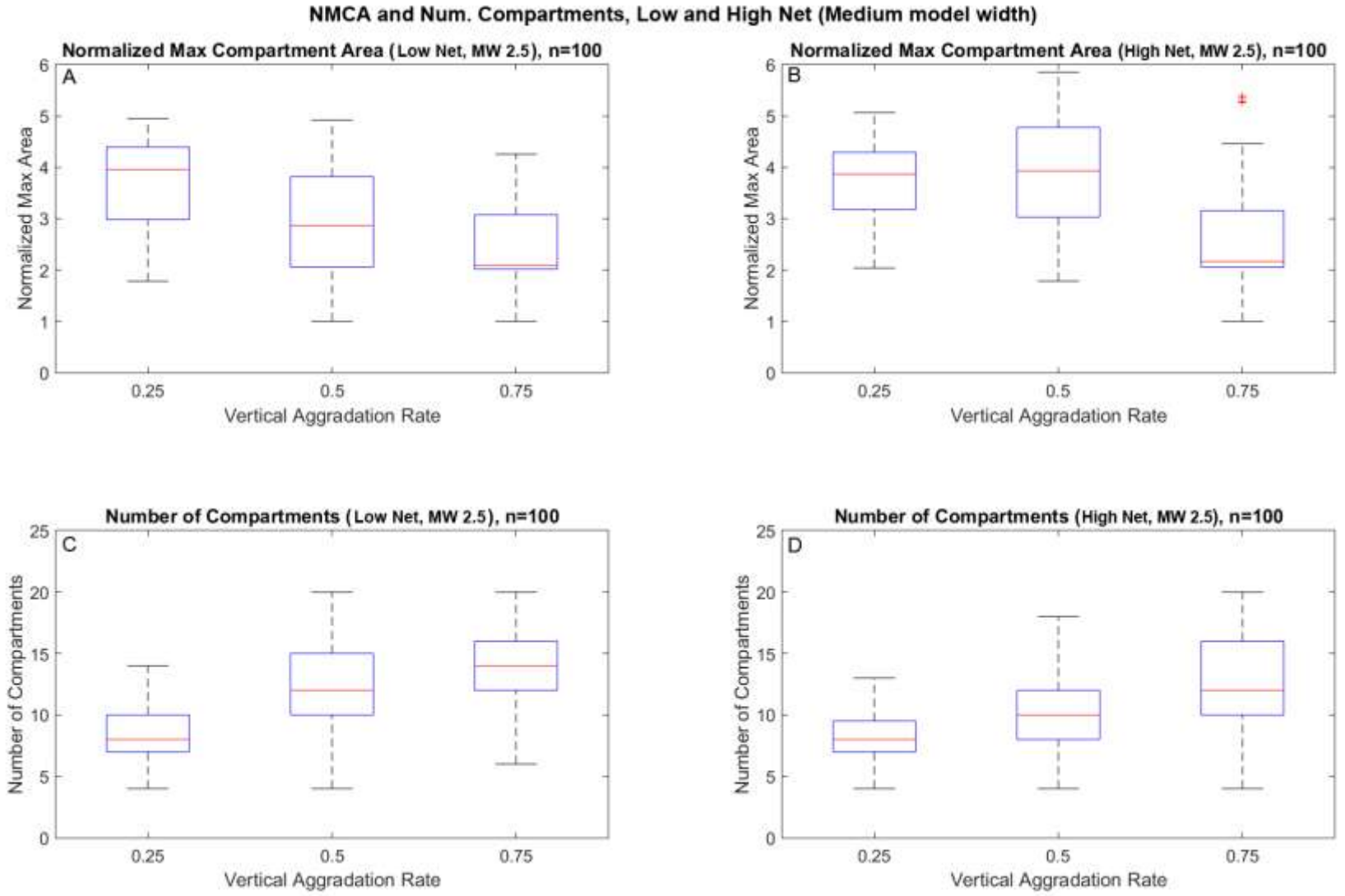

Fig. 4.2.8. Boxplots showing NMCA (top) and number of compartments (bottom) for low-net (left) and high-net (right) medium model width runs. Model width is constant while vertical aggradation varies from 0.25 to 0.75 times the element height.

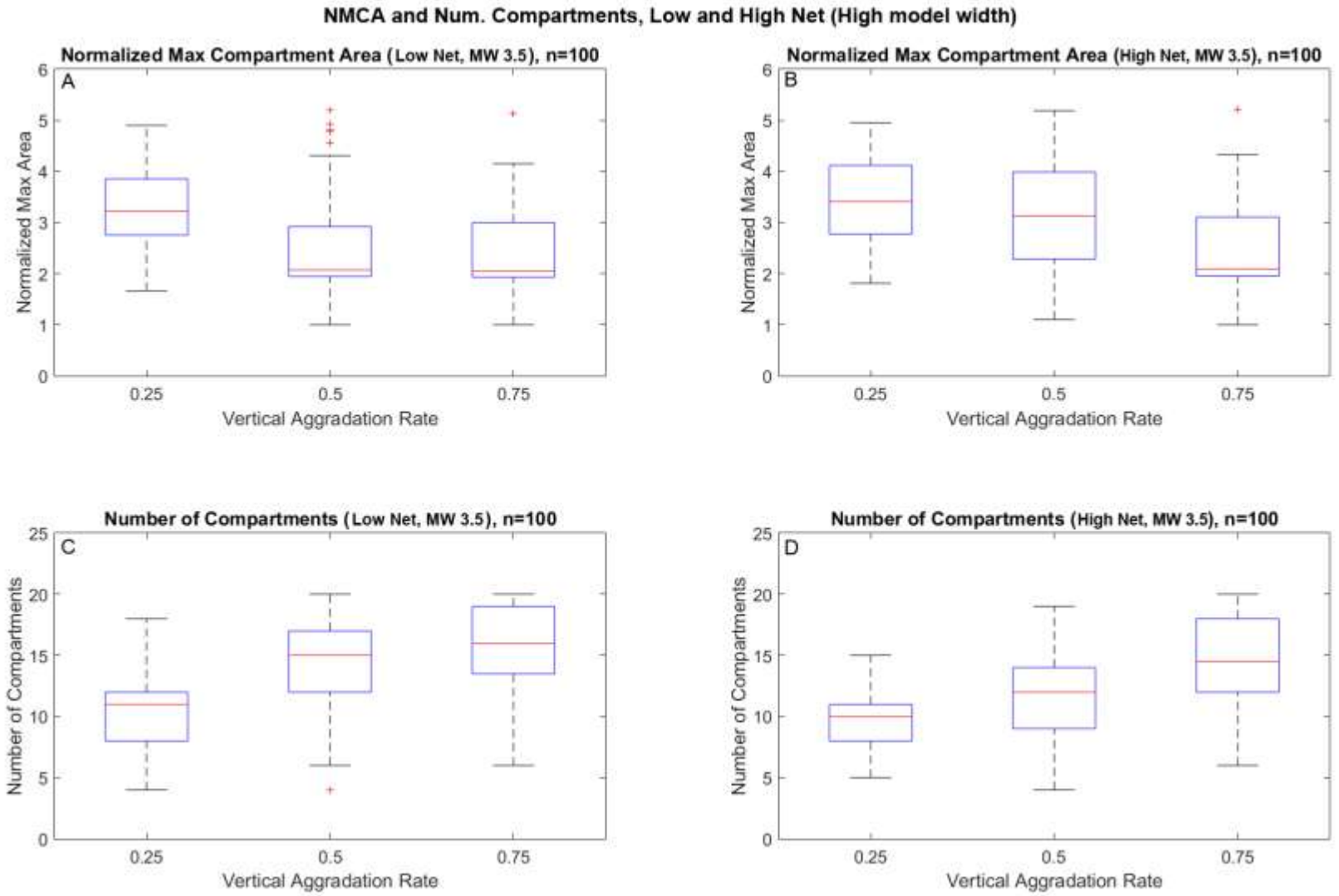

Fig. 4.2.9. Boxplots showing NMCA (top) and number of compartments (bottom) for low-net (left) and high-net (right) high model width runs. Model width is constant while vertical aggradation varies from 0.25 to 0.75 times the element height.

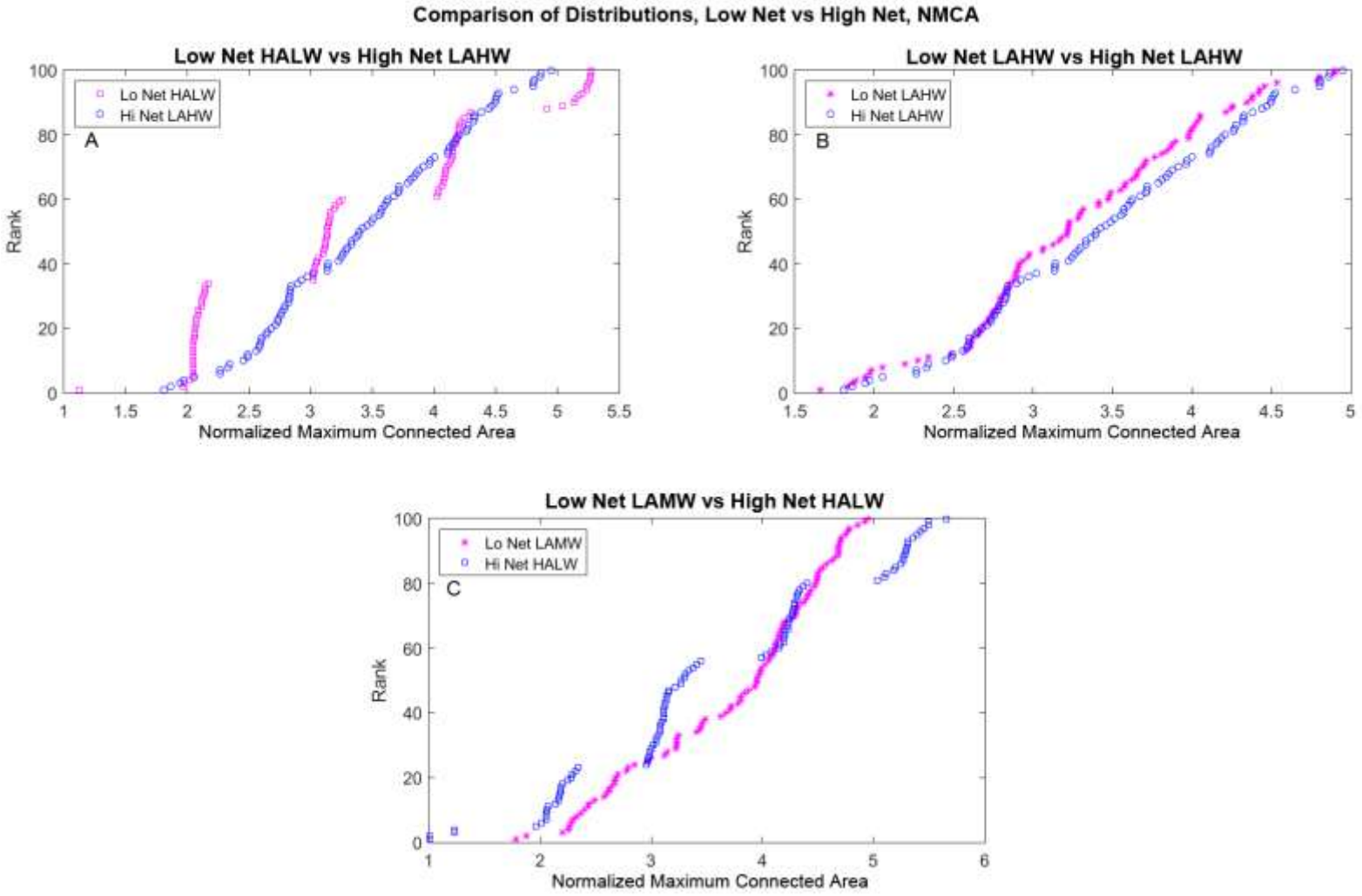

Fig. 4.2.10. Cumulative distributions of NMCA. Data from all 100 model runs was sorted from least to greatest NMCA. Low-net represented by pink stars; high-net represented by blue circles.

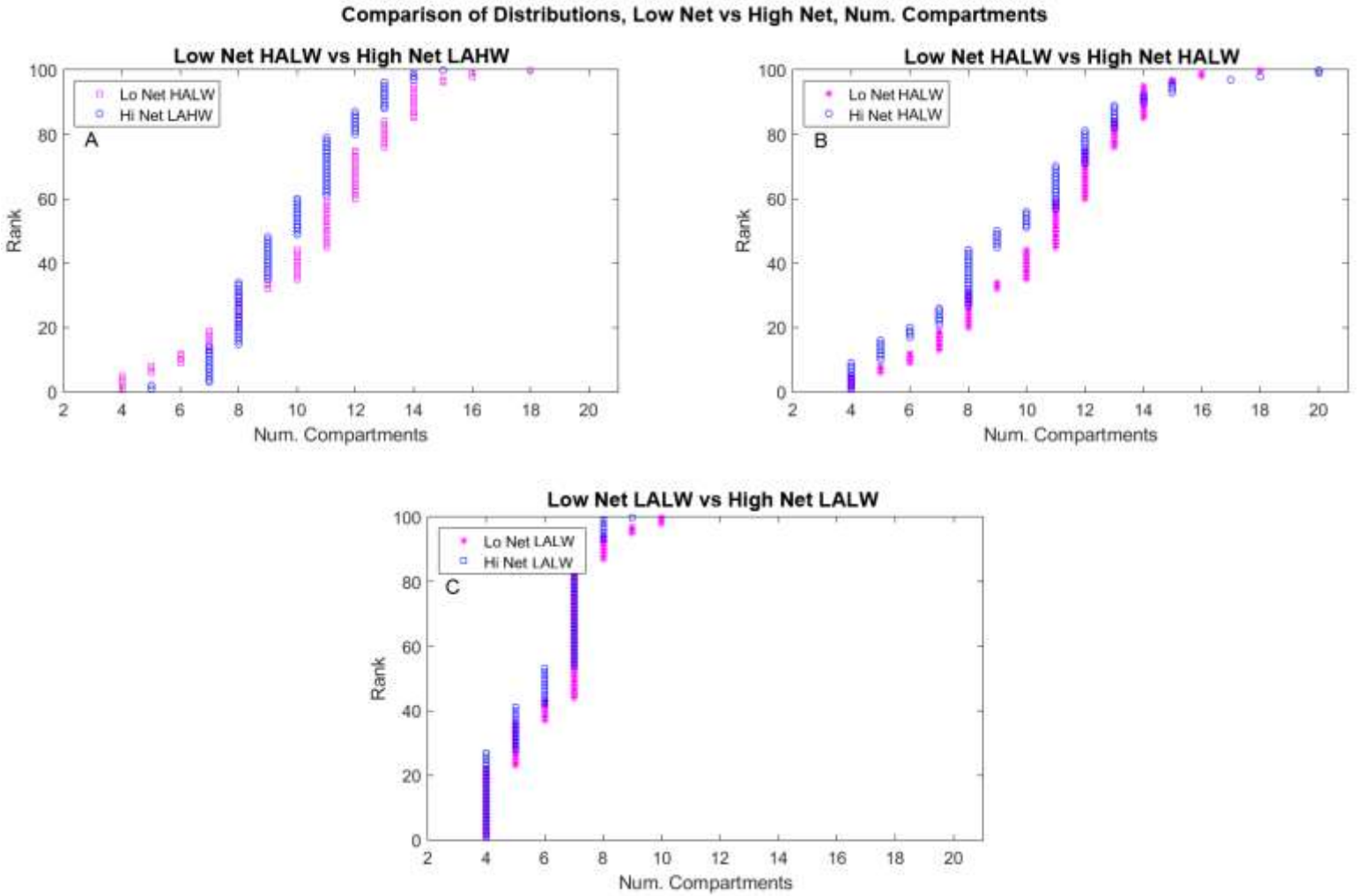

Fig. 4.2.11. Cumulative distributions of number of compartments. Data from all 100 model runs was sorted from least to greatest number of compartments. Low-net represented by pink stars; high-net represented by blue circles.

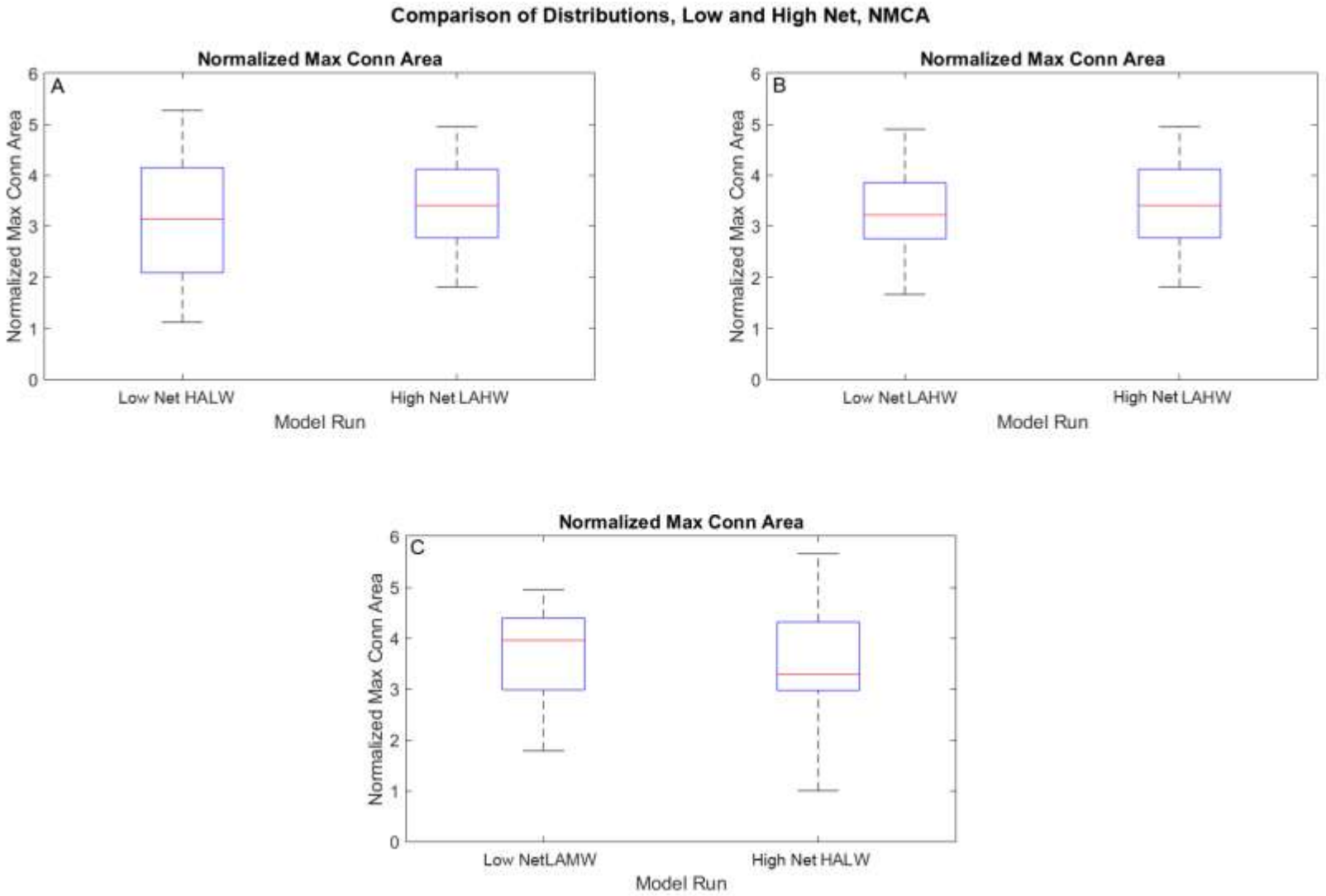

Fig. 4.2.12. Boxplots showing statistically similar cases of NMCA.

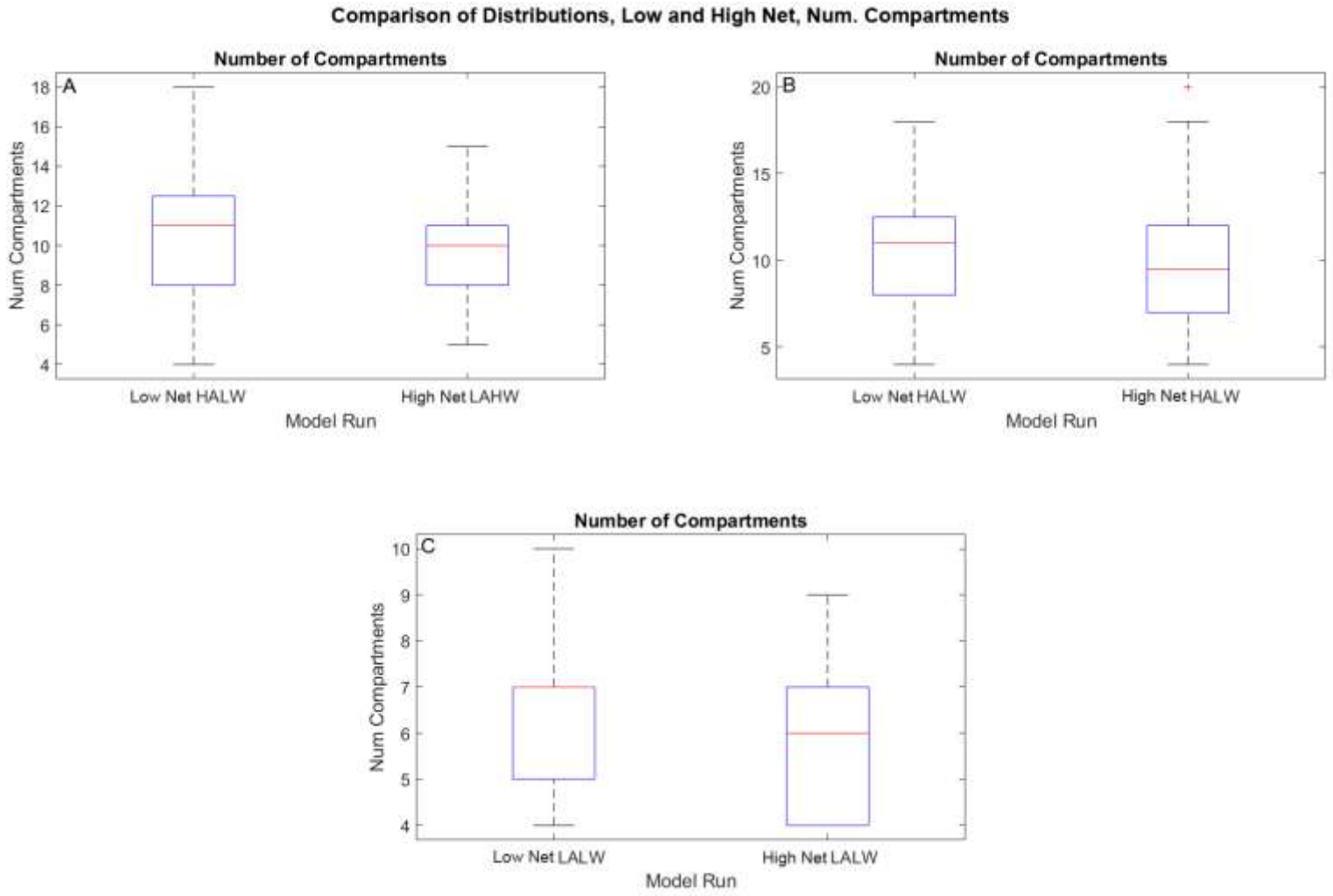

Fig. 4.2.13. Boxplots showing statistically similar cases of number of compartments.

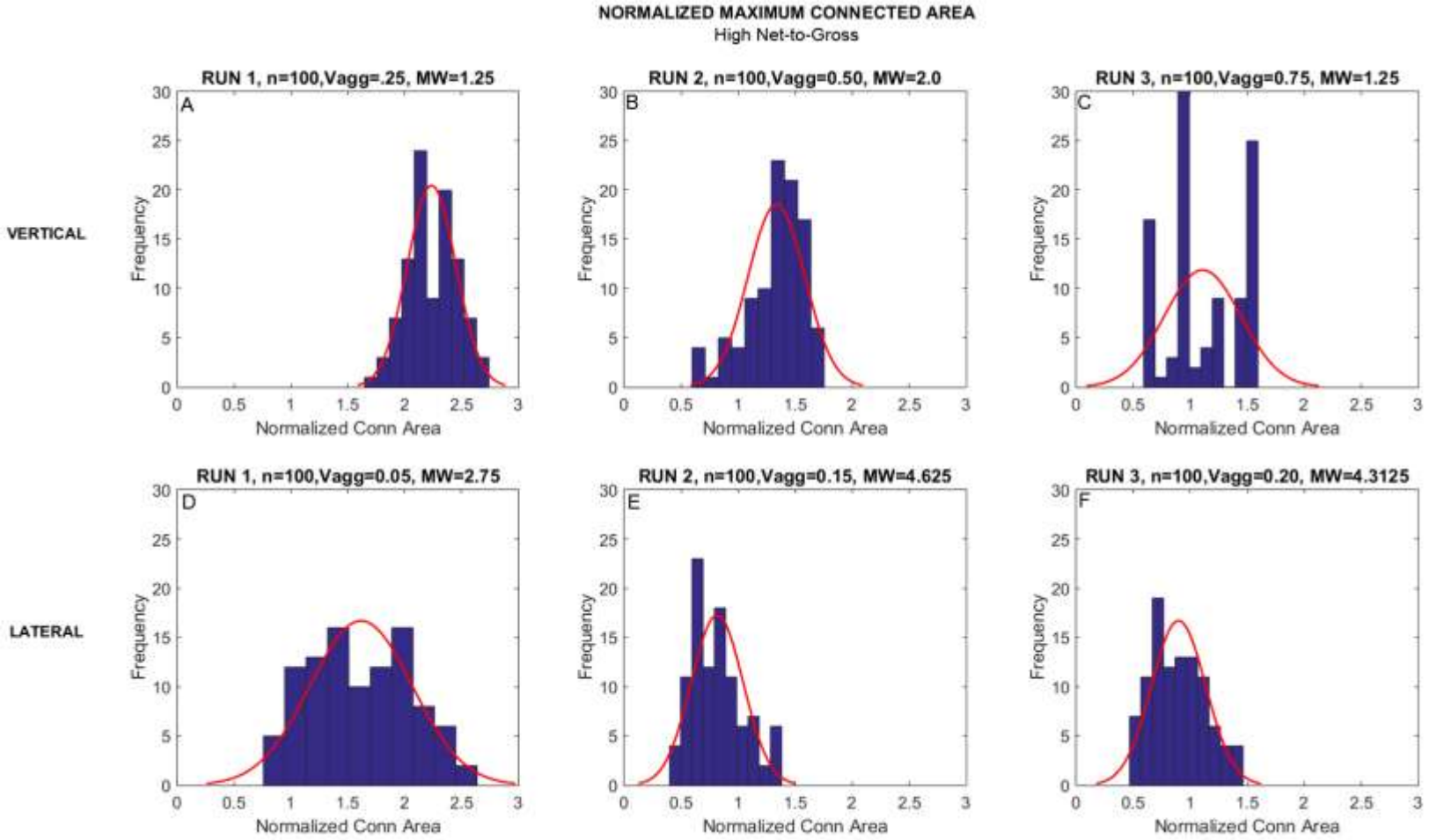

Fig. 4.2.14. Histograms showing NMCA for high-net vertical (top) and lateral (bottom) stacking model runs

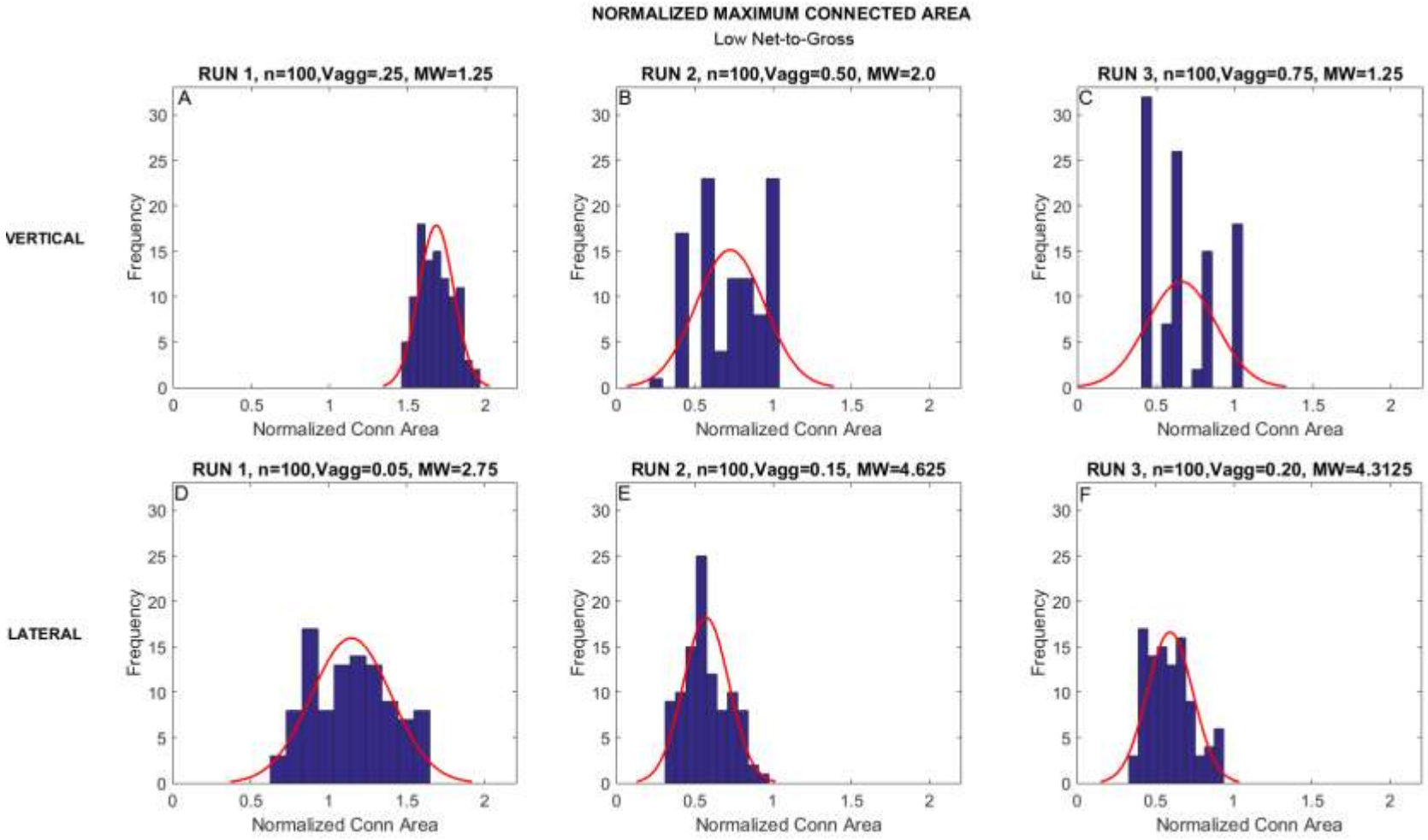

Fig. 4.2.15. Histograms showing NMCA for low-net vertical (top) and lateral (bottom) stacking model runs

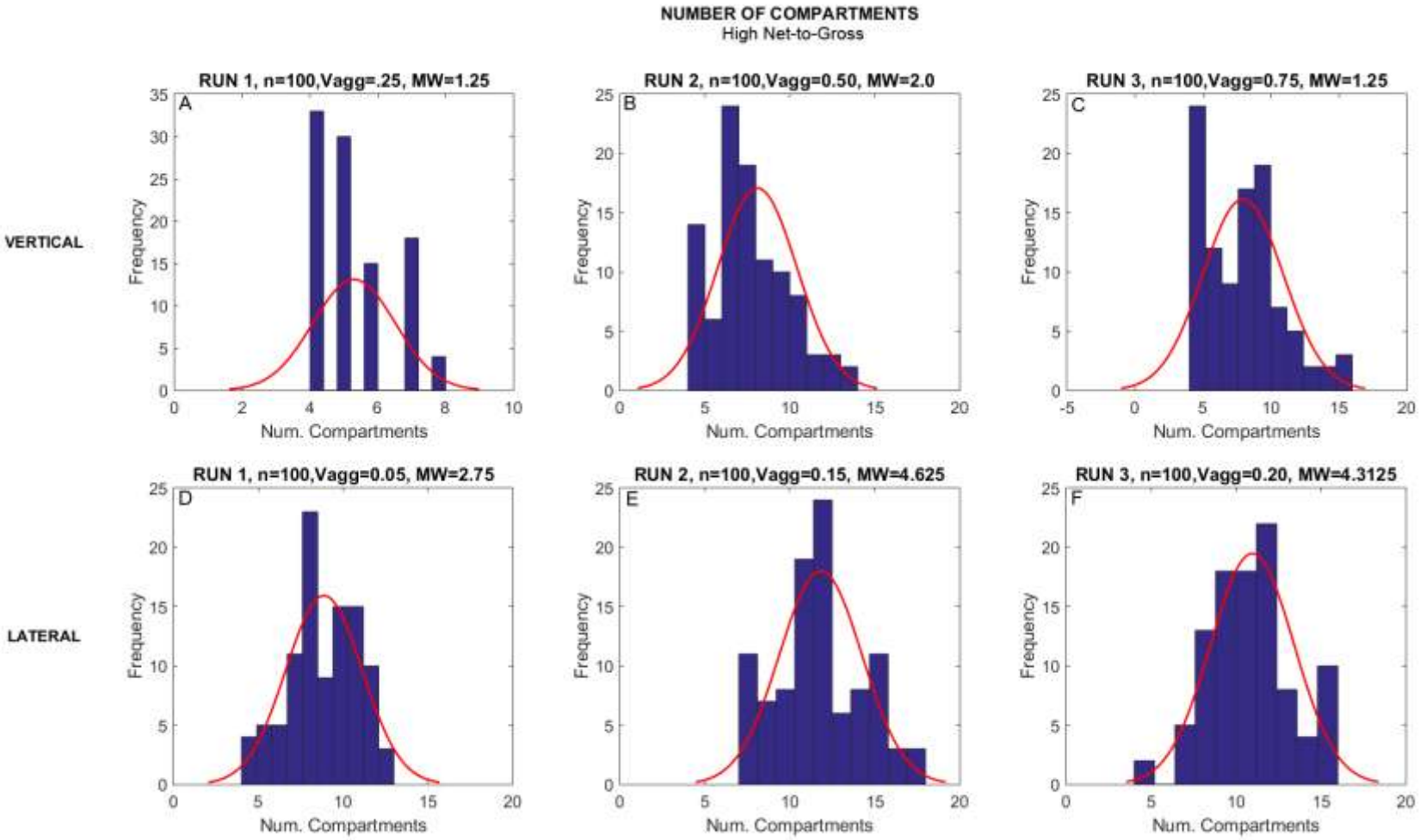

Fig. 4.2.16. Histograms showing number of compartments for high-net vertical (top) and lateral (bottom) stacking model runs.

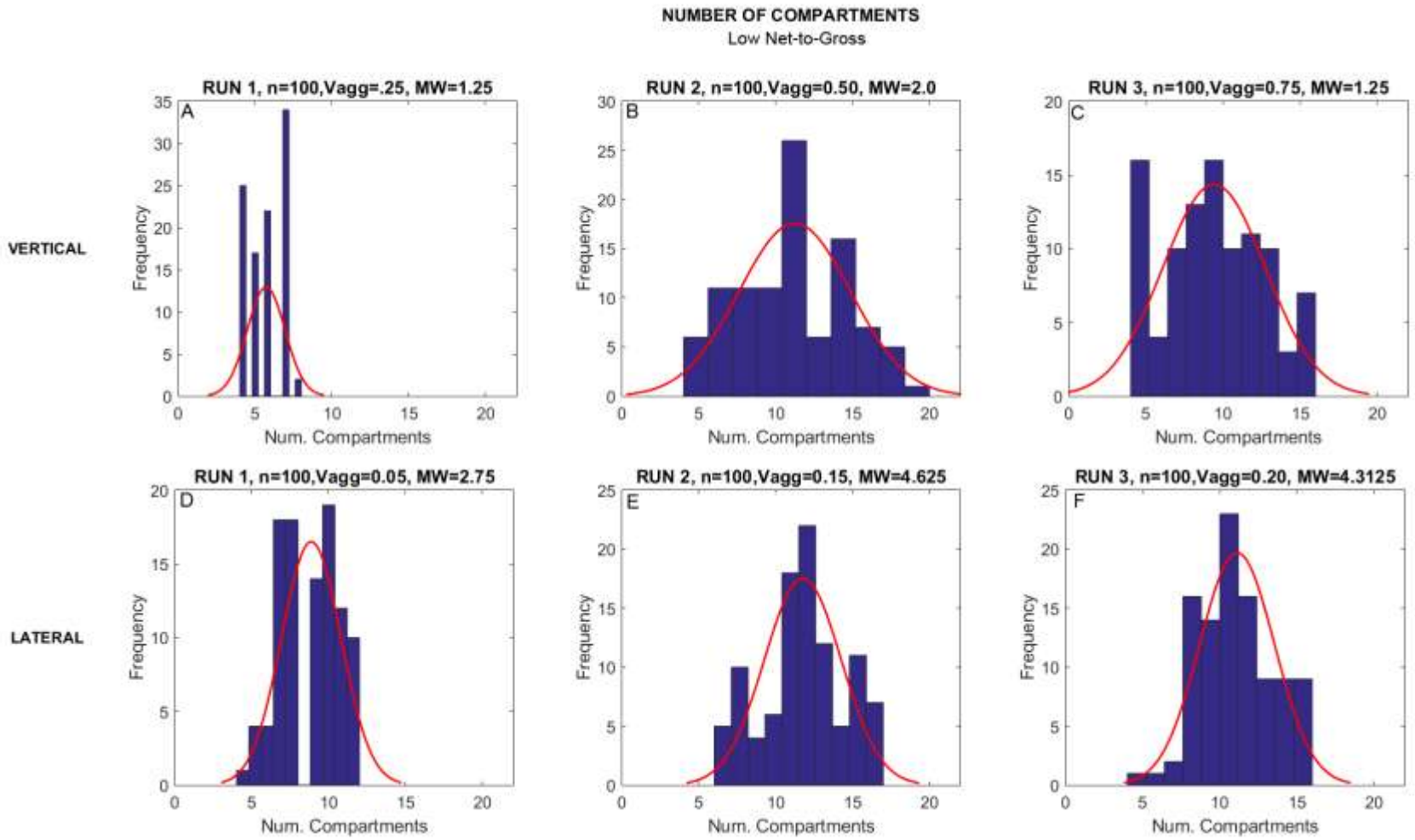

Fig. 4.2.17. Histograms showing number of compartments for low-net vertical (top) and lateral (bottom) stacking model runs.

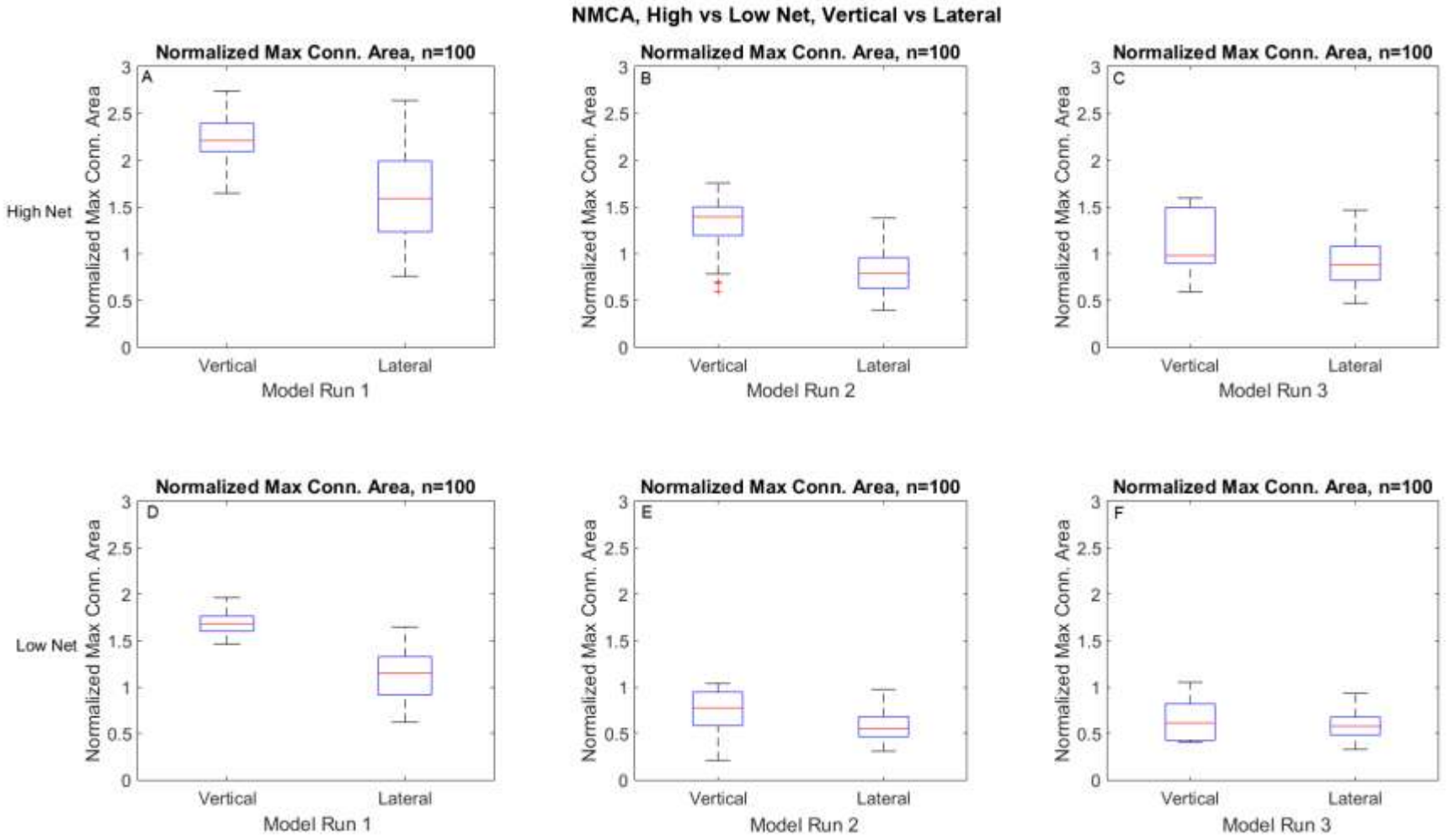

Fig. 4.2.18. Boxplots showing NMCA for vertical and lateral stacking model runs. High-net cases (top) and low-net cases (bottom).

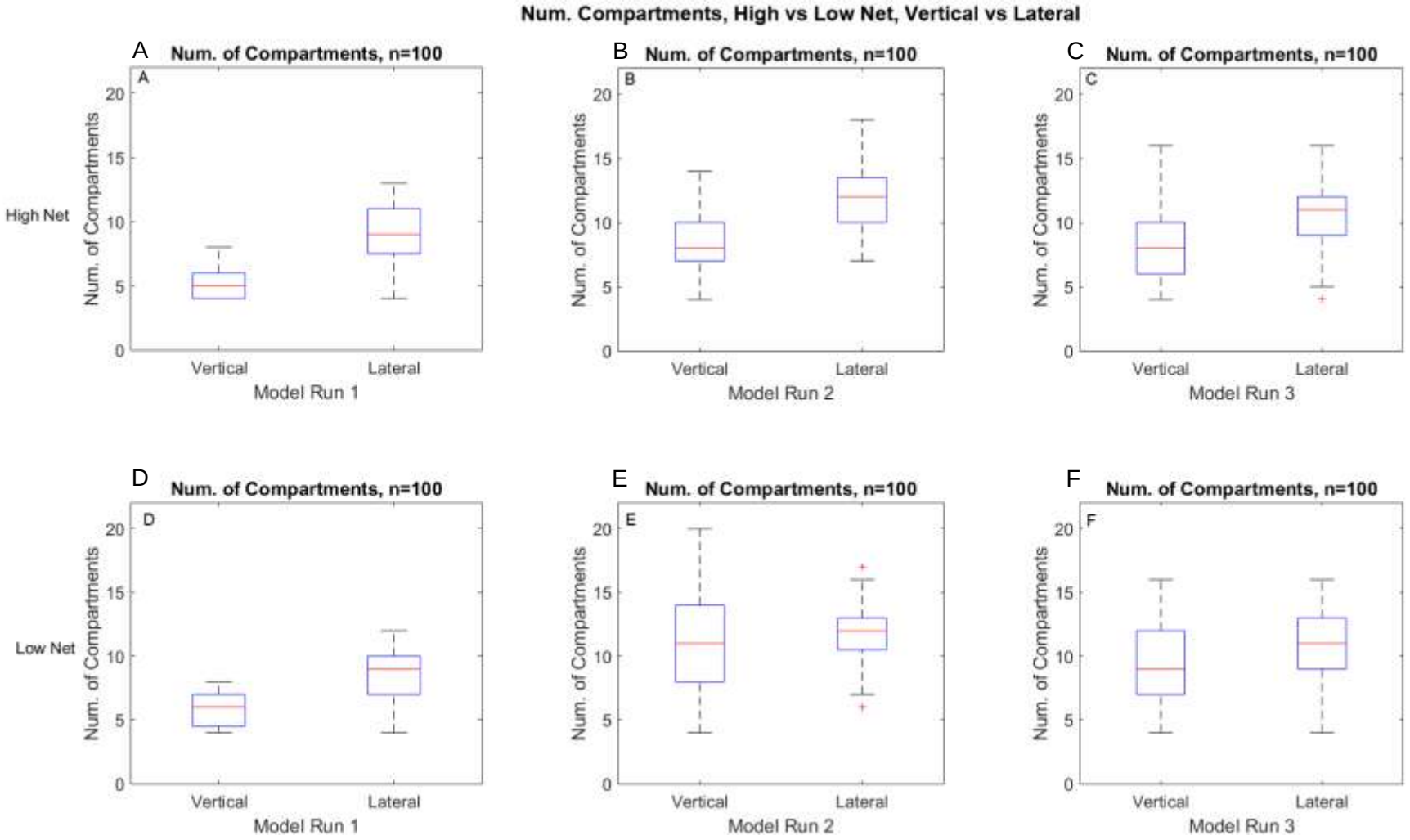

Fig. 4.2.19. Boxplots showing number of compartments for vertical and lateral stacking model runs. High-net cases (top) and low-net cases (bottom).

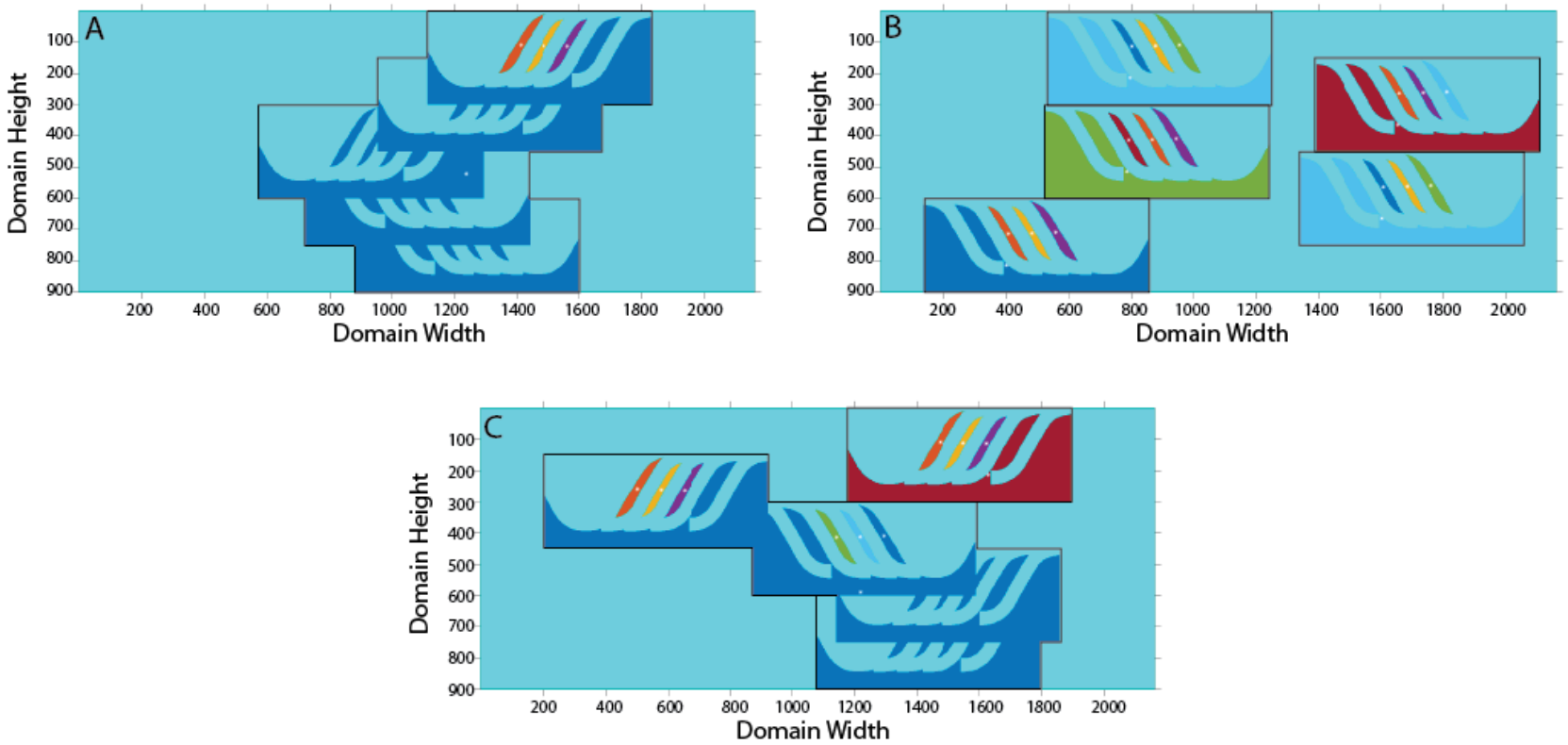

Fig. 4.2.20. Range of compartmentalization for the Model Run Low-V2. Vertical aggradation is 0.5 and model domain width is 2x element width. Connected compartments are the same color. White stars are compartment centroids. Light-blue represents background and channel muds. A) Minimum compartmentalization occurred when all large compartments of each element were connected; the three compartments formed by mud drapes are the only isolated bodies. B) Maximum compartmentalization occurred when none of the elements were in contact. C) Intermediate compartmentalization may result from the orientation of individual elements or juxtaposition of the elements.

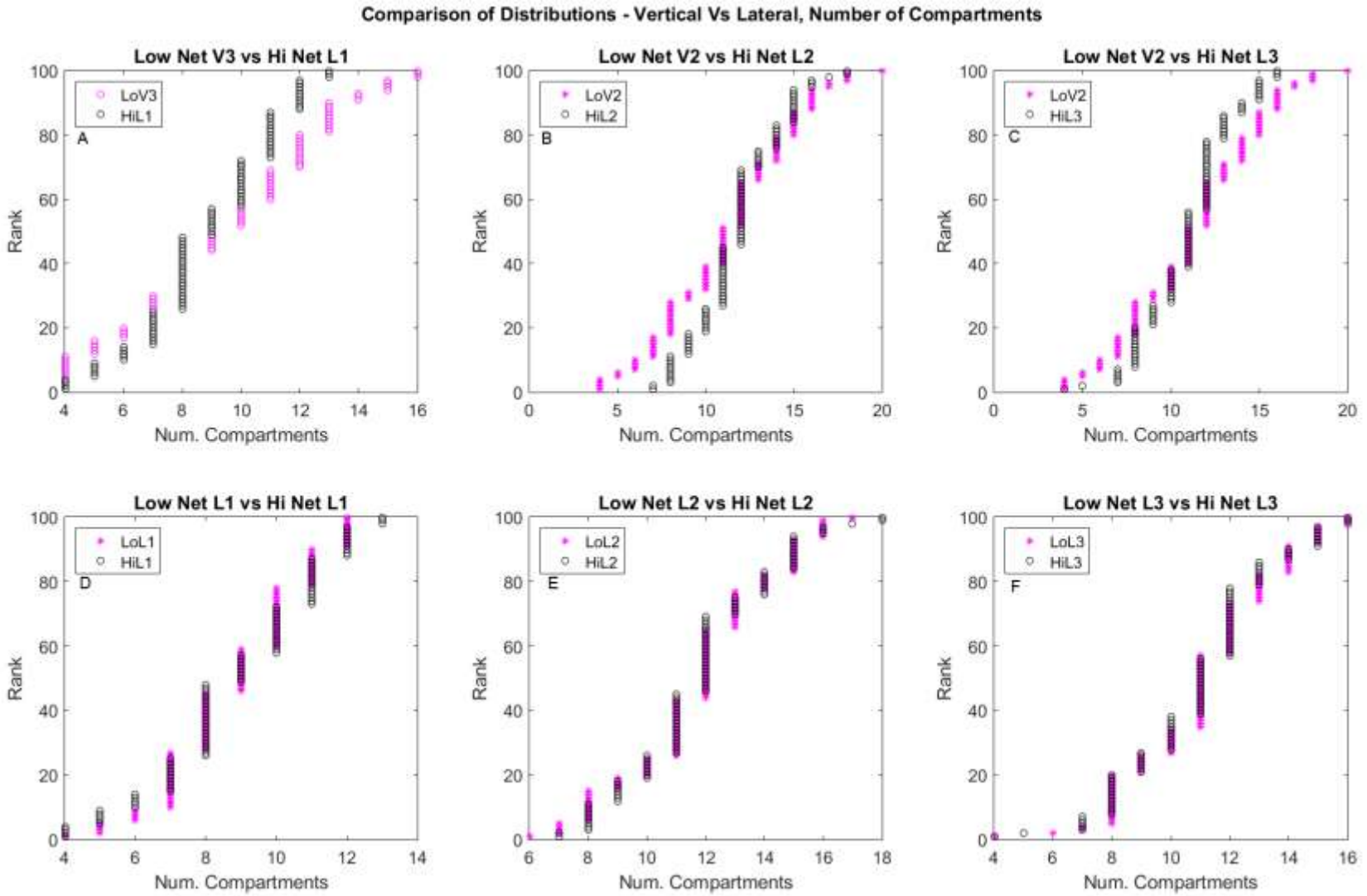

Fig. 4.2.21. Cumulative distributions of number of compartments. Low-net represented by pink circles; high-net represented by black circles.

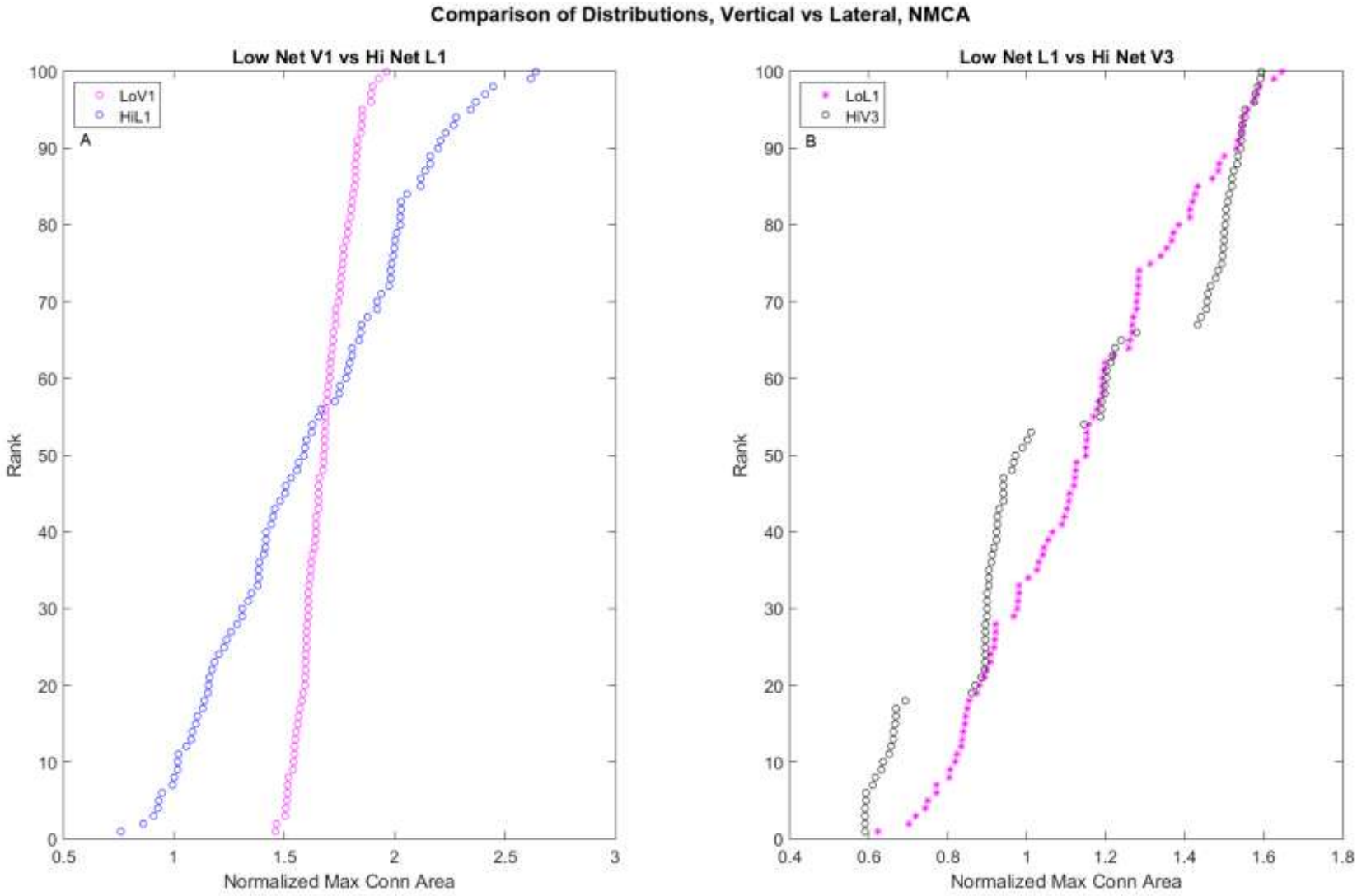

Fig. 4.2.22. Cumulative distributions of NMCA. Data from all 100 model runs was sorted from least to greatest NMCA. Low-net represented by pink circles; high-net represented by blue and black circles.

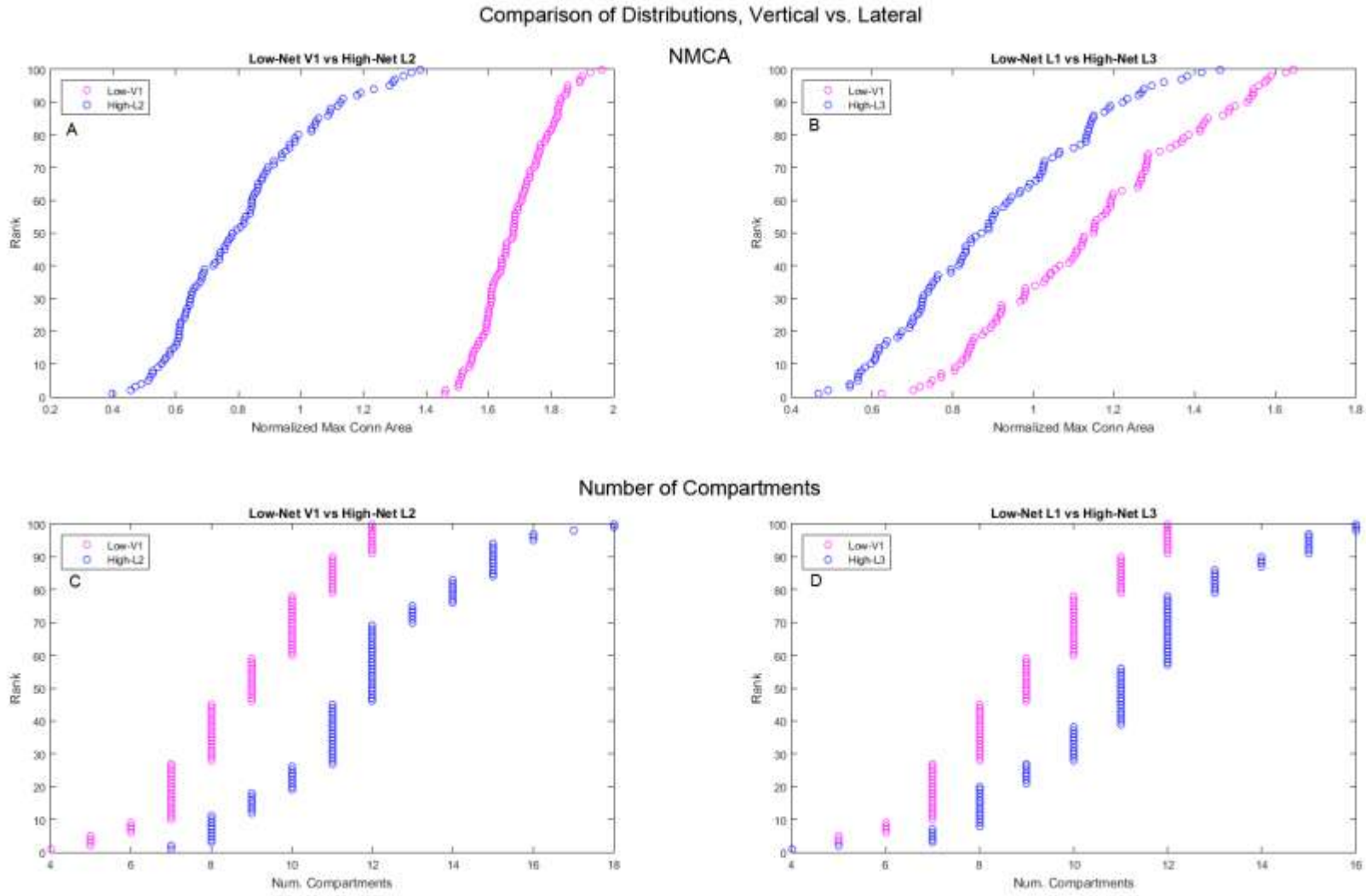

Fig. 4.2.23. Cumulative distributions of NMCA and Number of Compartments for Vertical versus Lateral runs. Data from all 100 model runs was sorted from least to greatest NMCA. Low-net represented by pink circles; high-net represented by blue circles.

Table 4.2.1. ANOVA Results: Number of compartments, High-net

	LALW	LAMW	LAHW	MALW	MAMW	MAHW	HALW	HAMW	HAHW
LALW	x	1	1	1	1	1	1	1	1
LAMW	x	x	1	1	1	1	1	1	1
LAHW	x	x	x	1	0	1	0	1	1
MALW	x	x	x	x	1	1	1	1	1
MAMW	x	x	x	x	x	1	0	1	1
MAHW	x	x	x	x	x	x	1	0	1
HALW	x	x	x	x	x	x	x	1	1
HAMW	x	x	x	x	x	x	x	x	1
HAHW	x	x	x	x	x	x	x	x	x

Table 4.2.1. ANOVA results for number of compartments of high-net model runs. 0 represents a p-value greater than the 0.05 confidence level, indicating statistically similar model runs (highlighted in light gray). 1 represents no statistical similarity. Abbreviations indicate aggradation rate and model domain width. Ex) LALW = low aggradation, low width.

Table 4.2.2. ANOVA Results: NMCA, High-net

	LALW	LAMW	LAHW	MALW	MAMW	MAHW	HALW	HAMW	HAHW
LALW	x	0	1	1	0	1	0	1	1
LAMW	x	x	1	1	0	1	0	1	1
LAHW	x	x	x	1	1	0	0	1	1
MALW	x	x	x	x	1	1	1	1	1
MAMW	x	x	x	x	x	1	0	1	1
MAHW	x	x	x	x	x	x	0	1	1
HALW	x	x	x	x	x	x	x	1	1
HAMW	x	x	x	x	x	x	x	x	1
HAHW	x	x	x	x	x	x	x	x	x

Table 4.2.2. ANOVA results for NMCA of high-net runs. 0 represents a p-value greater than the 0.05 confidence level, indicating statistically similar model runs (highlighted in light gray). 1 represents no statistical similarity. Abbreviations indicate aggradation rate and model domain width. Ex) LALW = low aggradation, low width.

Table 4.2.3 ANOVA Results: Number of compartments, Low-net

	LALW	LAMW	LAHW	MALW	MAMW	MAHW	HALW	HAMW	HAHW
LALW	x	1	1	1	1	1	1	1	1
LAMW	x	x	1	0	1	1	1	1	1
LAHW	x	x	x	1	1	1	0	1	1
MALW	x	x	x	x	1	1	1	1	1
MAMW	x	x	x	x	x	1	1	1	1
MAHW	x	x	x	x	x	x	1	0	1
HALW	x	x	x	x	x	x	x	1	1
HAMW	x	x	x	x	x	x	x	x	1
HAHW	x	x	x	x	x	x	x	x	x

Table 4.2.3. ANOVA results for number of compartments of low-net model runs. 0 represents a p-value greater than the 0.05 confidence level, indicating statistically similar model runs (highlighted in light gray). 1 represents no statistical similarity. Abbreviations indicate aggradation rate and model domain width. Ex) LALW = low aggradation, low width.

Table 4.2.4. ANOVA Results: NMCA, Low-net

	LALW	LAMW	LAHW	MALW	MAMW	MAHW	HALW	HAMW	HAHW
LALW	x	1	1	0	1	1	1	1	1
LAMW	x	x	1	1	1	1	1	1	1
LAHW	x	x	x	1	1	1	0	1	1
MALW	x	x	x	x	1	1	1	1	1
MAMW	x	x	x	x	x	1	0	1	1
MAHW	x	x	x	x	x	x	1	0	1
HALW	x	x	x	x	x	x	x	1	1
HAMW	x	x	x	x	x	x	x	x	0
HAHW	x	x	x	x	x	x	x	x	x

Table 4.2.4. ANOVA results for NMCA of low-net model runs. 0 represents a p-value greater than the 0.05 confidence level, indicating statistically similar model runs (highlighted in light gray). 1 represents no statistical similarity. Abbreviations indicate aggradation rate and model domain width. Ex) LALW = low aggradation, low width.

Table 4.2.5 ANOVA Results: Number of Compartments, High vs. Low-net

		Hi Net								
		LALW	LAMW	LAHW	MALW	MAMW	MAHW	HALW	HAMW	HAHW
Low Net	LALW	0	1	1	0	1	1	1	1	1
	LAMW	1	0	1	1	1	1	1	1	1
	LAHW	1	1	1	1	1	1	1	1	1
	MALW	1	1	1	1	0	1	0	1	1
	MAMW	1	1	1	1	1	0	1	0	1
	MAHW	1	1	1	1	1	1	1	1	0
	HALW	1	1	0	1	0	1	0	1	1
	HAMW	1	1	1	1	1	1	1	1	0
	HAHW	1	1	1	1	1	1	1	1	1

Table 4.2.6 ANOVA Results: NMCA, High vs. Low-net

		Hi Net								
		LALW	LAMW	LAHW	MALW	MAMW	MAHW	HALW	HAMW	HAHW
Low Net	LALW	1	1	1	1	0	1	1	1	1
	LAMW	0	0	1	1	0	1	0	1	1
	LAHW	1	1	0	1	1	0	1	1	1
	MALW	1	1	1	1	1	1	1	1	1
	MAMW	1	1	1	1	1	0	1	1	1
	MAHW	1	1	1	1	1	1	1	0	0
	HALW	1	1	0	1	1	0	0	1	1
	HAMW	1	1	1	1	1	1	1	1	0
	HAHW	1	1	1	1	1	1	1	1	0

Tables 4.2.5 and 4.2.6. ANOVA results for high-net versus low-net model runs. Number of compartments, top, and NMCA, bottom. 0 represents a p-value greater than the 0.05 confidence level, indicating statistically similar model runs (highlighted in light gray). 1 represents no statistical similarity. Abbreviations indicate aggradation rate and model domain width. Ex) LALW = low aggradation, low width.

Table 4.2.7. ANOVA Results: Number of Compartments, Low-net, Vertical vs. Lateral

	V1	V2	V3	L1	L2	L3
V1	x	1	1	1	1	1
V2	x	x	1	1	0	0
V3	x	x	x	0	1	1
L1	x	x	x	x	1	1
L2	x	x	x	x	x	0
L3	x	x	x	x	x	x

Table 4.2.7. ANOVA results for number of compartments of low-net, vertical versus lateral runs. 0 represents a p-value greater than the 0.05 confidence level, indicating statistically similar model runs (highlighted in light gray). 1 represents no statistical similarity. Abbreviations indicate vertical or lateral runs.

Table 4.2.8. ANOVA Results: NMCA, Low-net, Vertical vs. Lateral

	V1	V2	V3	L1	L2	L3
V1	x	1	1	1	1	1
V2	x	x	1	1	1	1
V3	x	x	x	1	1	1
L1	x	x	x	x	1	1
L2	x	x	x	x	x	0
L3	x	x	x	x	x	x

Table 4.2.8. ANOVA results for NMCA of low-net, vertical versus lateral runs. 0 represents a p-value greater than the 0.05 confidence level, indicating statistically similar model runs (highlighted in light gray). 1 represents no statistical similarity. Abbreviations indicate vertical or lateral runs.

Table 4.2.9. ANOVA Results: Num. Compartments, High-net, Vertical vs. Lateral

	V1	V2	V3	L1	L2	L3
V1	x	1	1	1	1	1
V2	x	x	0	1	1	1
V3	x	x	x	1	1	1
L1	x	x	x	x	1	1
L2	x	x	x	x	x	1
L3	x	x	x	x	x	x

Table 4.2.9. ANOVA results for number of compartments of high-net, vertical versus lateral runs. 0 represents a p-value greater than the 0.05 confidence level, indicating statistically similar model runs (highlighted in light gray). 1 represents no statistical similarity. Abbreviations indicate vertical or lateral runs.

Table 4.2.10. ANOVA Results: NMCA, High-net, Vertical vs. Lateral

	V1	V2	V3	L1	L2	L3
V1	x	1	1	1	1	1
V2	x	x	1	1	1	1
V3	x	x	x	1	1	1
L1	x	x	x	x	1	1
L2	x	x	x	x	x	1
L3	x	x	x	x	x	x

Table 4.2.10. ANOVA results for NMCA of high-net, vertical versus lateral runs. 0 represents a p-value greater than the 0.05 confidence level, indicating statistically similar model runs (highlighted in light gray). 1 represents no statistical similarity. Abbreviations indicate vertical or lateral runs.

Table 4.2.11. ANOVA Results: Num. Compartments
High vs. low-net, vertical vs. lateral

		High Net					
		V1	V2	V3	L1	L2	L3
Low Net	V1	1	1	1	1	1	1
	V2	1	1	1	1	0	0
	V3	1	1	1	0	1	1
	L1	1	1	1	0	1	1
	L2	1	1	1	1	0	1
	L3	1	1	1	1	1	0

Table 4.2.11. ANOVA results for number of compartments of high versus low-net, vertical versus lateral runs. 0 represents a p-value greater than the 0.05 confidence level, indicating statistically similar model runs (highlighted in light gray). 1 represents no statistical similarity. Abbreviations indicate vertical or lateral runs.

Table 4.2.12. ANOVA Results: NMCA, High vs. low-net, vertical vs. lateral

		High Net					
		V1	V2	V3	L1	L2	L3
Low Net	V1	1	1	1	0	1	1
	V2	1	1	1	1	1	1
	V3	1	1	1	1	1	1
	L1	1	1	0	1	1	1
	L2	1	1	1	1	1	1
	L3	1	1	1	1	1	1

Table 4.2.1.12. ANOVA results for NMCA of high versus low-net, vertical versus lateral runs. 0 represents a p-value greater than the 0.05 confidence level, indicating statistically similar model runs (highlighted in light gray). 1 represents no statistical similarity. Abbreviations indicate vertical or lateral runs.

4.3 Discussion

Results show that 1) high net-to-gross scenarios typically produce less compartmentalized reservoirs with larger NMCAs, relative to low-net cases and 2) with few exceptions, vertical stacking of channel elements produces reservoirs with larger NMCA and less compartmentalization, relative to lateral stacking.

4.3.1 High-net versus low-net model runs

For any reservoir, the first-order control on connectivity is net-to-gross. High-net systems have been shown to produce reservoirs that are better connected (Allen, 1978; Larue and Hovadik, 2006; Pranter et al., 2011.) Model results typically agree, and the high-net runs, on average, produce higher mean NMCA and are less compartmentalized. However, exceptions do occur. For example, low-net, HALW cases produce larger NMCA than high-net, LAHW cases. The proposed explanation stems from the degree of preservation in the HALW case. Higher aggradation leads to larger compartment areas, as the "incising" channel element does not erode as much of the underlying channel, while low model width reduces the chance of compartmentalization. Contrarily, low aggradation results in higher amalgamation, thus less preserved sand. This, coupled with high model width, results in reservoirs consisting of a high number of smaller compartments.

One factor contributing to the smaller NMCA in low-net cases is the thickness of bar-top muds and abandonment fill. Not only does this decrease the size of the isolated compartments, but there are combinations of model width, aggradation rate, centroid location and orientation of channel elements which would prevent the smaller

compartments from being breached (e.g. Fig. 4.3.1). The absence of abandonment fill at the top of the high-net case makes compartmentalization of this form less common.

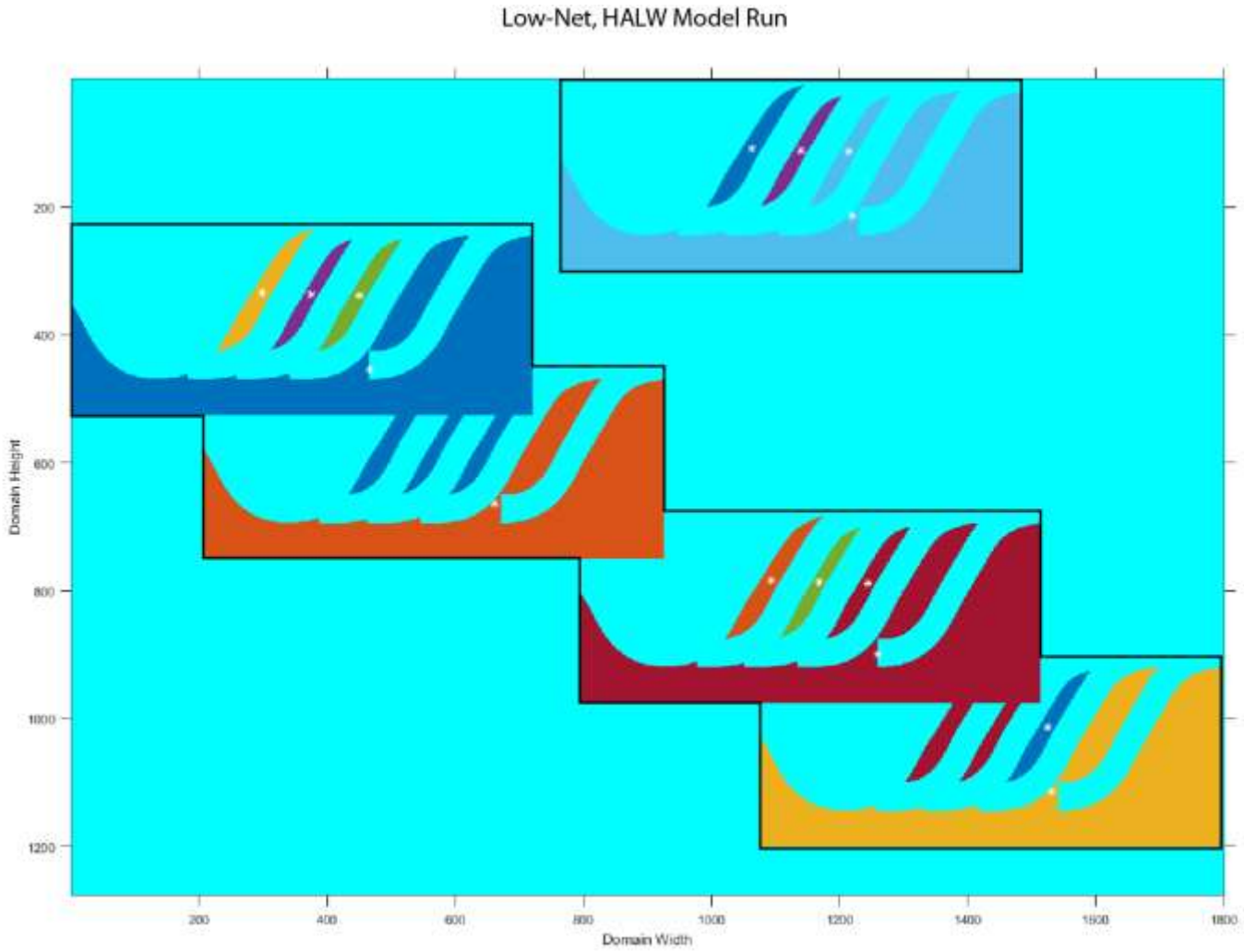

Fig 4.3.1. Low-net, HALW model run. Thick bar-top muds and abandonment fill prevent amalgamation, resulting in several isolated compartments.

4.3.2 Vertical versus lateral stacking

The first group of model run scenarios indirectly tested the impacts of vertical versus lateral stacking, through varying model domain areas. ANOVA testing revealed several cases of statistically similar compartmentalization and NMCA, but we focus specifically on two cases. Of the nine scenarios, LAHW and HALW represent end-member cases of lateral and vertical stacking, respectively. For low and high-net cases, internally, all LAHW and HALW runs produce statistically similar results for NMCA and compartmentalization (Tables 3.3 – 3.6). Across net-to-gross scenarios, the low-net HALW and high-net LAHW runs also produced similar results. The high-net case shows a higher median NMCA, but vertical stacking in the low-net case yields a higher maximum NMCA. The low-net HALW case is more likely to produce larger reservoirs, but relatively lower potential for compartmentalization in the high-net case suggests lateral stacking is marginally preferential.

The second group of model runs more directly investigated the quality of lateral versus vertical stacked reservoirs by forcing a domain area that tended towards either pattern. The better connected reservoirs created by Low-V1 are the result of higher aggradation and lower model width, relative to the high-L2 and high-L3 runs. With such low aggradation, the potential NMCA was limited. Coupled with high model width, isolated sand bodies were more likely to form than amalgamated sheet sands, which can serve as high quality reservoirs (Larue and Hovadik, 2006, Labourdette, 2011). Other than these cases, high quality reservoirs were dominantly high net-to-gross and characterized by vertical stacking. Following results from the previous section, lateral stacking was more likely to compartmentalize reservoirs, regardless of net-to-gross. The

models suggest it is extremely difficult to breach the smaller compartments without some component of vertical stacking. Results are consistent with a study of deepwater channels that showed vertical stacking of architectural elements led to higher connectivity of architectural elements (Funk et al., 2012).

4.3.3 Implications for predicting reservoir quality

Results suggest that for a given aggradation rate and floodplain width, large scale trends in reservoir connectivity may be predictable and that vertical stacking of channel-belt-scale sand-bodies results in relatively higher connectivity. Compartmentalization increased consistently with model width and aggradation rate. Estimates of net-to-gross will help further constrain predicted reservoir quality. Since channel-belt-scale features can be well-imaged in seismic data, stacking patterns may be analyzed to determine if vertical or lateral arrangement dominates. Coupled with inferences on basin-conditions, exploration geologists may better target reservoirs of apparent higher quality.

4.3.3.1 Theoretical approach for predicting connectivity

Given floodplain width (W), floodplain aggradation rate (r), avulsion frequency (f), channel width (w), and depth (d), the probability of channel-belt-scale sand-bodies being connected is a function of the preceding variables and is represented by a non-dimensional number, p:

$$p = f\left(\frac{W * r}{w * d * f}\right) = f\left(\frac{W * r}{A * f}\right)$$

where A is the cross-sectional area of a channel. This non-dimensional number can ultimately be tested against field data or high-resolution seismic data from various fluvial systems to investigate its effectiveness in predicting large-scale sand-body connectivity.

4.3.4 Limitations

This study approached avulsion-based MSB generation and its impacts on reservoir quality from a relatively large scale. It is well known that various scales of heterogeneity exist within reservoirs (Jordan and Pryor, 1992), ranging from pore to field-scale. We considered large, channel-belt-scale connectivity, but acknowledge the fact that smaller scale heterogeneities can have significant impacts on reservoir quality and exploitation (Larue and Friedmann, 2005).

Additionally, two-dimensional models may not accurately approximate the true, three-dimensional connectivity of a reservoir. Architecture may vary upstream or downstream from the simulated locations (Bridge and Mackey, 1995), resulting in increased or decreased reservoir volumes. Furthermore, shale drapes on bars may potentially be discontinuous, creating flow-paths which connect what would be otherwise compartmentalized sand bodies (Pranter et al., 2007). While the connected compartments we generated may be reasonable proxies for drainage areas in conventional reservoirs, the geometry and configuration of compartments would be a critical factor in steam-assisted-gravity-driven heavy-oil production.

The method by which channel elements in these models aggraded vertically also limits application of this study. While lateral position was random determined, vertical position was fixed for each aggradation rate. Given clustered, compensational, or purely random stacking, connectivity results may differ. Implementation of these stacking patterns in a similar model may provide further insight on reservoir quality in relation to large-scale channel organization and preservation of fine-grained facies which can compartmentalize reservoirs.

5. Conclusions

The goal of this study was to use field-based observations of multi-story sand bodies to develop reservoir models that test the hypothesis that vertical stacking of avulsion-generated reservoirs produces better connected, larger reservoirs. Field results show that the three members of the Wasatch Formation have distinct channel styles. Atwell Gulch meandering channels produced thin, laterally restricted, single story sand bodies. An increase in sand-content, coupled with a transition to a higher-energy braided river system deposited thick, multi-storied, and laterally extensive sheet sands in the Molina. MSBs of the Shire Member are relatively thick, wide and exhibit a range of characteristics suggesting mixed process origins.

Simplified channel elements, informed by field observations, were used to generate MSBs in various vertical aggradation and model width scenarios. Results suggest net-to-gross is a first order control on reservoir quality. High-net scenarios produce larger, better connected reservoirs, relative to low-net scenarios. As aggradation and model width increase, reservoir area generally decreases while compartmentalization increases. Vertical stacking typically results in higher reservoir quality, regardless of net-to-gross. Given low aggradation and high model width, laterally stacked, high-net channels yield lower quality reservoir than low-net, vertically stacked channels. Knowledge of basin conditions (i.e. avulsion frequency, floodplain width, aggradation rates) combined with seismic data capable of resolving channel-belt-scale features may allow for better prediction of reservoir connectivity.

References

Allen, J.R.L. “Studies in Fluviatile Sedimentation: An Exploratory Quantitative Model for the Architecture of Avulsion-Controlled Alluvial Suites.” *Sedimentary Geology* 21.2 (1978): 129–147.

Allen, J.R.L. "Studies in Fluviatile Sedimentation: Bars, Bar-Complexes and Sandstone Sheets (low-Sinuosity Braided Streams) in the Brownstones (L. Devonian), Welsh Borders.” *Sedimentary Geology* 33.4 (1983): 237–293.

Blakey, Ronald C., and R. Gubitosa. “Controls of Sandstone Body Geometry and Architecture in the Chinle Formation (Upper Triassic), Colorado Plateau.” *Sedimentary Geology* 38.1-4 (1984): 51–86.

Bridge, J S, and M. R. Leeder. “A Simulation Model of Alluvial Stratigraphy.” *Sedimentology* 26.September (1979): 617–644.

Bristow, C. S., and J. L. Best. “Braided Rivers: Perspectives and Problems.” *Geological Society, London, Special Publications* 75.1 (1993): 1–11.

Chamberlin, Ellen P, and E. A. Hajek. “Interpreting Paleo-Avulsion Dynamics from Multistory Sand Bodies.” *Journal of Sedimentary Research* 85 (2015): 82–94.

Donnell, John R. *Paleocene and Lower Eocene Units in the Southern Part of the Piceance Creek Basin Colorado*. Vol. 1274–M. N.p., 1969.

Donselaar, Marinus E., and I. Overeem. “Connectivity of Fluvial Point-Bar Deposit: An Example from the Miocene Huesca Fluvial Fan, Ebro Basin, Spain.” *AAPG Bulletin* 92.9 (2008): 1109–1129.

Eaton, B. C., and T. Giles. “Monitoring and Numerical Modelling of Riverbank Erosion Processes: A Case Study along the Cecina River (central Italy).” *Earth Surface Processes and Landforms* 724.December 2008 (2009): 712–724.

Flood, Yvette S, and G. J. Hampson. “Facies and Architectural Analysis to Interpret Avulsion Style And Variability: Upper Cretaceous Blackhawk Formation, Wasatch Plateau, Central Utah, U.S.A.” *Journal of Sedimentary Research* 84 (2014): 743–762.

Foreman, Brady Z., P. L. Heller, and M. T. Clementz. “Fluvial Response to Abrupt Global Warming at the Palaeocene/Eocene Boundary.” *Nature* 000 (2012): 1–4.

Friend, P. F., M. J. Slater, and R. C. Williams. “Vertical and Lateral Building of River Sandstone Bodies, Ebro Basin, Spain.” *Journal of the Geological Society* 136.1 (1979): 39–46.

Funk, Jonathan E., R. M. Slatt, and D. R. Pyles. “Quantification of Static Connectivity between Deep-Water Channels and Stratigraphically Adjacent Architectural Elements Using Outcrop Analogs.” *AAPG Bulletin* 96.2 (2012): 277–300.

Gibling, Martin. “Width and Thickness of Fluvial Channel Bodies and Valley Fills in the Geological Record: A Literature Compilation and Classification.” *Journal of Sedimentary Research* 76.5 (2006): 731–770.

Hajek, Elizabeth A, and D. Edmonds. “Is River Avulsion Style Controlled by Floodplain Morphodynamics?” *Geology* 42.3 (2014): 199–202.

Hajek, Elizabeth A, P. L. Heller, and B. A. Sheets. “Significance of Channel-Belt Clustering in Alluvial Basins.” *Geology* 38.6 (2010): 535–538.

Heller, Paul L, and C. Paola. “Downstream Changes in Alluvial Architecture; an Exploration of Controls on Channel-Stacking Patterns.” *Journal of Sedimentary Research* 1996: 297–306.

Johnson, Ronald C, and R. M. Flores. “Piceance Basin Guidebook.” *Piceance Basin Guidebook*. Rocky Mountain Association of Geologists, 2003. 21–61.

Johnson, Samuel Y. “Phanerozoic Evolution of Sedimentary Basins in the Uinta-Piceance Basin Region, Northwestern Colorado and Northeastern Utah.” *USGS Bulletin* 1787-FF (1992): 1–38.

Jones, H. L., and E. A. Hajek. “Characterizing Avulsion Stratigraphy in Ancient Alluvial Deposits.” *Sedimentary Geology* 202.1-2 (2007): 124–137.

Labourdette, Richard. “Stratigraphy and Static Connectivity of Braided Fluvial Deposits of the Lower Escanilla Formation, South Central Pyrenees, Spain.” *AAPG Bulletin* 95.4 (2011): 585–617.

Labrecque, Phillip A., J. L. Jensen, and S. M. Hubbard. “Cyclicity in Lower Cretaceous Point Bar Deposits with Implications for Reservoir Characterization, Athabasca Oil Sands, Alberta, Canada.” *Sedimentary Geology* 242.1-4 (2011): 18–33.

Larue, D. K., and F. Friedmann. “The Controversy Concerning Stratigraphic Architecture of Channelized Reservoirs and Recovery by Waterflooding.” *Petroleum Geoscience* 11.2 (2005): 131–146.

Larue, D. K., and J. Hovadik. “Connectivity of Channelized Reservoirs: A Modelling Approach.” *Petroleum Geoscience* 12.4 (2006): 291–308.

Lorenz, John C, and G. C. Nadon. “Braided-River Deposits in a Muddy Depositional Setting: The Molina Member of the Wasatch Formation (Paleogene), West-Central Colorado, U.S.A.” *Journal of Sedimentary Research* 72.3 (2002): 376–385.

Lynds, Ranie M., and E. A. Hajek. “Conceptual Model for Predicting Mudstone Dimensions in Sandy Braided-River Reservoirs.” *AAPG Bulletin* 90.8 (2006): 1273–1288.

Mackey, Scudder D, and J.S. Bridge. “Three-Dimensional Model of Alluvial Stratigraphy; Theory and Applications.” *Journal of Sedimentary Research* 65 .1b (1995): 7–31.

Miall, Andrew D. “Architectural-Element Analysis: A New Method of Facies Analysis Applied to Fluvial Deposits.” *Earth Science Reviews* 22 (1985): 261–308.

Pranter, Matthew J., A. I. Ellison, R. D. Cole, and P. E. Patterson. “Analysis and Modeling of Intermediate-Scale Reservoir Heterogeneity Based on a Fluvial Point-Bar Outcrop Analog, Williams Fork Formation, Piceance Basin, Colorado.” *AAPG Bulletin* 91.7 (2007): 1025–1051.

Pranter, Matthew J., Rex D. Cole, H. Panjaitan, and N. Sommer. “Sandstone-Body Dimensions in a Lower Coastal-Plain Depositional Setting: Lower Williams Fork Formation, Coal Canyon, Piceance Basin, Colorado.” *AAPG Bulletin* 93.10 (2009): 1379–1401.

Pranter, Matthew J., and N. Sommer. “Static Connectivity of Fluvial Sandstones in a Lower Coastal-Plain Setting: An Example from the Upper Cretaceous Lower Williams Fork Formation, Piceance Basin, Colorado.” *AAPG Bulletin* 95.6 (2011): 899–923.

Reijenstein, Hernán M., H. W. Posamentier, and J. P. Bhattacharya. “Seismic Geomorphobgy and High-Resolution Seismic Stratigraphy of Inner-Shelf Fluvial, Estuarine, Deltaic, and Marine Sequences, Gulf of Thailand.” *AAPG Bulletin* 95.11 (2011): 1959–1990.

Stouthamer, Esther, and H. J. A. Berendsen. “Avulsion Frequency, Avulsion Duration, and Interavulsion Period of Holocene Channel Belts in the Rhine-Meuse Delta, The Netherlands.” *Journal of Sedimentary Research* 71.4 (2001): 589–598.

Thomas, Richard G. et al. “Inclined Heterolithic stratification—Terminology, Description, Interpretation and Significance.” *Sedimentary Geology* 53.1-2 (1987): 123–179.

Willis, B. J., and H. Tang. “Three-Dimensional Connectivity of Point-Bar Deposits.” *Journal of Sedimentary Research* 80.5 (2010): 440–454.

Appendix A

Interpreted Outcrop Locations

ID	Latitude	Longitude	Gigapan
Atwell Gulch-1	39°17'56.09"N	108°19'4.86"W	http://gigapan.com/gigapans/162237
Atwell Gulch-2	39°16'59.26"N	108°21'50.39"W	http://gigapan.com/gigapans/139404
Atwell Gulch -3	39°16'22.87"N	108°12'5.12"W	http://gigapan.com/gigapans/162220
Atwell Gulch -4	39°17'57.42"N	108°19'7.18"W	http://gigapan.com/gigapans/162237
Molina-1	39°17'3.54"N	108° 9'57.48"W	http://gigapan.com/gigapans/162480
Molina -2	39°19'2.45"N	108° 9'45.61"W	http://gigapan.com/gigapans/162476
Molina -3	39°18'54.84"N	108° 9'37.81"W	http://gigapan.com/gigapans/162415
Molina -4	39°19'2.32"N	108°10'48.94"W	http://gigapan.com/gigapans/162642
Shire-1	39°24'11.44"N	108° 6'45.09"W	http://gigapan.com/gigapans/139447
Shire -2	39°23'28.31"N	108° 8'1.79"W	http://gigapan.com/gigapans/162389
Shire -3	39°24'41.37"N	108° 5'49.98"W	http://gigapan.com/gigapans/162248
Shire -4	39°24'25.60"N	108° 6'26.85"W	http://gigapan.com/gigapans/150058

Table A1.1 – GPS coordinates for all interpreted outcrops. Photomosaics are available online via Gigapan.com.

A Google map of these outcrop locations can be accessed online here:
http://tinyurl.com/OutcropLocationsBaisden

Appendix B

Sand body measurements

Story/Element ID	Element Width (m)	Element Thickness (m)	Basal Surface	Incision Depth (m)	Vertical Stacking Ratio	Lateral Stacking Ratio	Migration Distance
Overall	99	3.43	Planar	--	Single Story		1.4
1a	30	1.15	Planar	--			
1b	27	1.07	Convex	--			
1c	28	1.50	Convex	--			
1d	--	1.30	Convex	--			
1e	--	1.10	Convex	--			
1f	--	1.09	Convex	--			
Average	28.30	1.20					

Table B2.1 – Atwell Gulch-1 measurements. Aspect ratio is approximately 30:1. No vertical or lateral stacking ratio is determined for single-story sand bodies. Elements are bars of one bar-set. Migration distance is reported in average bar widths.

Story/Element ID	Element Width (m)	Element Thickness (m)	Basal Surface	Incision Depth (m)	Vertical Stacking Ratio	Lateral Stacking Ratio	Migration Distance
Overall	78	5.3	Convex to planar	1.5m	Single Story		1.6
1a	25.4	1.59	Convex	--			
1b	26.5	1.37	Convex	--			
1c	23.0	1.71	Convex	--			
Average	25	1.56					

Table B2.2 – Atwell Gulch-2 measurements. Aspect ratio is approximately 15:1. No vertical or lateral stacking ratio is determined for single-story sand bodies. Elements are bars of one bar-set. Migration distance is reported in average bar widths.

Story/Element ID	Element Width (m)	Element Thickness (m)	Basal Surface	Incision Depth (m)	Vertical Stacking Ratio	Lateral Stacking Ratio	Migration Distance
Overall	243.35	4.1	Relatively planar	--	5:2.87	5:1.95	
1	50.6	1.75	Planar	--			
1a	33	1.55	Planar	--			2.1
1b	30	1.73	Convex	--			
1c	14	1.45	Convex	--			
1d	16	1.29	Convex	--			
2	136	2.59	Convex to planar	1.7			
3	60	1.39	Planar	--			
4	131	3.42	Convex to planar	2.36			
5	46	1.69	Convex	0.98			
Average	58.25	1.88					

Table B2.3 – Atwell Gulch-3 measurements. Aspect ratio is approximately 60:1. Story 1 is one bar-set, comprising four bars which migrated 2.1 average bar widths. Stacking ratio calculated using overall story thicknesses and widths.

Story/Element ID	Element Width (m)	Element Thickness (m)	Basal Surface	Incision Depth (m)	Vertical Stacking Ratio	Lateral Stacking Ratio	Migration Distance
Overall	97	4.2	Planar	--	Single Story		1.7
1	26.3	1.239	Planar	--			
2a	48	1.458	Convex	--			
2b	62	2.184	Convex	--			
Average	45.4	1.63					

Table B2.4 – Atwell Gulch-4 measurements. Aspect ratio is approximately 23:1. Two bar-sets comprise this sand-body. Migration distance was measured on bar-set 2.

Story/Element ID	Element Width (m)	Element Thickness (m)	Basal Surface	Incision Depth (m)	Vertical Stacking Ratio	Lateral Stacking Ratio	Migration Distance
Overall	117.36	10.56	Convex	--	3:1.13	3:3.05	--
1	57.9	2.82	Convex	--			
2	105.23	4.19	Convex	1.81			
3	148.86	3.39	Convex	0.64			
3a	148.86	2.45	Convex	--			
3b	69.75	1.96	Planar	--			
Average	104.00	3.47					

Table B2.5 – Molina-1 measurements. Aspect ratio is approximately 12:1. Stacking ratio calculated using overall story thicknesses and widths.

Story/Element ID	Element Width (m)	Element Thickness (m)	Basal Surface	Incision Depth (m)	Vertical Stacking Ratio	Lateral Stacking Ratio	Migration Distance
Overall	109.78	7.11	Convex	--	2:1.33	2:1.84	--
1	93	3.46	Convex	1.64			
2	72	4.27	Convex	--			
2a	71	3.88	Relatively Planar	1.45			
2b	23.54	2.29	Convex	--			
2c	16	2.1		1.23			
Average	82.5	3.86					

Table B2.6 – Molina-2 measurements. Aspect ratio is approximately 16:1. One bar-set with three downstream accreting bars comprise story 2 and represent one channel belt. Stacking ratio calculated using overall story thicknesses and widths.

Story/Element ID	Element Width (m)	Element Thickness (m)	Basal Surface	Incision Depth (m)	Vertical Stacking Ratio	Lateral Stacking Ratio	Migration Distance
Overall	88.29	19.77	Planar	--	5:1.32	5:4.87	--
1	52.24	3.27	Convex	1.23			
2	77.87	5.15	Convex	1.42			
3	81.21	4.21	Convex	0.78			
3a	75.03	2.16	Planar	--			
3b	80.76	2.76	Planar	--			
4	70.16	4.02	Planar	--			
4a	63.5	2.09	Planar	--			
4b	59.42	1.63	Planar	--			
5	52.5	3.64	Convex	3.57			
Average	66.8	4.06					

Table B2.7 – Molina-3 measurements. Aspect ratio is approximately 4:1. Stories 3 and 4 both show lateral accretion surfaces, but stacking ratios reflect bar-set geometry. Overall story thickness and width was used to calculate stacking ratios.

Story/Element ID	Element Width (m)	Element Thickness (m)	Basal Surface	Incision Depth (m)	Vertical Stacking Ratio	Lateral Stacking Ratio	Migration Distance
Overall	223	8.5	Planar	--	2:1.25	2:2.06	--
1	136.79	2.84	Planar	--			
2	220	5.40	Planar	--			
2a	222.7	3.09	Planar	--			
2b	217.9	4.97	Planar, locally convex	3.609			
Average	178.40	4.12					

Table B2.8 – Molina-4 measurements. Aspect ratio is approximately 28:1. Story 2 comprises two bars, representing one channel belt. Overall story thickness and width was used to calculate stacking ratios.

Story/Element ID	Element Width (m)	Element Thickness (m)	Basal Surface	Incision Depth (m)	Vertical Stacking Ratio	Lateral Stacking Ratio	Migration Distance
Overall	102.15	12.46	Planar	--	2:1.56	2:2.04	--
1	100.03	9.64	Planar	--			
1a	94.09	2.07	Planar	--			
1b	100.03	7.41	Convex	1.49			
2	30.58	2.56	Planar	--			
Average	65.31	6.10					

Table B2.9 – Shire-1 measurements. Aspect ratio is approximately 8:1. Stacking ratio calculated using overall story thicknesses and widths.

Story/Element ID	Element Width (m)	Element Thickness (m)	Basal Surface	Incision Depth (m)	Vertical Stacking Ratio	Lateral Stacking Ratio	Migration Distance
Overall	220.7	16.77	Convex	--	3:1.02	3:3.12	--
1	220.75	5.3	Convex	3.27			
2	219.24	4.31	Convex	2.56			
3	206.99	6.49*	Planar	--			
3a	135.71	7.16	Planar	--			
3b	77.6	5.8	Planar	--			
Average	163.33	5.65					

Table B2.10 – Shire-2 measurements. Aspect ratio is approximately 14:1. Two bar-sets of one channel belt comprise story 3. Stacking ratio calculated using overall story thicknesses and widths. *Story 3 thickness is average thickness of bar-sets 3a and 3b.

Story/Element ID	Element Width (m)	Element Thickness (m)	Basal Surface	Incision Depth (m)	Vertical Stacking Ratio	Lateral Stacking Ratio	Migration Distance
Overall	123.82	27.07	Planar	--	4:1.16	4:3.89	--
1	111.10	5.09	Planar	--			
2	135	6.3	Locally convex	--			
2a	134.59	2.5	Planar	--			
2b	134.28	3.45	Planar	--			
3	83.88	2.91	Convex	1.7			
4	96.9	13.51	Convex	2.3			
4a	62.03	7.09	Convex	--			
4b	96.9	6.58	Planar	--			
Average	106.72	6.95					

Table B2.11 – Shire-3 measurements. Aspect ratio is approximately 4.5:1. Stacking ratio calculated using overall story thicknesses and widths.

Story/Element ID	Element Width (m)	Element Thickness (m)	Basal Surface	Incision Depth (m)	Vertical Stacking Ratio	Lateral Stacking Ratio	Migration Distance
Overall	53.55	5.68	Convex	--	2:1.0	2:2.04	--
1	52.57	2.71	Convex	1.29			
1a	50.67	1.7	Convex	--			
1b	48.5	1.19	Planar	--			
2	53.78	2.85	Convex	1.07			
2a	47.8	1.46	Convex	--			
2b	53.78	.9	Planar	--			
Average	53.18	2.78					

Table B2.12 – Shire-4 measurements. Aspect ratio is approximately 10:1. Each story comprises one bar-set. Stacking ratio calculated using overall story thicknesses and widths.

Appendix C

Sand body descriptions

Atwell Gulch Member

Sand-body Atwell Gulch-1

Atwell Gulch-1 (Fig. 3.3.1) is a single-story sand-body, well-exposed in many orientations. A relatively planar lower bounding surfaces marks where AWG-1 incised directly into distal floodplain deposits, which are moderately-developed, bright red paleosols. A total of six bar clinoforms, comprising one bar-set, were interpreted. The three right-most bars (1a-1c) were measured to determine a lateral migration distance of about 1.4 bar widths. These bars, in particular, can be traced for some distance into the surrounding floodplain deposits, before they become poorly exposed. This is represented by dashed lines in the interpreted section. The convex surfaces marking contact between each bar are distinguishable and largely sand-on-sand; however, packages of floodplain material near the right margin of each bar are present. These may represent periods of lower flow where finer grained material is preferentially deposited. Based upon facies, and external and internal geometry, this sand-body likely formed as a result of intra-channel-belt processes, i.e. bar migration.

Sand-body Atwell Gulch-2

Atwell Gulch-2 (Fig. 3.3.2) is a single-story sand-body, isolated in poorly developed, gray floodplain paleosol. The cut is nearly perpendicular to paleoflow and the left margin of the sand-body is clearly visible. The convex, basal scour surface is well defined and is marked by ~1.5m of incision. Internally, three relatively well-defined bar

clinoforms of one bar-set have been interpreted, with a measured migration distance of 1.6 average bar-widths. Similar to AWG-1, bar contacts are sand-on-sand, and packages of finer grained sediment separate the bars where they become more difficult to trace into the floodplain. Based on internal geometry, lateral migration is the interpreted formative processes for AWG-2.

Sand-body Atwell Gulch-3

Atwell Gulch-3 (Fig. 3.3.3) is the only multi-story sand-body interpreted in this member. The outcrop cut here also provides a nearly 3-dimensional view in two faces. The lowermost story, 1, is marked by a convex basal scour, and incised directly into floodplain deposits. It comprises a series of migrating bars (1a-1d; Fig 2.6B-C) which show a migration distance of 2.1 average bar widths (1b-1d). Note, however, the measurement may have been skewed due to the outcrop curving around a nose at this point. Story 1 is truncated by story 2, which incised into proximal overbank and splay deposits. This story potentially contains two bar-sets, though poor exposure and cover limits this interpretation. Story 3 has been interpreted as a separate channel belt; the basal scour occurs above the base of and does not trace laterally into story 2. Story 4 represents another channel belt which incised directly into stories 2 and 3. Remnant proximal overbank deposits are preserved beneath the well-defined wings of the sand-body. To the left of story 4 and above story 3, a mud-plug, representing channel abandonment, has been interpreted, based upon the convex lower surface and channel-approximating geometry. A final, 5^{th} story was interpreted to the right and above story 1. Proximal overbank deposits isolate this story from the rest of the sand-body. Lateral stacking

dominates, though some stories exhibit a component of vertical stacking. Internal geometry, preserved overbank deposits, and stepped margins (external geometry) indicate bar migration, as well as channel-belt abandonment/reoccupation as formative processes for AWG-3.

Sand-body Atwell Gulch-4

Atwell Gulch-4 (Fig. 3.3.4), like most sand bodies of this member, is single-story and isolated, but not as well exposed as others. Unlike previously interpreted sand bodies, two bar sets comprise the single story. The lower bar-set (1) is a lozenge shaped element, which was truncated by a second bar-set (2a) of the same channel belt, possibly in a meander cutoff. The upper bar-set is typical of Atwell Gulch channels, with the exception that the packages of fines which separate individual bars are relatively thicker here. Calculated migration distance is about 1.7 average bar widths. At the left margin of the sand-body, the bar-sets thin and eventually give way to an interpreted mud-plug. Interpreted bar clinoforms and internal geometry indicate lateral migration and other intra-channel-belt processes as the dominant formative processes here.

Molina Member

Sand-body Molina-1

Molina-1 (Fig. 3.3.5), a three story sand-body, occurs near the top of the Molina section. Each story was interpreted as a separate channel belt, with convex story boundaries expressed in outcrop as continuous, recessed surfaces. Some portions of these surfaces are sharp, erosional sand-on-sand contacts, while others are lined with channel fines, which represent interbar muds or abandonment fill. Internally, the stories are dominantly massive, with one or two surfaces present, marking bar clinoforms. The top of story 1 can be traced laterally to the top of a paleosol horizon. Coupled with the stepped external geometry of the stories, channel-belt abandonment/reoccupation was likely the dominant process of formation for Molina-1. This channel incised ~1.8m directly into poorly developed, splay rich floodplain deposits. Vertical stacking of these channel belts almost exclusively dominates.

Sand-body Molina-2

Molina-2 (Fig. 3.3.6) has been interpreted as a two-story sand-body, with each story representing a separate channel belt. The lower story is massively bedded, with some high angle, planar laminations, but no accretion surfaces. The story boundary is marked by a continuous surface, which is dominantly sand-on-sand, though some portions are lined with channel fines. Three nested bar-sets make up the upper story, and are likely downstream accreting bars of a braided river. Interbar fines, indicated by a gap in the sand bodies where the bars thin, are present between each, though more pronounced between 2a and 2c. A thin package of finer material separates the lower and

upper story near element 2b, and the left margins of elements 1 and 2a are stepped, indicating abandonment-reoccupation as the most likely process origin. Intra-channel-belt processes resulted in the downstream accreting bars of the second story. Between the lower and upper story, stacking is dominantly vertical. Though the bar-sets of the upper story are not avulsion generated and represent one channel belt, the elements stack laterally.

Sand-body Molina-3

Sand-body Molina-3 (Fig. 3.3.7) is located near Molina-2, slightly further up V-Road. Five-stories comprise this sand-body, with the lowest story representing a single channel belt that incised directly into proximal floodplain deposits, which are not readily visible here. A lower order accretion surface was interpreted near the middle of this story. Adjacent to and above story 1 is a package of proximal overbank deposits, containing poorly developed paleosol and splays, which story 2 incises into. Internal surfaces are noticeably absent, while a prevalent sand-on-sand contact and convex story bounding surface marks the transition to story 3.

Story 3 comprises two bar-sets and incises 1.4m into story 2. There is a discontinuous accretion surface between elements 3a and 3b; it occurs at the top of a finer grained, flaggy-bedded interval. The contact between story 3 and story 4 is mud-lined for much of its length, though sand-on-sand contact is visible towards the margins of the sand-body. Story 4 comprises two bars, separated by a partially mud-lined, continuous surface, and exhibits an internal structure similar to that seen in story 3. The contact between stories 4 and 5 is a well-defined, recessed boundary, likely due to the presence

of fine-grained abandonment fill. Story 5 is void of internal structure and incises 2.9m into underlying channel deposits. The juxtaposition of story 5 relative to story 4 suggests a channel-belt reoccupation. Internal to each story, intra-channel-belt processes (bar migration) dominate, while some instances of stepped margins suggest channel belt abandonment/reoccupation formed this MSB. Measurements show that Molina-3 is dominantly vertically stacked.

Sand-body Molina-4

Sand-body Molina-4 (Fig. 3.3.8) comprises two stories, with the lowermost incising into underlying floodplain deposits. Several discontinuous, lower order surfaces exist internal to story 1, but it is, overall, massively bedded. Story 2 incises into story 1, locally, and the story bounding surface is somewhat difficult to trace across the entire exposure. Two bar-sets are present in story 2, and their bounding surface is also difficult to resolve in some reaches. However, at both margins of the sand-body, the story bounding surface and bar-set surface are visible and were interpreted as sand-on-sand contacts. With only one true exposed margin and difficulty in resolving internal surfaces, confidence of this process based interpretation is relatively low. Nevertheless, the lack of internally preserved floodplain deposits, but presence of accretion surfaces suggest bar migration, i.e. intra-channel-belt processes, as the dominant mechanism of MSB formation. Vertical stacking dominates, with a slight component of lateral stacking.

Shire Member

Sand-body Shire-1

Two stories comprise sand-body Shire-1 (Fig. 3.3.9), which incised into moderately developed paleosol and overbank deposits. A higher order, convex surface is interpreted internal to the first story, marking two episodes of bar deposition. Several first order surfaces have been interpreted in both of these bars. At the left margin of the upper bar, a steep cut filled with channel fines is present. This may represent abandonment fill for this channel belt (i.e. a mud-plug), while an alternate hypothesis proposes the deposits are proximal overbank and splays related associated with a later channel. The upper bar (1b) and fine-grained fill are truncated by a 4th order surface, separating the lower and upper story. From this perspective, the scale of the upper story is much smaller than the lower. Internal architecture is dominated by lower order surfaces, similar to those seen in the first story. Based on the fine-grained fill above element 1b and geometry of the bar-scale features, this sand-body likely formed through bar-migration and abandonment/reoccupation. Stacking is dominantly vertical and incision is relatively high, which is typical of Shire sand bodies.

Sand-body Shire-2

Sand-body Shire-2 (Fig. 3.3.10) comprises three internally complex stories. Story 1 is underlain by proximal overbank deposits, and has a planar to convex basal bounding surface. Shallow dipping surfaces, possibly thinly bedded, inclined heterolithic strata, are present at the left margin of this story. A 2nd order surface towards the right margin marks lateral accretion of bar deposits. Preserved channel fines line a portion of the boundary

between story 1 and 2, which is a convex, 4th order basal scour. Similar to story 1, story 2 comprises two bars, separated by a well-defined, continuous surface. A mud-plug was interpreted at the top of story 2, indicating channel-belt abandonment. The surface bounding stories 2 and 3 is relatively planar and well-defined, likely due fine-grained material at the boundary. Elements 3a and 3b are nested bar-sets, with internal surfaces representing individual bars. Perspective becomes an issue here, as it appears that 3a and 3b should be connected. However, the base of 3b is higher than the top of 3a, suggesting that they are, indeed, separate. Overall, preserved abandonment fill, and stepped margins between stories 1, 2 and 3, suggest abandonment/reoccupation as the avulsion-based process origin. Intra-channel-processes were important for the formation of individual bars and bar-sets. Vertical stacking of stories dominates.

Sand-body Shire-3

Four stories make up sand-body Shire-3 (Fig. 3.3.11). The lowermost represents a single channel belt with several internal first-order surfaces. There is an interval of floodplain deposits separating stories 1 and 2 for the majority of their length, but the contact becomes sand-on-sand at the left end of the sand-body. Two bars are separated by a 2nd order, continuous surface in story 2, and both bars are of similar scale. Story 3 incises into story 2, with a prevalent surface marking the break. There is also a package of floodplain preserved between stories 2 and 3. Story 3 thins to the left, possibly transitioning from axial channel deposits to levee deposits. Facies, geometry, and arrangement described for stories 2 and 3 repeats between story 3 and story 4, which comprises two bars. The upper bar, 4B, thins to the left as well, with floodplain deposits

preserved between the margins of story 3 and 4. Story 4 incised nearly 2.5m into story 3, which is representative of deep incision common to the Shire Member. Stepped margins and encased floodplain deposits suggest an abandonment/reoccupation process origin, while a component of intra-channel-belt processes is inferred from the presence of migrating bar deposits. Stories are dominantly stacked vertically, with some lateral offset, especially apparent between stories 3 and 4.

Sand-body Shire-4

Shire-4 (Fig. 3.3.12) is a two story sand-body, with evidence of lateral migration. The lower story comprises two bars (1a, 1b), with first-order internal surfaces. It incised directly into proximal overbank deposits, including paleosols and splays. Interpreted interbar muds were deposited at the top of the second bar (1b). Story 2 truncates surfaces in story 1, and also incised 1m into the underlying channel deposits. The contact between the two stories is dominantly sand-on-sand. Two bar-sets, 2A and 2B, make up the second story, and are marked by first-order, internal surfaces. A small mud-plug has been interpreted at the top of element 2b, towards its left margin. Story 2 thins dramatically towards the right, where the margin of the sand-body is well-exposed. The smooth bounding surface here, coupled with the nested bar-sets indicates intra-channel-belt processes as the dominant mechanism of formation for this MSB. The stories stack slightly lateral, while vertical stacking is dominant.

Appendix D

Reservoir Model, MATLAB Code

```
%%%%%%%%%%%%%%%%%%%%%%%%%% StickModel_Tramond_ver5 %%%%%%%%%%%%%%%%%%%%%%%%%%
% Modified from code by EPC
% Last updated by TRB 07/17/2015
%
% Read in model dimensions based on channel element, 'element,' width (ch_w)
% and height (ch_z), and randomly select lateral channel position from model domain.
% Vertical position is set by constant "vertagg_rate", given as a proportion of the
% channel thickness.
%
% Output: Structure with Stats (area of each compartment, num of
% compartments, total white area, channel centroids, and element orientation)
%%%%%%%%%%%%%%%%%%%%%%%%%%%%%%%%%%%%%%%%%%%%%%%%%%%%%%%%%%%%%%%%%%%%%%%%%%%%%%%
```

```
%NOTE:
%User must manually load image file and name it 'c'!!!!!!!!
%READ IN CHANNEL ELEMENT
element=c;
element=element/255; %Normalize colors before rounding
element=round(element); %Round values to 0 (black/mud) or 1(white/sand)
```

BEGIN AUTOMATION LOOP

```
numruns = 100; %Number of model runs

for j=1:numruns
```

DEFINE MODEL DOMAIN

```
%%%%%%% Input variables

nits = 5; % number of iterations/number of channel elements

% DEFINE CHANNEL/FLOODPLAIN DEPOSITIONAL UNIT and AGGRADATION RATE
ch_z=size(c,1); %sand body height (generic length units) ---- channel element height,
read from matrix 'c'
ch_w=size(c,2); % pre-allocate channel width vector ---- channel element width, read from
matrix 'c'
ch_w(1)=ch_w; %initial sand body width (generic length units)
var=0.5; % channel height multiplier
vertagg_rate = var*ch_z; % vertical aggradation rate

% MODEL DOMAIN, TIMESTEPS, & MAXIMUM TOPOGRAPHIC RELIEF LIMIT
mw=2.5; % lateral position multiplier
model_w = mw*ch_w; % width of model domain
domain_w= model_w + ch_w; % width of background domain; adds buffer to either side equal
to 1/2 element width
model_idx = [(0.5*ch_w) (0.5*ch_w + model_w)]; % index values across model domain where
channel elements can be centered

% Pre-allocate channel centroids matrix
ch_center = nan(nits,2); % channel element centroids matrix
```

DEFINE CENTROIDS

```
        ch_center(:,1) = randi(model_idx,[nits,1]); % Randomly define x-position for
element centroid
        ch_center(:,2) = [(0.5*ch_z):vertagg_rate:((nits-1)*vertagg_rate+(0.5*ch_z))]; %
set y-coordinate using the vertical aggradation rate
        ch_center=flipud(ch_center);
```

PLOT CHANNEL ELEMENTS

```
%%%% Define model domain matrix
domain=zeros((nits*vertagg_rate)+(0.5*ch_z),domain_w);  %Defines domain in x-direction
(from domain width) and y-direction(from VAR); adds buffer of 1/2 ch_z to top

%%%% Replace zeros of domain matrix with channel element at x,y location,
%%%% for 'nits' elements
for i=1:nits

    x=(ch_center(i,1)-(ch_w(1)/2):ch_center(i,1)+(ch_w(1)/2)-1);
    y=(ch_center(i,2)-(ch_z/2)+1:ch_center(i,2)+(ch_z/2));

%%%%% RANDOMLY ORIENT ELEMENTS
orientation = round(rand(1,nits,1)); %Generates random vector of length "nits" holding 0s
and 1s
%Run loop to place channel elements in the domain with mudplug to left(0) or right(1)
if orientation(i) == 0;
       domain(y,x)=element;
    else
       domain(y,x)=fliplr(element);
    end
end
```

DISPLAY CHANNELS

```
%%%% CALCULATE CONNECTED AREA
cc=bwconncomp(domain); %Calculate total number of connected areas and their size in
pixels

%%%% CREATE LABEL MATRIX TO COLOR EACH COMPARTMENT
l=labelmatrix(cc); %Assign value to each compartment
label=label2rgb(l,@lines,'c','noshuffle'); %Assign each compartment a different color

%%Run region properties and plot centroids
s = regionprops(l,'all'); % Calculate all region properties
centroids = cat(1, s.Centroid); %Convert centroid structure to vector

%%%%% UNCOMMENT TO DISPLAY MODEL WITH COLORED COMPARTMENTS AND CENTROIDS
%figure;
%imshow(label,'InitialMagnification','fit')
%axis on
%hold on
%plot(centroids(:,1),centroids(:,2), 'w*') %Plot centroids on top of compartments
```

OUTPUT RESULTS

```
%Convert array of compartment area from each run into total whitearea
allarea=([s.Area]); %converts field of white area for each run to vector
%Create output structure
output_struc(j).Conn=cc; %Save conncomp for each run
output_struc(j).Orient=orientation; %Save orientation of each element
output_struc(j).ElementCent=ch_center; %Save element centroids
output_struc(j).TotalWhArea=sum(allarea); %Save total white area for each run (Sum of
"sand" pixels)
```

```
end
```

RUN STATISTICS

```
%Uncomment to run statistics

%Statistics %Use for LALW through HAHW models
%Stats_VertLat %Use for vertical versus lateral tests
```

Appendix E

Statistics, MATLAB Code

```
%%%%%%%%%%%%%%%%%%%%%%%%%%% Model Statistics %%%%%%%%%%%%%%%%%%%%%%%%%%%
%
% Output Synthesis for channel models
% Calculates max connected area, number of connected areas, and outputs
% centroids of each element
%
%                            Updated 07/02/2015
%%%%%%%%%%%%%%%%%%%%%%%%%%%%%%%%%%%%%%%%%%%%%%%%%%%%%%%%%%%%%%%%%%%%%%%%%%
```

Calculate number of elements in channel element

```
numel=numel(element);
```

Calculate max connected area and Store Number of Connected Areas

```
for i=1:numruns;
    area=[output_struc(i).RegionProps.Area];
    TotWh=[output_struc(i).TotalWhArea];

    MaxArea=max(area); %Stores max compartment area from each run
    ConnArea=length(area); %Stores number of compartments
%Calculate the max area, normalized to the area of the largest compartment in the element
    MaxAreaNorm=(5*MaxArea)/numel(elements);

    Stats(i).MaxArea=MaxArea; %Store max compartment size from each run
    Stats(i).MaxAreaNorm=MaxAreaNorm; %Store normalized max connected area
    Stats(i).Compartments=ConnArea; %Store number of compartments for each run
    Stats(i).TotalWhite=TotWh; %Store sum of compartment areas

end
```

Store Centroids of Elements and orientation of Elements

```
for i=1:numruns;
    ElemCent=output_struc(i).ElementCent;
    Orient=output_struc(i).Orient;
    Stats(i).ElemCent=ElemCent; %stores element centroids
    Stats(i).Orientation=Orient; %stores element orientations
end
```

Save Structures as .mat files

```
%MUST RENAME FILES (MODELRUNNAMEHERE)AND CHANGE PATH TO MATCH MODEL RUN!

q=sprintf('L:/PATH/[MODELRUNNAMEHERE]_VAgg_%d_ModWid_%d.mat', [var, mw]);  %%%%% CHANGE
TO REFLECT RUN
save(q, 'Stats'); %%% Save structure with max conn area, num conn area, centroids and
orientation of elements
```

Save final model run image

```
imshow(label,'InitialMagnification','fit')
axis on
saveas(gcf,
sprintf('L:/Thesis/Models/Results/LowMig_LowNG/Elements/MODELRUNNAMEHERE_VAgg_.75_ModWid_
3.5_Elements.tiff'));
close all
```

Appendix F

Statistics for Vertical v. Lateral Runs, MATLAB Code

```
%%%%%%%%%%%%%%%%%%%%%%%%%%% Model Statistics %%%%%%%%%%%%%%%%%%%%%%%%%%%
%
% Output Synthesis for channel models
% Calculates max connected area, number of connected areas, and outputs
% centroids of each element
%
%                            Updated 07/02/2015
%%%%%%%%%%%%%%%%%%%%%%%%%%%%%%%%%%%%%%%%%%%%%%%%%%%%%%%%%%%%%%%%%%%%%%%%%%
```

Calculate max connected area and Store Number of Connected Areas

```
for i=1:numruns;
    area=[output_struc(i).RegionProps.Area];
    TotWh=[output_struc(i).TotalWhArea];

    MaxArea=max(area); %stores max compartment area from each run
    ConnArea=length(area);
    MaxAreaNorm=(MaxArea*nits)/numel(domain); %Calculates the maximum area, normalized to
the domain area (to compare vert v. lateral)

    Stats(i).MaxArea=MaxArea; %stores max compartment size from each run
    Stats(i).MaxAreaNorm=MaxAreaNorm; %calculates and stores normalized compartment size
(to compar vert v. lateral)
    Stats(i).Compartments=ConnArea; %Stores number of compartments for each run
    Stats(i).TotalWhite=TotWh;      %stores sum of compartment areas
end
```

Store Centroids of Elements and orientation of Elements

```
for i=1:numruns;
    ElemCent=output_struc(i).ElementCent;
    Orient=output_struc(i).Orient;
    Stats(i).ElemCent=ElemCent; %stores element centroids
    Stats(i).Orientation=Orient; %stores element orientations
end
```

Save Structures as .mat files

```
q=sprintf('L:/PATH/[RUNNAMEHERE]_VAgg_%d_ModWid_%d.mat', [var, mw]);  %%%%% CHANGE TO
REFLECT RUN
save(q, 'Stats'); %%% Save structure with max conn area, num conn area, centroids and
orientation of elements
```

Save Last Element image

```
imshow(label,'InitialMagnification','fit')
axis on
saveas(gcf, sprintf('L:/Thesis/Models/Results/Vertical v
Lateral/Elements/LowMig_LoNG_Vagg_%d_ModWid_%d.tiff',[var, mw]));
close all
```

Appendix G

Model output (raw)

Excel spreadsheets containing all connected areas, normalized connected area, , number of compartments, and total “sand” area for each model run can are available online through Google Drive at:

http://tinyurl.com/ResModBaisden